UC Berkeley
UC Berkeley Electronic Theses and Dissertations

Title
Methods for Process Monitoring to Accurately Detect and Quantify Material Holdup in Advanced Recycle Facilities

Permalink
https://escholarship.org/uc/item/3j91s8kn

Author
Batie, Grey

Publication Date
2022

Peer reviewed|Thesis/dissertation

eScholarship.org Powered by the California Digital Library
University of California

METHODS FOR PROCESS MONITORING TO ACCURATELY DETECT AND QUANTIFY MATERIAL HOLDUP IN ADVANCED RECYCLE FACILITIES

by

Grey Batie

A dissertation submitted in partial satisfaction of the

requirements for the degree of

Doctor of Philosophy

in

Engineering - Nuclear Engineering

in the

Graduate Division

of the

University of California, Berkeley

Committee in charge:

Professor Kai Vetter, Chair
Professor Per Peterson
Professor Michael Nacht

Fall 2022

METHODS FOR PROCESS MONITORING TO ACCURATELY DETECT AND QUANTIFY MATERIAL HOLDUP IN ADVANCED RECYCLE FACILITIES

Copyright 2022
by
Grey Batie

Abstract

Safeguarding spent fuel reprocessing facilities and other bulk material handling facilities is a challenge. These high throughput facilities typically operate continuously and produce thousands of significant quantities worth of special nuclear material annually. This, combined with the high measurement uncertainties and extremely high radiation fields present, makes the timely detection of the diversion of a single significant quantity difficult. It is in these facilities where accurate and precise techniques are vital for the detection and prevention of both inadvertent and deliberate hold-up.

Our goal was to develop novel near-real-time accountancy techniques that take advantage of advanced radiation detection and imaging technologies, in combination with non-radiation signals present in bulk handling facilities. Fault detection and isolation methods were used to investigate material holdup and diversion in a closed-loop hydraulic system. An initial experimental loop was constructed to model the movement of nuclear material between material balance areas in a commercial PUREX reprocessing plant, and accurately induce material holdup and diversion. This process was done using commercially available and diluted radiotracers such as Tc-99m and F-18, to simulate the various radiation signals present in spent fuel. Not all faults in this loop were completely isolable and more collimation was needed to reduce the cross talk between radiation detectors.

The Next Generation Loop (NGL) was a re-designed reprocessing loop which can operate in a variety of configurations and boasts control of individual process streams while employing both radiation and non-radiation sensors to observe and detect off-normal behavior. Off-normal behavior that can be simulated may include material holdup and diversion, which can correspond to plant inefficiencies, faults such as blockages or leaks, or unknown/unauthorized nuclear material streams. A model network was utilized to detect and quantity off-normal behavior. With this improved reprocessing loop, all faults were completely isolable and material diversion was detected with reasonable accuracy.

Using advanced hybrid methods to reduce the computational burden associated with running high precision simulations of complex facility models, the previous two experiments served as benchmarks for variance reduction tools such as ADVANTG. An MCNP model of a concrete shielded Input Accountability Tank (IAT) inside of a commercial PUREX reprocessing plant was created. The source term was generated using the Separations and Safeguards Performance Model (SSPM) developed at Sandia National Laboratories. This data was used to inform the type and placement of radiation detectors as well as the collima-

tion and shielding required to obtain and verify fuel characteristics such as burn up, initial enrichment, and cooling time. A high purity germanium detector and a 1 cm diameter cylindrical collimator through the concrete hot cell wall produced count rates on the order of 10^5 cps. Pu-239, Eu-154, Ag-110, Bi-214, and Y-88 were detected in the input accountability tank. Cs-134 and Cs-137 were expected to be observed but were not.

This work serves as a basis for the safeguards by design process within bulk handling facilities including advanced reactor facilities such as molten salt reactors. Using fault diagnostics and all available signals bulk handling facilities can leverage the collective expertise of the various stakeholders in the system design process to ultimately improve plant performance, reduce maintenance concerns, and communicate information about the facility's operation to better safeguard nuclear material.

For Barbara.

Contents

List of Figures

List of Tables

Acknowledgements

Firstly I would like to thank the Creator for allowing me to complete this work.

I *must* acknowledge the stolen land on which this research was completed on: the territory of **xučyun (Huichin)**, the unceded ancestral landscape of the Chochenyo speaking Ohlone people, the successors of the sovereign Verona Band of Alameda County. I recognize that every member of the Berkeley community has benefited, and continues to benefit from the use and occupation of this land since the institution's founding in 1868.

Thank you to my academic advisor **Professor Kai Vetter** for his never ending support, invaluable advice, and patience throughout this process. I could not have had a better advisor and mentor. Thank you **Professor Per Peterson** and **Professor Michael Nacht** for your mentorship, advice, and feedback. I am humbled to have you both be apart of my graduate experience. Thank you also to **Dr. Lucian Mihailescu** and **Dr. Alan Bolind**. You both were instrumental in the successful design and implementation of my experiments.

Additionally, I would like to express gratitude to the Department of Energy's Nuclear Energy University Program (DOE-NEUP) for funding this research, and the other students supported by this grant who helped accomplish this work: **Vanessa Goss**, **Dr. Christopher Poresky**, **Dr. James Kendrick**, **Laura Shi** and **Cameron Cage**.

I could never thank my loving partner **Janae Anderson** enough, nor my loyal friends **Rasheed Auguste**, **Grace Tuyiringire**, **Sherron Pearson**, **Katrina Miller**, **Nkechi Kai**, **Devin Cornish**, **Taylor Holeman**, and **Maria Velazquez**. I could not have gotten here without each and every one of you. This degree is as much mine as it is all of yours. I am extremely grateful for my sister **Michelle Washington**, my nephew **LeMar Batie**, and the rest of the Washington Family for their unconditional love.

Thank you to Berkeley Applied Research on the Imaging of Neutrons and Gamma rays (BeARING) group at UC Berkeley, especially **Michael Bondin**, **Kalie Knecht**, **Darrell Stepter**, **Jake Hecla**, **Dr. Matthew Marshall**, and **Dr. Rebecca Krentz-Wee**. Within the greater Berkeley community a special thanks goes to **Meltem Erol**, **Professor Kara Nelson**, and **Dr. Fatima Alleyne**. You all really held me down through the trials

and tribulations that are graduate school.

A special shout-out goes out to the black women who came before me in the field of nuclear engineering: **Dr. Tomi Akindele**, **Dr. Ciara Sivels**, and **Dr. Mareena Robinson Snowden**. I'm honored to have you all as friends and to be joining your ranks!

Lastly, I would like to recognize my advisors/mentors from before my time at Berkeley, such as **Dr. Ronald Wakai**, **Dr. Douglass Henderson**, and **Dr. Chanda Prescod-Weinstein**. I could not have undertaken or completed this journey without your support and the shining examples you set for what a professor should be.

Chapter 1

Introduction

1.1 Project Motivation

The International Atomic Energy Agency (IAEA) is an autonomous international organization within the United Nations system, tasked with promoting the safe, secure, and peaceful use of nuclear technologies. Their mission is carried out through technical measures, or safeguards, which are used to verify the peaceful use of all nuclear material within a country and ensure that such material is not diverted to produce nuclear weapons or other nuclear explosive devices [30].

Safeguarding facilities where the material is in bulk form, or is not individually identifiable for accountancy purposes, can be difficult since conventional item-counting safeguards techniques are not applicable, and facilities vary widely in function, layout and design. In aqueous spent fuel reprocessing facilities for example, not only is material accountancy more difficult due to the material being in an aqueous salt form, but there are large amounts of material cycling through these facilities continuously and consequently large measurement uncertainties. Additionally, the nuclear material is difficult to access due to its high radioactivity and highly corrosive nature, making it even more challenging to perform conventional material accountancy measures [16]. Unattended monitoring systems with greater accuracy and more precision are needed to minimize the IAEA's impact on plant operations and ensure that safeguards technology is keeping pace with the next generation of nuclear facilities.

Two prime examples of the need for improved near-real-time material accountancy measures were the recent accidents that occurred in two bulk handling facilities. On April 21, 2004, at the Sellafield Thermal Oxide Reprocessing Plant (THORP) in Sellafield, UK, a fractured pipe between two accountancy tanks led to the leakage of 83 m^3 of clarified radioactive fluid into a recovery pan directly below the two tanks [44]. The fluid, which had just been dissolved and was about to begin treatment, contained an estimated 20 tons of uranium and 200 kg of plutonium. This leak was not discovered until April 21, 2005, and once discovered caused the entire plant to shut down. Fortunately, no radioactive material was released into the environment thanks to the building's three containment barriers which were still intact.

The pipe fracture was discovered to be due to a mechanical failure of a nozzle connected to the accountancy vessel, caused by vibration induced fatigue [27].

At the Columbia Fuel Fabrication Facility (CFFF) in Hopkins, South Carolina, a routine annual inspection performed on May 28, 2016 discovered a large amount of solid material had accumulated in the inlet transition of the S-1030 scrubber system [54]. This system served to ventilate hoods, vessels, cleaning operations, and scrap recovery in UF_6 conversion areas to remove fumes and particulates from effluent air. Approximately 87 kg (192 lb) of unaccounted for material containing between 34 to 55 weight percent of uranium was discovered. This far exceeded the criticality safety evaluation (CSE) mass limit of 29 kg. Fortunately, this did not result in criticality, however this incident still represented a criticality safety concern since no physical controls or measures existed to detect such an event. Management was said to have lacked a questioning attitude and conservative bias required for a healthy nuclear safety culture, and did not ensure the organization had sufficient procedures and training to recognize and respond to deviations from the safety basis described in criticality safety evaluation conducted post-accident [15].

Incidents like these are expensive and resulted in losses from operation being halted, costly new recommendations to be implemented, and fines for the operator. Had these facilities been equipped with some sort of in-process-cell radiation imaging system, the rise in radioactivity could have been detected and indicated the accumulation of radioactive material outside of the accountancy tanks or above operational limits within machinery.

1.2 Research Proposal

This body of work intends on meeting the need for more advanced safeguards techniques in bulk handling facilities by using recent developments in radiation detection and imaging, combined with advances in radiation transport methods, and strategies for non-radiation based leak and diversion detection. Using these three research areas the new technology developed will detect, localize, and quantify the diversion of significant quantities of special nuclear material in near real time.

These aims were accomplished through two main research thrusts: 1) an experimental component involving the construction of two aqueous reprocessing loops to simulate the movement of material from one material balance area (MBA) to another within a bulk handling facility, and 2) a simulation component to confirm the system responses of the experimental work and optimize the proposed detection system to be employed in future advanced recycle facilities.

1.3 Outline for this Work

Safeguarding nuclear material in bulk handling facilities is an important and necessary challenge. As today's nuclear fleet ages and the next generation of reactors emerge, safeguards

techniques must also keep pace with them. The ability to detect and quantify diversion and material hold up in near real time will be vital in these increasingly complex facilities. Chapter 2 of this manuscript will provide more background information on bulk handling facilities and the safeguards technology that currently exists within them. Chapter 3 will discuss the design and operation of the first generation reprocessing loop. Chapter 4 will describe the Next Generation Loop and the experimental results obtained from its operation. Chapter 5 will focus on the modeling and simulation work done which explored the complex radiation environments present in spent fuel reprocessing facilities. And finally, Chapter 6 will summarize the implications of this work and look forward to future avenues for investigation. The goal of this work is to better safeguard existing bulk handling facilities and encourage the implementation of these methods in the safeguards by design approach for future facilities.

Chapter 2

Background

The treaty on the Non-Proliferation of Nuclear Weapons (NPT) is an international treaty whose objective is to "prevent the spread of nuclear weapons and weapons technology, to promote cooperation in the peaceful uses of nuclear energy, and to further the goal of achieving nuclear disarmament [21]." The NPT was ratified in 1968 and designated the International Atomic Energy Agency (IAEA) as its verification agency; this required all non-nuclear weapons states to negotiate an agreement with the IAEA which gave the agency the authority to monitor nuclear programs and inspect nuclear facilities, in order to verify that countries were fulfilling their treaty obligations.

The technical measures that are applied by the IAEA to independently verify that nuclear facilities are not misused and nuclear material is not diverted from peaceful uses are often referred to as safeguards [87]. Safeguards serve to assure the international community that NPT member States are adhering to the NPT and its additional protocols. They also serve to deter (a) the diversion of safeguarded nuclear materials to the production of nuclear explosives or for other military purposes and (b) the misuse of safeguarded facilities with the aim of producing unsafeguarded nuclear material [40].

2.1 Significant Quantities and Timeliness of Detection

The technical objective of safeguards according to the NPT is "the timely detection of the diversion of significant quantities of nuclear material from peaceful nuclear activities ... and deterrence of such diversion by risk of early detection [21]." The term significant quantity (SQ) was created to establish an IAEA inspection goal, and is defined as the approximate amount of nuclear material for which the possibility of manufacturing a nuclear explosive device (NED) cannot be excluded [34].

A significant quantity depends on the material type and material category. Material type refers to the element contained in the material, and, for uranium, the degree of enrichment. The primary material types are plutonium, highly enriched uranium, ^{233}U, depleted, natural, and low enriched uranium, and thorium. The material category classifies nuclear material

according to its irradiation status and suitability for conversion into NED components. The categories are: unirradiated direct use material, irradiated direct use material, and indirect use material [34].

- *Direct use material*: nuclear material that can be used to make a nuclear explosive device without transmutation or further enrichment. Direct use materials include: plutonium containing less than 80% ^{238}Pu, highly enriched uranium, ^{233}U, chemical compounds, mixtures of direct use materials (e.g. mixed oxide (MOX)), and plutonium in spent reactor fuel. Direct use materials can be further split into subgroups based on its irradiation status. Unirradiated direct use material does not contain substantial amounts of fission products, therefore requiring less time and effort to be converted to components for a nuclear explosive device. Conversely, irradiated direct use materials such as plutonium in spent reactor fuel contains substantial amounts of fission products and would require much more processing time to implement into a NED.
- *Indirect use material*: all nuclear material except direct use material. It includes depleted, natural and low enriched uranium, and thorium, all of which must be further processed in order to produce direct use material.

By taking into account both the type and form of the material, the IAEA established its detection timeliness goals. These ultimately determine the frequency of inspections the IAEA performs and the containment and surveillance measures implemented. The detection timeliness goal, defined as the maximum time that may elapse between diversion and its detection by IAEA safeguards, should correspond in order of magnitude to conversion time. Tables 2.1 and 2.2 summarize this information and lists the SQ values and timeliness goals that are currently in use.

Table 2.1: Definitions of Significant Quantities (SQ)

Material	SQ
Direct use nuclear material	
Pu[a]	8 kg Pu
^{233}U	8 kg ^{233}U
HEU (^{235}U $\geq$ 20%)	25 kg ^{235}U
Indirect use nuclear material	
U (^{235}U <20%)[b]	75 kg ^{235}U (or 10 t natural U or 20 t depleted U)
Th	20 t Th

[a] For Pu containing less than 80% ^{238}Pu

[b] Including low enriched, natural and depleted uranium

Table 2.2: IAEA Detection Timeliness Goals

Classification ∗Direct use ∗∗Indirect use	Pu, HEU, U-233 unless stated	Conversion Time	Timeliness Goal
1*	metal	7-10 d	1 m
2*	oxides, nitrates	1-3 w	1 m
3*	irradiated fuel	1-3 m	3 m
4**	<20% $^{235}U/^{233}U$, Th	12 m	12 m

The IAEA safeguards system functions as a confidence-building measure, an early warning mechanism, and the trigger that sets in motion other responses by the international community if and when the need arises [22]. This early warning system should also serve as a deterrence to dissuade any State from contemplating material diversion or the misuse of nuclear facilities. But in order to be considered effective, the system must be seen as and be technically capable of promptly detecting diversion [40]. This task remains a challenge as nuclear facilities continue to evolve.

2.2 Safeguards by Design (SBD)

At the 2008 IAEA workshop on "Facility Design and Plant Operation Features that Facilitate the Implementation of IAEA Safeguards" it was reported that safeguards considerations are often introduced after a facility is fully designed or even after advanced construction has already taken place [32]. This can result in costly facility redesign, project delays, and reduced efficiency and effectiveness of the safeguards that are eventually implemented [35]. To avoid costly and time-consuming redesign work, Safeguards by Design is a viable alternative.

Safeguards by Design (SBD) is an approach whereby international safeguards are fully integrated into the design process of a facility: from the initial planning through design, construction, operation, and decommissioning. With SBD, facility designers are equipped with a general knowledge of safeguards and can make informed design choices that are the result of an optimum confluence of economic, operational, safety, and security factors and which include the application of international safeguards.

2.2.1 SBD Stakeholders

It is important to note that designers are just one of multiple stakeholders of nuclear facilities. Others include the facility owners/operators, the IAEA, safeguards regulatory authorities, equipment suppliers, and the scientific community. These stakeholders share common goals such as the reduction of resources needed to implement all requirements; the reduction of project risk against schedule delays; the avoidance of compensatory measures or

'workarounds'; and the avoidance of extra construction associated with retrofits. In addition to these shared goals each stakeholder also has their own individual responsibilities and incentives for implementing SBD as early as possible [32].

1. **Facility owners/operators**: The facility owner/operator is responsible for providing the information to the safeguards authority in order to meet the requirements of the relevant safeguards agreements, and to facilitate access for IAEA safeguards inspectors. Their incentives for choosing a design that best accommodates safeguards requirements are to minimize the impact of these requirements on the overall cost of the facility and to reduce the intrusiveness of safeguards activities during observation. If this isn't done, IAEA safeguards activities can significantly impact a facility's ability to operate during inspections.

2. **Designers/constructors**: Designers/constructors can improve the effectiveness of safeguards by simplifying the path the nuclear material takes within the facility or reducing the number or size of penetrations and access openings along that path. Designers can also reduce the number of storage locations or reduce operational flexibility to make it more difficult to reconfigure systems for the production of undeclared nuclear material.

   SBD encourages designers to be made aware of the potential safeguards requirements such as containment considerations, penetrations, camera views, sealing, locations of potential measurement stations, etc. Improving access and illumination for example, are some of the many ways designers can reduce the impact inspections have on facility operations. Such improvements can reduce project risks, prevent construction delays, and avoid costs associated with retrofitting the facility late in the licensing/construction process.

3. **The IAEA**: The primary goal of the IAEA is to safeguard nuclear materials and detect diversion in a timely manner. To facilitate the implementation of safeguards the IAEA establishes high level facility specific safeguards guidelines and communicates these to the stakeholders at appropriate times during the design process. Benefits of this include improved inspection conditions, the implementation of more effective and efficient safeguards, and the increased awareness of safeguards goals among all stakeholders. This will help establish a 'safeguards culture', which can benefit the international community as a whole in the long term.

4. **Safeguards regulatory authorities**: The safeguards regulatory authority is the formal, legally recognized entity responsible for implementation of the State's international safeguards obligations, and serves as the primary interface between the State, including companies within the State, and the IAEA. Since the NPT does not confer its obligations directly on the facility designers, an intermediate safeguards authority is responsible for communicating the IAEA's safeguards requirements with the operators

and designers. It is the State's responsibility to ensure all safeguards considerations are addressed and that the operator's plans comply with all regulatory requirements.

The State authority submits all formal declarations to the IAEA, including data obtained from remote acquisition and other data transmission techniques. The State is therefore responsible for the quality, completeness, and accuracy of these declarations. By preparing for the incorporation of advanced safeguards technology early in the design phase, the State authority can reduce the incidence of human error, communication failure, anomalies, and inconclusive results; thus, reducing the State's workload to resolve such issues.

5. **Equipment suppliers**: Multiple subcontractors are often employed to provide safeguards equipment and software. Some suppliers provide operator equipment to collect and report information to the safeguards authority, measure nuclear material, or monitor operational processes. Other subcontractors could supply IAEA equipment to provide measurement, containment, and surveillance in both attended and unattended applications. International safeguards rely on this equipment to facilitate the inspector verification process. If suppliers are aware of the safeguards specifications they can improve their equipment to meet the international safeguards requirements. Some of these specifications include measurement uncertainty limits, interface specifications, repair and maintenance responsibility, procurement mechanisms, authentication, and data security.

6. **The scientific community and technical support organizations**: The academic and scientific community can help with addressing new technological challenges and informing the public about the issues, risks, and risk reduction with regards to the construction and operation of nuclear facilities. There is a dire need for better, cost-effective tools that facilitate decision making, point out gaps in safeguards approaches, and help identify opportunities for innovation. By engaging with the next generation of scientists, engineers, and policy makers, and instilling in them the importance of international safeguards, they can be better advocates and innovators of safeguards friendly technology and designs.

2.2.2 A Brief History of SBD in Reprocessing Plants

One of the largest and most recent examples of the successful implementation of the Safeguards by Design approach was at the Rokkasho Reprocessing Plant in Japan. This feat was made possible through decades of IAEA collaboration with multiple States and their reprocessing facilities. Beginning with the West Valley Reprocessing Plant in West Valley, New York, the United States voluntarily offered the IAEA access to the facility in 1969 to help define international safeguards measures. With no models or guidelines available to be used as a reference, the first ever IAEA inspection of a reprocessing plant was conducted.

The primary lesson learned during this campaign was of the need for a greater number of independent verification measures of nuclear material [49].

In the following decade numerous advances in safeguards design and technology were made. For example, the Wiederaufarbeitungsanlage Karlsruhe (WAK) facility in Germany, became the first reprocessing facility to actually require an enhanced IAEA inspection regime since it existed within a non-Nuclear Weapons State. At WAK, IAEA inspectors were granted open access to operating records for the first time, and with the help of facility operators, developed K-edge/Hybrid K-Edge densitometers for in-field measurements [68]. Additionally, routine solution monitoring and measurements of undissolved solids were taken.

At the Tokai Reprocessing Plant (TRP) in Tokai, Japan, the next reprocessing plant to come under international safeguards, near-real-time-accountancy (NRTA) was implemented for timely safeguards assessment. Electromanometers for volume measurements, containment and surveillance (C/S) approaches, and non-destructive assay (NDA) techniques were explored. The conclusions drawn by the IAEA from these studies were published in the TRP Improvement Plan [47]. The key takeaways from the improvement plan were that the IAEA did not sufficiently understand the plant's operations and that safeguards had not been the priority during building or operation. The IAEA had little to no input in the early design phase of the plant, and attempts to retrofit the plant for safeguards were unusable or inadequate and needed strengthening. It was recommended that:

1. Design information by the operator/State be submitted as early as possible to allow for IAEA consultations on safeguards requirements for equipment and verification measures, and for the early determination of resource requirements

2. Advanced nuclear material accountancy methods be developed to provide NRTA with improved accuracy and reasonable measurement uncertainties, including online analysis

3. Containment and surveillance measures be applied wherever possible to maintain continuity of knowledge of material flows and reduce re-measurement requirements

4. A method be formulated to authenticate the operator's instruments, although installation of independent safeguards measurement and surveillance systems are preferable

5. An on-site laboratory should be constructed to reduce sample shipping costs and provide timely analyses of safeguards sample

6. Research and development between the IAEA, State, and operator continue to be conducted to determine on-going needs

Soon after these recommendations were formulated the IAEA was put to the test to create a credible safeguards approach. Japan had decided to construct the Rokkasho Reprocessing Plant (RRP), a large scale commercial reprocessing plant with an estimated throughput of 800 tHM/year. Using the lessons learned from WAK and TRP as a blueprint, the IAEA worked closely with the JAEA, Japan's safeguards regulatory authority, and JNFL, the

facility operator, to incorporate new and existing safeguards approaches in the design phase. Preliminary designs were provided to the IAEA very early on, allowing for early visits to the site and resource planning, and for the discussion of design changes or modification to accommodate safeguards[1].

Together they optimized plant design features to provide easier access for verification of nuclear material and operational status, and to provide more transparency in declared process operations. This resulted in the construction of a state-of-the-art on-site laboratory, jointly used equipment, over 50 in situ measurement/monitoring systems, and approximately 70 surveillance systems [28]. Specific examples of some of the monitoring systems will be explained in more detail in Section 2.5.

2.3 Bulk Handling Facilities

The goal of IAEA safeguards is to provide timely detection of the diversion of a significant quantity of nuclear material. Meeting this goal is much more challenging when the material is in bulk form. Bulk nuclear material is material in bulk/loose form, such as liquid, gas or powder, or in a large number of small units (e.g. pellets or pebbles) that are not each individually identifiable for nuclear material accountancy purposes [34]. Example of facilities that use bulk material include plants for conversion, fuel fabrication, enrichment, reprocessing, or molten salt reactors. Table 2.3 lists the most common bulk handling facilities and the various forms special nuclear material exists within each facility [5]. This work focuses on the safeguarding of bulk materials in both spent fuel reprocessing facilities and molten salt reactors (MSRs). It is within these facilities where novel safeguards technologies are needed.

Bulk Handling Facility	**Special Nuclear Material Form**
Conversion	U_3O_8, uranyl nitrate (UNH), ammonium diuranate (ADU), UF_4, U metal
Enrichment	UF_6
U Fuel Fabrication	UO_2 (pellets, powder, scrap)
MOX Fuel Fabrication	Pu and U solutions, PuO_2, MOX (powder, pellets, scrap)
Reprocessing	Input solutions, products, high activity liquid waste
Molten Salt Reactors	Liquid molten salt fuels and/or coolants

Table 2.3: Material Form in Bulk Handling Facilities

[1]It is worth noting that some design changes were difficult to make because of the operator's contractual agreements. Also, IAEA was unable to detail their safeguards requirements early in the design stage because of its lack of experience in safeguarding this type/size of a facility [49].

2.3.1 Molten Salt Reactors

Molten salt reactors use nuclear fission to generate power. The key difference between molten salt reactors and pressurized water reactors (PWRs) is that the nuclear fuel and/or primary coolant in MSRs is in molten salt form. Figure 2.1 depicts a molten salt reactor with molten salt fuel and molten salt coolant. To keep their fuel in a liquid state, these reactors operate at higher temperatures compared to PWRs. These higher temperatures result in higher thermal efficiencies for generating electricity, and gives the plant operator the option of using the excess heat for other high-temperature process heat applications such as desalination or hydrogen production [83],[33]. MSRs' negative temperature coefficient and lower operating pressures also reduce the risk of a large break or loss of coolant accident, thereby enhancing the inherent safety of the reactor [37].

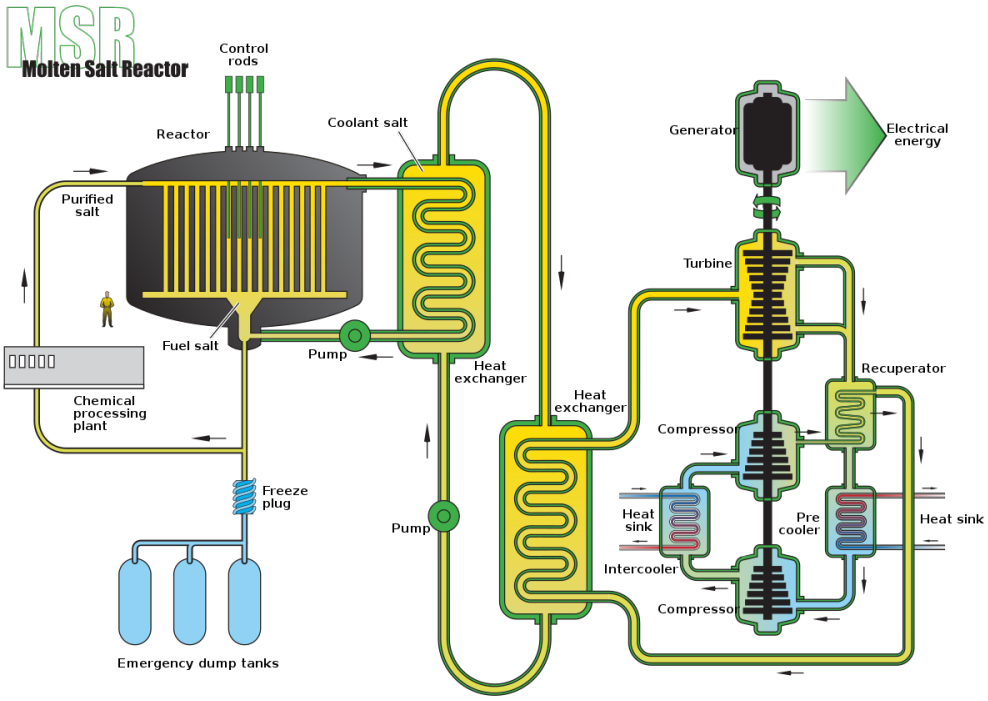

Figure 2.1: A schematic representation of a molten salt reactor [23]

MSRs vary widely in design. Some versions such as the Fluoride Salt-Cooled High-Temperature Reactor (FHR) use solid TRISO-based fuel and cool it with liquid molten salt [64], while others use molten salt fuel. Researchers at Oak Ridge National Laboratory (ORNL) have successfully demonstrated MSRs' ability to utilize all three major types of fuel: ^{233}U, ^{235}U, and ^{239}Pu [79]. MSRs can be burners, meaning they burn more fuel than

they produce, or breeders that generate more fissile material than they use during operation (via the $^{238}U/^{239}Pu$ cycle or the $^{232}Th/^{233}U$ cycle).

In the 1960s, because of rising energy demands and predictions of uranium deposits running out, the United States felt like breeder reactors were a logical choice for investment. However molten salt breeder reactors advanced much slower than expected and were becoming increasingly expensive. This coupled with the discovery of additional uranium deposits led to the eventual abandonment of commercial breeder reactors [80]. Presently, breeder reactors remain much less cost effective than disposing of fuel directly.

The neutron spectrum within these reactors can be fast, thermal, or epithermal, and coolants can be mixtures of fluoride or chloride salts, for example the mixture of lithium and beryllium salt called FLiBe. The fuel cycle in the reactor itself can be once-through or closed; a closed cycle MSR containing molten salt fuel would have the potential to remain online while refueling or fuel reprocessing occurs. Research has shown that continuous fuel salt cleanup is possible to separate the fission products from the fuel via pyrochemistry.

Another method to reduce the amount of fission products in the salt is by designing the MSR to be an actinide burner reactor to transmute the long-lived isotopes into shorter-lived fission products [7],[81]. The benefits of actinide burners aren't clear; in theory, reducing the presence of long-lived radioisotopes would simplify risk assessments of geologic repositories for spent fuel. However, the dose risks are usually dominated by long-lived fission products, which will remain in the waste even if actinides are removed and burned off in future reactors [74].

Molten salt reactors do have some disadvantages worth considering. The high operating temperature and highly corrosive nature of the salts makes finding compatible structural materials difficult. This corrosiveness is worsened if the fuel salt comes in contact with moisture, sulfur, or free oxygen ions [59]. The liquid form of the fuel fluid means that different considerations need to be taken for containment and maintenance. Lastly, the mobile form of the special nuclear material and the potential for fissile breeding means that IAEA safeguards would need to monitor fuel in bulk form, which is more challenging than conventional nuclear reactors with fuel that can be monitored as discrete items.

2.3.2 Spent Fuel Reprocessing Facilities

Spent fuel reprocessing is the process of extracting fissile and fertile materials from spent nuclear fuel. Once a spent fuel assembly leaves the reactor it still contains over 95% of uranium and about 1% of plutonium (Figure 2.2). This material is recoverable and can be put towards creating fresh mixed oxide fuel, or MOX fuel. MOX fuel replaces a nearly equivalent amount of enriched uranium and thus reduces the need for considerable mining and enrichment operations [43].

This process of recovering and recycling the uranium and plutonium also reduces the volume of material being disposed of as high-level waste and contributes to national energy security. These advantages are often outweighed by the present fact that direct disposal is

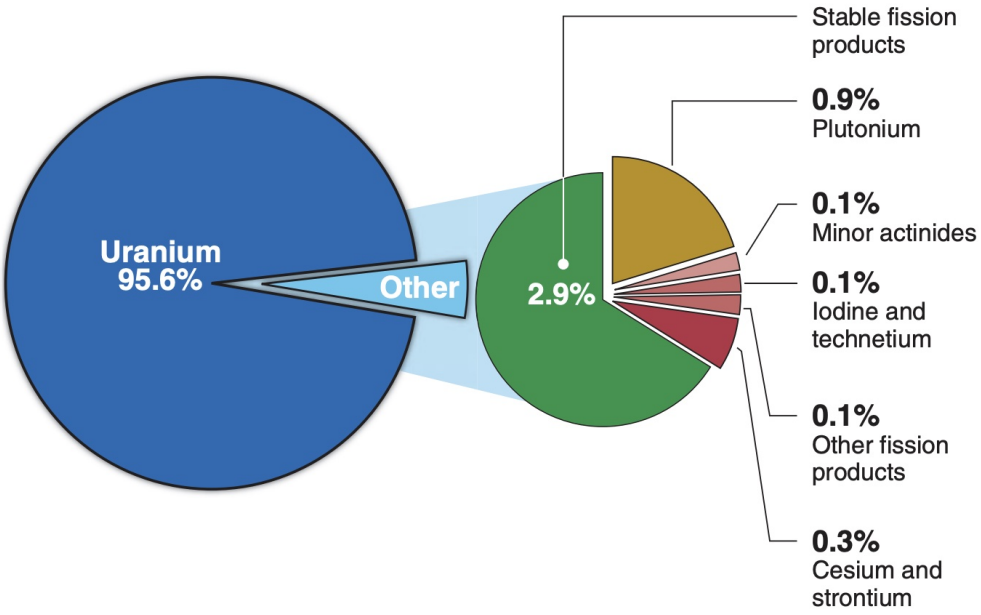

Figure 2.2: Composition of spent nuclear fuel from a standard PWR 33 GW/ton with a 10-year cooling time (without cladding) [89]

much cheaper than reprocessing and that uranium has remained readily available at relatively low prices in recent years [9].

Currently only five countries reprocess spent fuel worldwide: France, Russia, Japan, the UK, and India; no country has a completed permanent spent fuel repository [43]. Finland and Sweden have completed licensing and are constructing long-term spent fuel repositories based on the Swedish KBS-3 spent fuel disposal method [31]. The U.S. has operated a geologic disposal facility called the Waste Isolation Pilot Plant (WIPP) since 1999, although this plant is restricted to only dispose of defense generated transuranic wastes [56]. As the amount of spent fuel being stored worldwide continues to increase, and no agreed upon long term storage option exists, spent fuel reprocessing will remain a viable, albeit not yet economical, option for spent fuel waste reduction.

The PUREX Process

PUREX, or the Plutonium URanium EXtraction process, is an aqueous/organic solvent extraction process developed to recover uranium and plutonium from spent nuclear fuel. PUREX is the primary extraction method used worldwide for reprocessing spent fuel and is best suited for continuous, large scale, remote operation. PUREX utilizes an extractant called tributyl phosphate (TBP) diluted in an inert hydrocarbon solvent such as kerosene.

Spent fuel is dissolved using boiling concentrated nitric acid in a continuous or batch process and undergoes clarification to remove insoluble fission products and cladding [45].

This clarified fluid undergoes intensive mixing with the TBP/kerosene solution to achieve U/Pu separation from the fission products. The well mixed solution is allowed to settle and at higher nitric acid concentrations the uranium and plutonium partition to an organic solvent phase and the fission products stay in an aqueous nitric phase as seen in Figure 2.3. This can be done using mixer settlers, pulsed columns, or centrifuges.

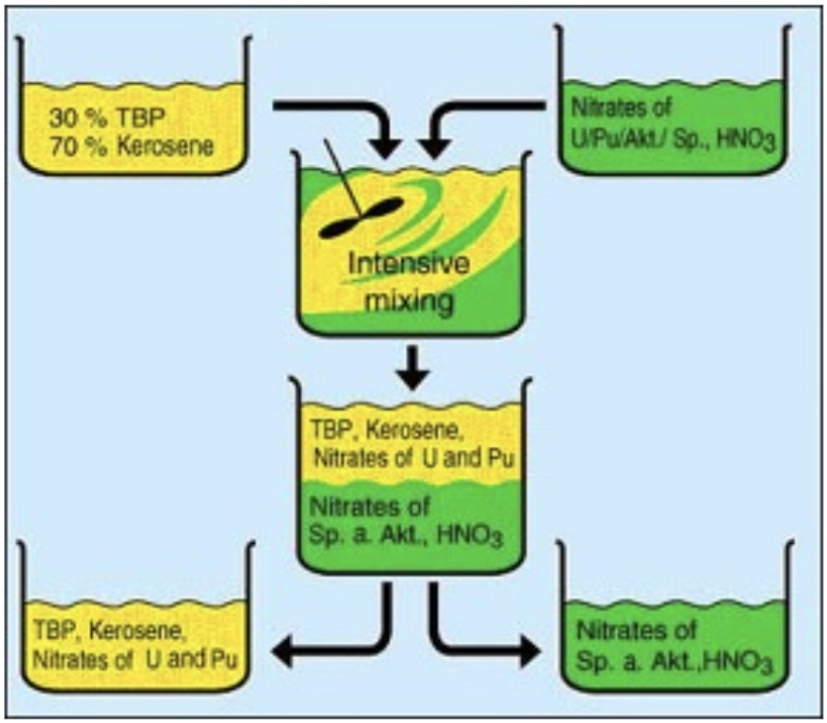

Figure 2.3: PUREX extraction process using TBP and Kerosene [85]

Once separated from the fission products, a reductant is added to the aqueous stream to reduce plutonium into a state that is not soluble in an organic solvent, leaving just uranium remaining. That remaining uranium is stripped from the nitric acid solution and stored as UO_2 while the removed plutonium is stored as PuO_2. The liquid high-level waste containing the fission products is eventually solidified by mixing it with molten glass and allowing it to harden, a process known as vitrification [90]. A process flow diagram is included in Figure 2.4.

The PUREX process has its advantages: low solvent volatility and flammability, higher chemical and radiation stability of the solvent, and lower operating costs [43]. The primary disadvantage to PUREX is that the purified plutonium will be a direct use material and

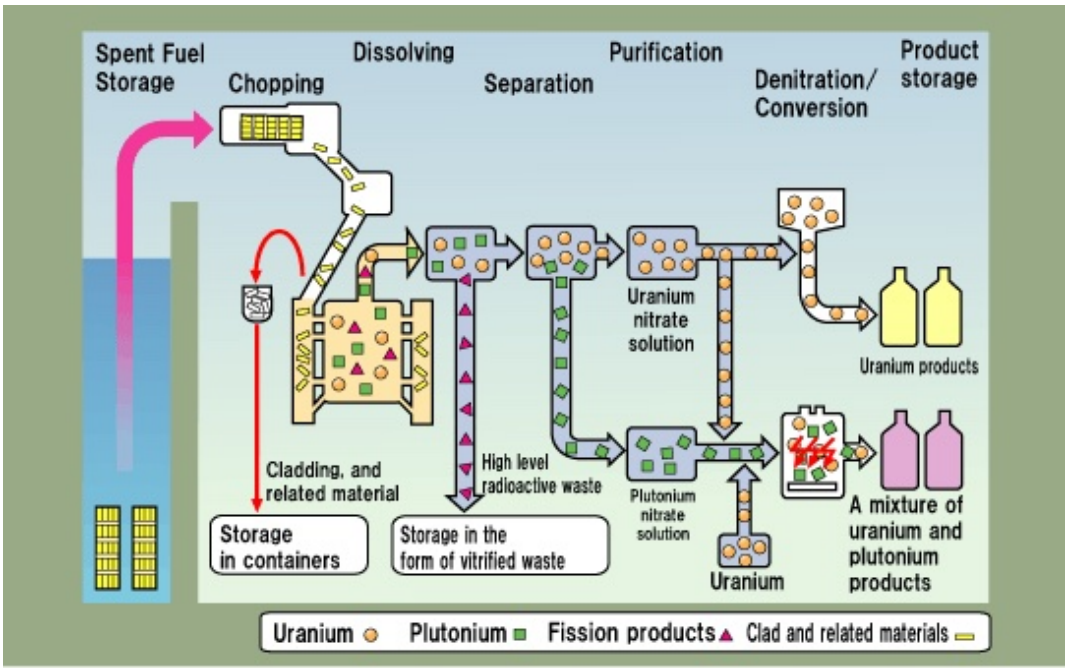

Figure 2.4: Flow of LWR spent fuel in an aqueous reprocessing facility [46]

presents an attractive target for theft. Thus spent fuel reprocessing facilities require highly effective physical protection, equivalent to Category I facility protection in the United States [38].

Other PUREX alternatives include UREX, or the URanium Extraction process, which results in a pure uranium stream and leaves the plutonium in the fuel with the fission products and minor actinides, UREX+ which removes both uranium and technetium, and pyroprocessing.

Pyroprocessing

Pyroprocessing is a process which uses high temperature oxidation and reduction reactions involving inorganic molten salts, gases, and liquid metals as process media to remove uranium from spent nuclear fuel [42]. This can be done with electrolytic separation or electrorefining. Electrorefining involves using the impure metal (the spent fuel) as an anode and virtually pure uranium is collected at a solid mandrel cathode. A mixture of transuranic elements such as plutonium, americium, neptunium, curium and other rare-earth fission products are collected at a liquid cadmium cathode suspended in an electrolyte salt [55]. A schematic of the electrorefining process is shown in Figure 2.5.

Pyroprocessing has a few benefits compared to PUREX: it has a significantly lower proliferation risk, it costs less because the organic extractants used in PUREX such as TBP are

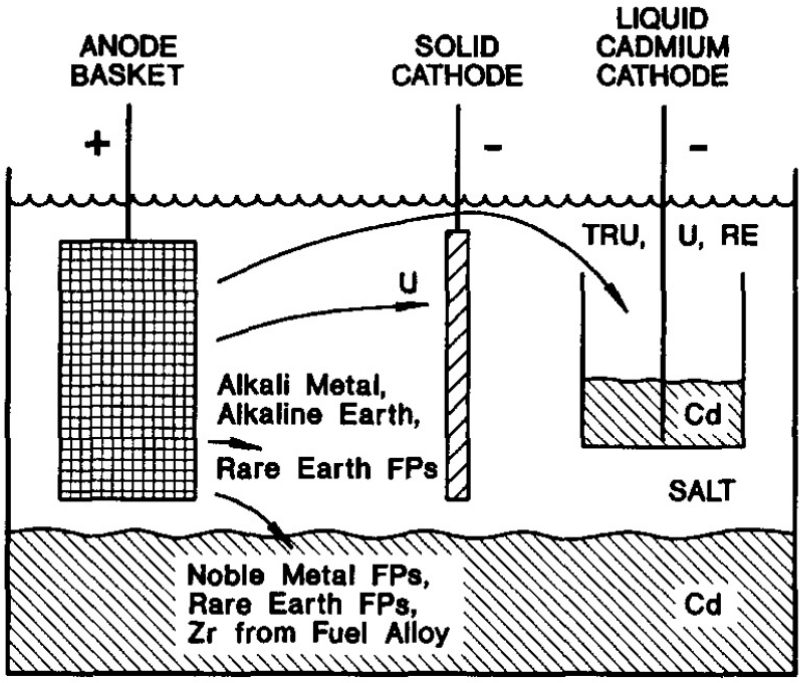

Figure 2.5: Schematic diagram of the electrorefining process [55]

more susceptible to radiolysis-induced breakdown and require replacement, it produces less secondary waste, and the spent fuel it uses requires shorter cooling times because intense radiation levels are acceptable during operation. Additionally, pyroprocessing facilities can be more compact because larger quantities of spent fuel can be handled at one time. This is because the chloride dissolution salt used is a neutron absorber, in contrast to water which is an effective neutron moderator. The chloride salt thus reduces the risk of inadvertent criticality accidents relative to aqueous reprocessing criticality accidents. On-site reprocessing could occur at or within proximity of a nuclear reactor, reducing spent fuel transportation costs as well.

The main drawback to pyroprocessing is that it has not yet been fully industrialized so it is not economically viable in any country [42]. Current methods involve batch-wise processing making it difficult to scale up to on the order of hundreds of tons per year. For these reasons, it will not be studied in this body of work.

2.3.3 Challenges with Safeguarding Bulk Handling Facilities

Bulk handling facilities can vary widely in function, layout, and design. This makes standardizing safeguards techniques difficult, especially as the facilities continue to evolve. In

the bulk handling facilities of particular interest for this research (aqueous reprocessing facilities and molten salt reactors) the bulk material has a higher proliferation risk due to the material type and form. These large-scale facilities can operate continuously, perform online refueling, and handle as much as several hundred tons of heavy metal per year. With a modest 5% measurement uncertainty, this can result in the potential loss of hundreds of significant quantities of special nuclear material annually.

The constantly changing isotopics and concentrations of material adds to the difficulty in accurate accountancy measures. This is further complicated by the high operating temperatures, high radioactivity, and highly corrosive environment the material exists within [16]. That being said, technical measures do exist within existing bulk handling facilities. This technology will be discussed in more detail in Section 2.5. The following section will examine some of the signatures of interest from a safeguards and material accountancy perspective.

2.4 Signatures of Interest

2.4.1 Non-Radiation Signals

Process monitoring is a key part of nuclear material accountancy for safeguards in bulk handling facilities. Process monitoring in this context applies to structures, systems, and components within a facility which handle specific nuclear material using non-radiation means (process stream flow rates, material mass and volume measurements, system pressures, etc.). As the available non-radiation signals within these types of facilities have increased in number and in resolution, there is a large potential for leveraging these non-radiation signals to complement the traditional radiation signal measurement and analysis that is fundamental to implementing strong nuclear safeguards [10],[61].

This project aims to coordinate the collection and analysis of both radiation and non-radiation signals. Together, these signals augment understanding of the operation and behavior of facilities containing fluid streams of special nuclear material. This subsection discusses the non-radiation signals that may be available in facilities where diversion and/or holdup is possible and any considerations for collection if these signals can be measured by existing instrumentation [50]. A wide range of potential non-radiation signals are mentioned even when they may not be particularly applicable or where additional instrumentation would be required. This expanded signal option set is presented so that future research and facility designers may find useful solutions here even though we choose not to use some of these signals.

Inventory Control

Inventory control signals indicate changes in the inventory in major components or structures, such as holding tanks and reaction vessels. Signals in this group include free surface levels and fluid inventory weights. An important consideration for these signals is whether the

process is a continuous process or a batch process. It is also important to know whether these processes are expected to have steady-state operating conditions.

There are two primary methods of measuring fluid levels in a facility: directly through level inspection and indirectly through weight measurements. Weight measurements are much simpler in theory and yet may require complex means of facility integration. Both measurement methods are online, passive, and continuous. In all cases, these measurements rely heavily on compatible materials and environments and may not be appropriate depending on the application.

Fluid flow rate

Fluid flow rate measurements indicate the amount of fluid flow in specific flow paths such as pipes. The total exchange of material in a system or component is possible to capture if fluid flow rate signals are collected for all flow paths to and from the system or component. Important considerations for this signal are the type of flow rate measured (volume flow rate, mass flow rate, fluid velocity) and complementary signals (fluid temperature, density, quality, etc.), whether flow rate is measured in all flow paths/branches of a system, whether the system is expected to have steady-state operating conditions, and if there are additional mass exchange operations in the system.

Fluid flow rate measurements depend significantly on the environment and the fluid under measurement. Accuracy is also particularly challenging, and the instrument selected depends heavily on the accuracy needed; this could range from simply having a qualitative understanding of flow rate (i.e. is the fluid flowing, and if so, relatively the same as normal or more or less) to having a high-accuracy measurement that can be used to determine whether very small amounts of fluid are being lost in the facility as it operates. Fluid flow rate measurements are generally in situ, online, passive, and continuous.

Vibration

Vibration signals typically result from the continuous movement of dynamic components such as pumps, bearings, mixers, and fans, and can be produced from moving fluids as well. Vibration signals may be useful for indicating deviations from steady-state operation of processes; an important consideration is whether the system or component is expected to have steady-state operating conditions. If vibration signals that closely couple to fluid flow through structures can be measured (such as flow through piping networks, pumps, and internal fluid movement from agitators), these may provide high-accuracy and high-precision measurements of the movement of fluid through a facility and thus diversion and/or holdup.

Vibration instruments are in general directly coupled to the motors of rotating components (pumps, fans, blowers, etc.) and therefore are generally decoupled from the extreme environments of the facility.

Temperature

Temperature is a fundamental signal for understanding a thermal system's performance and thus provides important process and state information to the system operator. Examples of important process information that temperature signals may provide include: when a fluid begins to boil, how long a fluid has been cooling in a tank, if there is fluid in a pipe (for batch processes), if environmental conditions change, and whether structural elements exceed temperature limits. Temperature measurements can be made for fluids (liquids and gases) and solid materials, making these signals particularly flexible for a wide range of structures, systems, and components.

Both aqueous reprocessing facilities and molten salt facilities present significant chemical challenges and may require special coatings or surface processing for in situ instruments. A common work-around is to install temperature instruments in physical penetrations into the fluid stream or to use instrumentation to measure component and structure surface temperatures as surrogates for fluid temperatures.

Pressure

Pressure, like temperature, is a fundamental signal in fluid systems that provides process and state information and thus an understanding of a system's operation and performance. Although typically more difficult to measure than temperature, pressure signals are just as valuable in providing insight into a system's operation and performance, particularly in off-normal conditions where slight deviations from normal behavior are easily detected.

Because of pressure signals' strong correlation to the dynamic behavior of bodies of fluid, pressure signals are incredibly useful for indicating abnormal performance expected in diversion and/or holdup. Pressure sensors must be in situ to measure the pressure of a fluid and are generally online, passive, and continuous measurement devices.

Structure Strain and Acceleration

Strain is a measurement of the physical distortion of a structure. In fluid systems, strain signals provide clear indications of structures' performance under varying temperature conditions (due to thermal expansion/contraction), deflection under loads, and expansion/contraction under pressure. Strain signals are also critical for tracking creep of high-temperature structures when they're loaded in tension over an extended period of time.

Acceleration signals indicate changes in the movement of structures. Structures and components in dynamic systems are expected to move – what is revealing in acceleration signals are relative changes, or changes in the way that structures and components are moving over time. Together, strain and acceleration signals give steady-state and dynamic measurements of the physical condition of the facility during operation. Depending on the sensitivity of the signals, they may be used to define and understand the facility during normal operation so that off-normal events are easy to identify, thus targeting diversion and holdup.

Like vibration sensors, instruments for strain and acceleration measurement may be relatively decoupled from the harsh conditions of the facility by placing them on the surface of structures and components of the facility that are away from the fluid environment. In general, like vibration sensors, these instruments are in situ although outside the harshest environment in the facility, online, passive, and continuous.

Visual/Infrared Photography

Photography, both in the visual and infrared light ranges, is incredibly useful for monitoring the operation of a structure, system, or component. These signals are relatively easy to collect, are collected at a distance, and potentially contain a significant amount of information in each image captured. Visual photography signals help indicate off-normal behavior and may be critical forensic signals for identifying root causes of accidents or other adverse conditions. Infrared photography signals are similar yet complementary to visual photography and may help clarify images where not enough visual light is present. Infrared photography also is generally indicative of the temperatures in an environment and thus provides relative temperature signals from a distance.

Signals from photography are critical for monitoring any facility during and outside of operation, and thus are important for detecting diversion, holdup, or any abnormal event. Fortunately, these systems are generally commonplace in most facilities. Special thought should be given to the placement of photography systems (partially in the design phase of plant commissioning) so that they are maximally effective in monitoring the facility for signals of interest and so that they are not easily tampered with or disabled.

Visual and infrared photography (and videography) are ex-situ (although within line-of-sight of the component of interest), online, passive, and continuous. The primary considerations for the selection of these systems are measurement requirements (frequency of images, resolution, sensor count, etc.) rather than environmental considerations.

System Power Input/Output

Power input and output signals are typically not directly measured signals in systems but are important for capturing and understanding the energy inputs and outputs of the system. Understanding the dynamic energy balance in a system provides powerful insight into the system's operation, performance, and dynamic behavior. Typical power input and outputs in a system include heating, cooling, pumping/blowing, and pressurization. If these signals are high-resolution in both time and energy, they may help identify the small energy-based signals relevant to diversion and holdup.

In general, there are no specific instruments for directly measuring power input and output within a facility. Instead, these values are calculated using other signals such as flow rate, temperature, current, voltage, and pressure differential.

Thus far, in discussing the signals available from facilities that may be used to detect and identify material diversion and/or holdup we have focused our attention on instrument signals

that measure specific technical parameters of the facility. In addition to these signals, data-based signals such as equipment health monitoring, personnel movements, signal metadata, plant performance metrics, and controls actuation may provide additional insight into the operation and performance of the facility, including whether and how material is diverted or unintentionally held up.

2.4.2 Radiation Signals

More than a thousand fission products (FPs) are generated by the nuclear fission process [1]. By detecting and quantifying the decay radiation from these fission products and other isotopes present in a material, we can gain insight into the isotopic composition in a non-destructive manner in near real time. Isotopes of particular interest from a radiological safety and waste management perspective are listed in Table 2.4. This table does not include high activity nuclides with low emitted radiation energies because these are typically eliminated by source shielding.

Table 2.5 lists the isotopes measurable by gamma rays in a typical irradiated fuel assembly. Special attention is paid to Cs-134, Cs-137, and Eu-154. Research has shown that a strong correlation exists between the ratio of Cs-134 and Cs-137 and the fuel burn up/cooling time [73]. The ratio of Cs-134 to Eu-154 has been shown to exhibit a correlation between initial enrichment as well. By employing high resolution spectroscopy the goal is to use these gamma signatures to remotely verify characteristics of the fuel and precisely estimate the amount of special nuclear material present.

With respect to neutrons, several isotopes have been shown to produce significant neutrons per gram per ton of uranium (Table 2.6). The sources of the neutrons in spent fuel vary from alpha particle induced reactions, spontaneous fission, to induced fission. Curium-244's spontaneous fission rate is commonly used in passive neutron detection systems to verify the presence of special nuclear material.

Using these relationships, properly positioned and collimated gamma and neutron spectroscopy systems can be employed to continuously verify the material composition at various stages within the reprocessing plant in near real time.

Nuclide	Half-life (years)	Burn-up credit	Radiological safety	Waste management	Comments
^{79}Se	2.95×10^5			■	
^{95}Mo	Stable	■			Metallic
^{90}Sr	28.9		■	■	Decay precursor of ^{90}Y
^{99}Tc	2.111×10^5	■		■	Metallic
^{101}Ru	Stable	■			Metallic
^{106}Ru	371.6 days		■		Metallic
^{103}Rh	Stable	■			Metallic
^{109}Ag	Stable	■			Metallic
^{125}Sb	2.7586		■		Metallic
^{129}I	1.6×10^7			■	Off gas during dissolution
^{133}Cs	Stable	■			
^{134}Cs	2.065		■		
^{135}Cs	2.3×10^6			■	
^{137}Cs	30.0		■	■	Burn-up indicator and precursor of ^{137m}Ba
^{139}La	Stable				Burn-up indicator
^{143}Nd	Stable	■			
^{145}Nd	Stable	■			
^{148}Nd	Stable				Burn-up indicator
^{144}Ce	284.9 days		■		Decay precursor of ^{144}Pr
^{147}Pm	2.623	■			Decay precursor of ^{147}Sm
^{147}Sm	1.06×10^{11}	■			
^{149}Sm	Stable	■			
^{150}Sm	Stable	■			
^{151}Sm	90	■			Decay precursor of ^{151}Eu
^{152}Sm	Stable	■			
^{151}Eu	Stable	■			
^{153}Eu	Stable	■			
^{154}Eu	8.59		■		
^{155}Eu	4.753	■			Decay precursor of ^{155}Gd
^{155}Gd	Stable	■			
^{234}U	2.455×10^5	■		■	
^{235}U	7.037×10^8	■		■	
^{236}U	2.342×10^7	■		■	
^{238}U	4.468×10^9	■		■	
^{237}Np	2.14×10^6	■		■	
^{238}Pu	87.71	■	■	■	
^{239}Pu	2.41×10^4	■	■	■	
^{240}Pu	6.56×10^3	■	■	■	
^{241}Pu	14.29	■		■	
^{242}Pu	3.75×10^5	■		■	
^{241}Am	433	■	■	■	
^{243}Am	7 370	■		■	
^{242}Cm	162.8 days		■		
^{243}Cm	29.1	■			MOX and high burn-up UOX fuel
^{244}Cm	18.1		■		
^{245}Cm	8.5×10^3	■	■		MOX and high burn-up UOX fuel

Table 2.4: Commonly measured nuclides of importance to different safety related spent fuel applications

Fission Product Isotopes	Half-Life		Fission Yield in ^{235}U (%)	Fission Yield in ^{239}Pu (%)	Gamma-Ray Energy (keV)	Branching Ratio (%)
^{95}Zr	64.0	days	6.50	4.89	724.2	43.1
					756.7	54.6
^{95}Nb	35.0	days	6.50	4.89	765.8	99.8
^{103}Ru	39.4	days	3.04	6.95	497.1	86.4
					610.3	5.4
^{106}Ru-Rh	366.4	days	0.40	4.28	622.2	9.8
					1050.5	1.6
^{134}Cs	2.06	years	1.27×10^{-5}	9.89×10^{-4}	604.7	97.6
					795.8	85.4
					801.8	8.7
					1167.9	1.8
					1365.1	3.0
^{137}Cs	30.08	years	6.22	6.69	661.6	85.1
^{144}Ce	284.9	days	5.48	3.74	696.5	1.3
					1489.2	0.3
					2185.6	0.7
^{154}Eu	8.59	years	2.69×10^{-6}	9.22×10^{-5}	996.3	10.3
					1004.8	17.4
					1274.4	35.5
Activation Products						
^{54}Mn	12.2	days			834.8	100.0
^{58}Co	70.3	days			811.1	99.0
^{60}Co	5.27	years			1173.2	100.0
					1332.5	100.0

Table 2.5: Isotopes measurable by gamma rays in a typical irradiated fuel assembly [78]

Nuclide	g/tU	n(SF)/s-tU	n(α,n)/s-tU
^{238}Pu	1.35×10^{2}	3.67×10^{5}	2.48×10^{6}
^{240}Pu	2.32×10^{3}	2.02×10^{6}	4.66×10^{5}
^{242}Pu	4.61×10^{2}	8.16×10^{5}	
^{241}Am	8.83×10^{1}		3.21×10^{5}
^{242}Cm	2.43	5.44×10^{7}	1.15×10^{7}
^{244}Cm	18.3	2.07×10^{8}	1.88×10^{6}

Table 2.6: Typical neutron production from metal oxide fuel [78]

2.4.3 International Target Values

Measurement uncertainties are an unavoidable part of material accountancy. In the 1970s the IAEA first defined a set of international standards for nuclear material accountancy which lists the target values of measurement uncertainties expected for a closing material balance in five types of nuclear facilities [34]. These values are defined as the measurement result minus the true value. This difference represents the combined effect of the many sources of error present in any measuring system, such as statistical sampling error, bulk measurement error, material sampling error, and others.

These international target values (ITVs) are said to be achievable in "conditions normally encountered in typical industrial laboratories or during actual safeguards inspections. They do not represent the measurement uncertainties which would only be achieved under exceptional or ideal laboratory conditions, or with most recently developed methods, which have not yet found wide use for daily and routine measurements [95]." These values will serve as a reference point for this work to validate the experimental uncertainties obtained in our laboratory.

The IAEA presented these target measurement uncertainty values in two components: the random uncertainty component $u(r)$ and the systematic uncertainty component $u(s)$. The random uncertainty refers to the random error associated with counting statistics or the repeatability of measurements under constant conditions. The systematic uncertainty is a short-term constant when taking measurements at a current setting, meaning they are a consistent or proportional difference. An example of a systematic error is the error caused by an incorrectly calibrated instrument.

These two errors are summed in quadrature to produce the ITVs for different materials, instruments, and measurement methods.

$$u_{ITV}^2 = u(r)^2 + u(s)^2$$

Table 2.7 discusses the agreed upon target values for bulk and density measurements including mass, volume, and density. There are distinctions between accountability tanks in newer facilities based on the idea that older facilities likely use dated instrumentation that provides less certainty in the measurements. Since accountancy takes place within the accountability tanks themselves more accuracy is expected for these direct bulk measurements. The concentrations being referred to in Table 2.7 relate to the special nuclear material present within each tank. For tanks with higher concentrations of uranium or plutonium, the operator and inspector want smaller uncertainties in the quantities they are estimating.

Verifying the presence or absence of special nuclear material is vital both from a safeguards perspective and a material accountancy perspective. One of the ways to do this non-destructively is using gamma or neutron spectroscopy. Table 2.8 highlights the usefulness of NaI and Ge gamma ray detectors. With a minimum measurement time of 300 seconds, NaI ITVs ranging between 3-16% can be obtained for a variety of material types. Germanium detectors offer better energy resolution and are allotted a total measurement uncertainty between 3 and 6% with the same minimum measurement time of 300 seconds.

Table 2.9 quotes the ITVs using various neutron detection systems, all of which employ ^{3}He tubes to detect thermal neutrons from a given sample or surrounding environment [17]. Some systems like the Active Well Coincidence Counter (AWCC) are specifically for plutonium and uranium quantification. The AWCC can employ a fast neutron detection mode allowing it to estimate masses of ^{235}U present up to 23 grams [3],[60]. The High Level Coincidence Counter (HLCC) was designed specifically to assay plutonium samples including PuO_2, mixed oxides, metal carbides, solution and scrap [4].

As the amount of material these detection systems are designed to quantify increases, from smaller scale sampling to larger assaying of containers and tanks, so do the target measurement uncertainties. The Waste Drum Assay System (WDAS) was built for low level waste assays to determine the transuranic activity of contaminated solid waste in containers of a finite volume [86].

The Hulls Monitor and Measurement System which exists at Rokkasho uses neutron detection to estimate the amount of ^{244}Cm in the leached hulls and fuel end-pieces. Using these estimates operators can relate the curium content to the uranium and plutonium based on U:Pu:^{244}Cm ratios from dissolver solutions [48]. The Vitrified Waste Canister Assay System (VCAS) was also developed and deployed at the Rokkasho Reprocessing Plant in Japan; VCAS was designed to detect gross and partial defects in the declared plutonium content of plutonium and MOX storage canisters during transfer to storage and process areas of the MOX fuel fabrication facility at RPP.

The next section lists example systems that employ the instrumentation mentioned above to generate continuous data to monitor processes occurring in different bulk handling facilities.

Table 2.7: International Target Values for Bulk and Density Measurements [95]

Measurement	**Instrument**	**Uncertainty (% rel.)**		**Notes**
		u(r)	**u(s)**	
Mass	Load-Cell Based Weighing System	0.05	0.05	
	Electronic Balance	0.05	0.05	
Volume[1]	Diptube	0.30	0.20	
	Electromanometer (Accountability tanks in newer facilities)	0.05	0.10	[2]
	Electromanometer (Process tanks; high concentration)	0.20	0.20	[3]
	Electromanometer (Process tanks; low concentration)	1	1	[4]
	Electromanometer (Accountability tanks in older facilities)	0.30	0.20	[5]
Density	Diptube	0.30	0.20	
	Vibrating Tube Density Meter	0.05	0.05	
	Electromanometer (Accountability tanks)	0.05	0.05	[6]
	Electromanometer (Process tanks; high concentration)	0.10	0.10	
	Electromanometer (Process tanks; low concentration)	0.70	0.70	

[1] Volume determinations are made on the basis of level pressure, density and temperature measurements. The volume measurement uncertainties are highly dependent on the homogeneity of the liquid, the quality of the density measurements and of the calibration equation determined in the calibration process. The volume measurements may also involve an absolute error component which has to be taken into consideration when determining the overall uncertainty of volume measurements

[2] For accountability tanks in newly built large-throughput facilities, uncertainties of 0.05% for u(r) and 0.1% for u(s) at full volume are achievable if: i.) A carefully designed calibration procedure has been implemented under well-controlled environmental and stable temperature conditions; and ii.) Measurements, using high precision electromanometers, are performed on a well-characterized and homogenized liquid

[3] Process tanks for high Pu concentration solutions are generally equipped with high precision electromanometers, however, the calibration effort and tank design specifications may be lower

[4] Equipped with standard electromanometers, lower calibration effort

[5] These values apply to older facilities where the tank design was not driven by optimized electromanometer volume measurement capabilities

[6] The same comments as given for the volume measurements apply; one additional important calibration parameter is the determination of the probe (dip tube) separation

Table 2.8: International Target Values for ^{235}U Abundance NDA Measurements [95]

Method	Material	Uncertainty (% rel.)		Notes
		u(r)	u(s)	
Multichannel Analyzer with NaI Detector [1]	$LEUF_6$	5	3	(2)(3)(4)
	NU (pure materials)[5]	5	3	(3)(4)
	LEU (pure materials)[5]	3	2	
	NU, LEU Scrap (dirty)[6]	15	5	
	LEU Rods	3	1	
	HEU Metal, Alloys	3	1	
Multichannel Analyzer with Ge Detector	$LEUF_6$	5	2	(2)(3)
	LEU Oxides[5]	3	2	(3)
	HEU Metal and Alloys	3	1	

[1] For materials not containing reprocessed uranium
[2] Includes uncertainty associated with ultrasonic thickness gauge measurement of the UF_6 cylinder
[3] Spectrum analysis: infinite thickness method (enrichment meter principle)
[4] Similar uncertainties should be achievable for peak fitting based spectrum analysis methods
[5] Includes scrap with low impurity content and suitable for recycling
[6] Uncertainties for dirty scrap can vary widely due to matrix heterogeneity

Table 2.9: International Target Values for Total U/Pu Mass NDA Measurements [95]

Method	Material	Uncertainty (% rel.)		Notes
		u(r)	(u(s)	
Active Well Coincidence Counter	HEU Metal, Alloys	5	3	(1)
	HEU Fuel Elements	3	3	
High Level Neutron Coincidence Counter	Pu Oxide	1	0.5	(2)
	MOX (>10% Pu)	2	0.5	
	MOX (<10% Pu)	4	1.5	
	MOX (clean scrap)	5	2	
Waste Drum Assay System	Pu Waste Drums	10	5	
Hulls Monitor and Measurement System	Hulls Drums	10	10	
Vitrified Waste Canister Assay System	Vitrified Waste Canisters	10	10	

[1] Measurement time 600 sec.; fast mode operation
[2] Measurement time 300 sec.

2.5 Existing Safeguards Technology

Although most in-field process measurement techniques such as x-ray fluorescence, K-edge densitometry, or mass spectrometry, have relatively small uncertainties, they typically require sampling and a laboratory (either on-site, off-site, or in a portable laboratory) which can still be time intensive [48]. Other techniques exist which can employed in real time and thus can improve timeless of detection compared to the aforementioned methods.

Near-real-time accountancy (NRTA) is the basic principle of frequently monitoring in-process inventories using a combination of direct measurements from in-process instruments, off-line analyses, and indirect assessments using computer simulations of the chemical process areas [87]. Further development of unattended NRTA monitoring systems can not only improve timeliness of detection while minimizing the IAEA's impact on plant operations, but also reduce the number Person-Days of Inspection required by the IAEA to adequately safeguard bulk handling facilities. Below are three examples of NRTA technology currently deployed in bulk handling facilities.

The Solution Measurement and Monitoring System (SMMS)

The Solution Measurement and Monitoring System (SMMS) is an example of an unattended NDA safeguards system which uses NRTA to provide timely inventory measurements within process lines at the Rokkasho Reprocessing Plant in Japan. SMMS is applied to the chemical liquid processing portion of the plant, which involves over 90 vessels or extractors. Using IAEA owned and authenticated high precision electromanometers connected directly to the operator's pneumatic dip tubes, the system measures the pressure at at least two different depths within each tank (see Figure 2.6).

Volume, density, and flow rate are calculated based on the temperature and pressure readings for each tank. These values are used to estimate the mass of Pu containing solution in 12 of the most strategic tanks in the process area. A volume measurement uncertainty of $\pm$ 0.05% was achieved during commissioning [19]. Advanced features were implemented recently to support inspector verification activities and in situ calibration of the manometers using an ad-hoc portable calibration system [76].

The Plutonium Inventory Measurement System (PIMS)

The Plutonium Inventory Measurement System (PIMS) is a non-intrusive monitoring system deployed at Rokkasho [36]. It consists of 142 commercially available ^{3}He neutron detectors situated throughout the facility near any areas that may contain significant quantities of plutonium. A simplified schematic of the system is shown in Figure 2.7.

The neutron detectors employ total neutron counting techniques to convert the overall count rate at each detector to the neutron emission rate from each plant item (i.e. vessels, glove boxes, etc.) based on a measured detector response determined during commissioning. This neutron emission rate is then used to calculate the quantity and distribution of pluto-

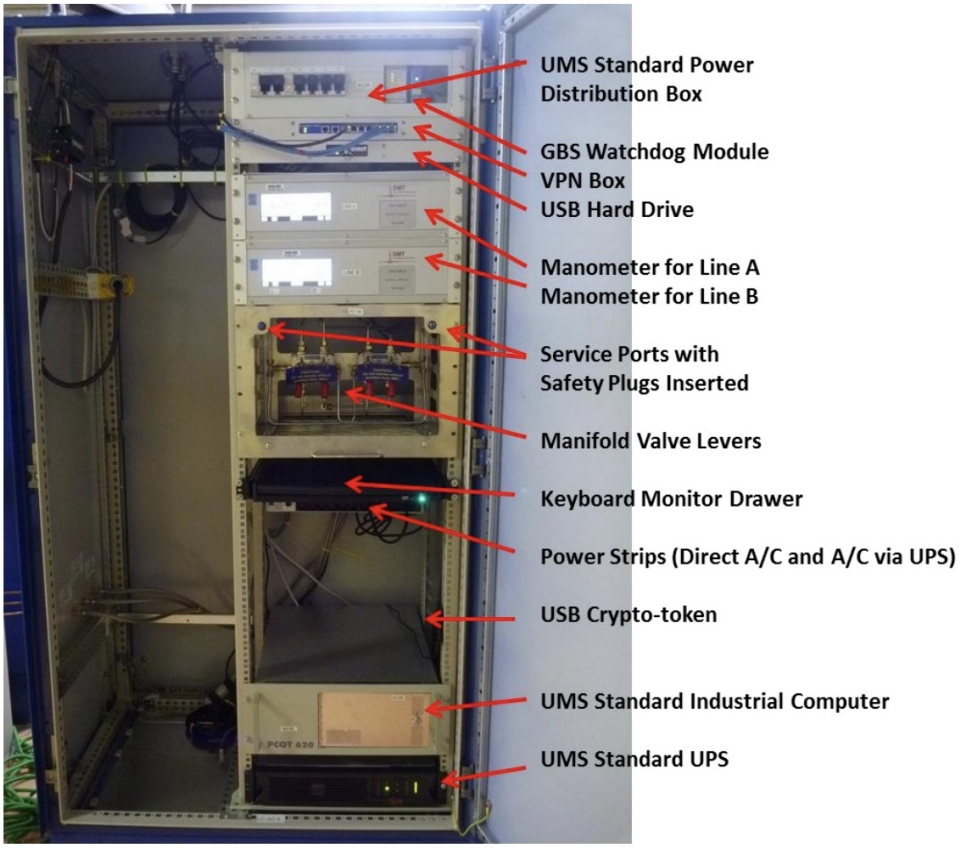

Figure 2.6: SMMS instrumentation cabinet at RRP

nium at various points in the plant using known or declared material characteristics such as isotopic or chemical composition [69]. This enables the determination of the distribution of material throughout the plant to be tracked in real time.

This continuously operating in situ system was developed specifically for high-speed distributed systems to provide optimum performance, high reliability, at minimum cost, without disturbing plant operation. PIMS is jointly used by the IAEA and JNFL which reduces the costs associated with such safeguards equipment to both the operator and the safeguards authorities. The target performance for the PIMS plant total inventory is to measure the expected or declared inventory to within an accuracy of $\pm$ 6% (1σ) during normal plant operations. For accuracy greater than that provided by SMMS and PIMS, samples are drawn and independently analyzed by the IAEA at the on-site laboratory [36]. This process is both time and resource intensive and highlights the need for more accurate and precise NRTA technology to safeguard nuclear material.

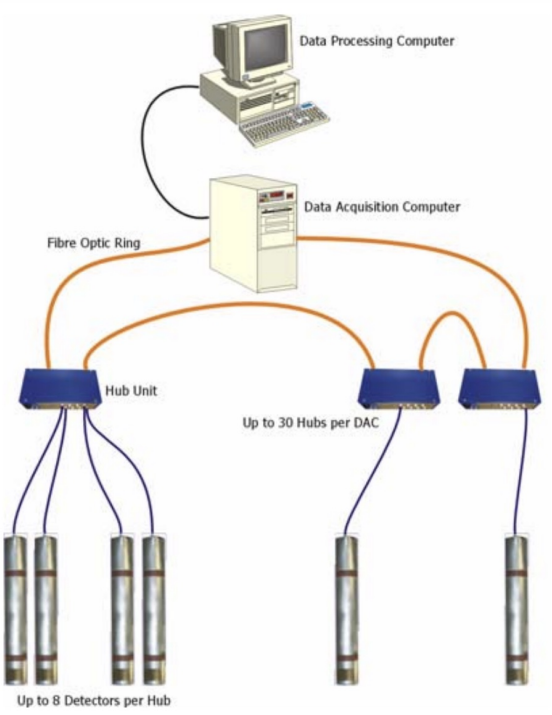

Figure 2.7: Schematic of a typical PIMS electronics platform

On Line Enrichment Monitor (OLEM)

One final example of NRTA in a bulk handling facility is the On Line Enrichment Monitor (OLEM) [84]. OLEM is an unattended system which continuously monitors the enrichment of UF_6 gas going into or being withdrawn from cylinders at gaseous centrifuge enrichment plants. A collimated NaI(Tl) gamma spectrometer, a temperature probe, and a manometer are used to estimate the enrichment at specific points and together constitute one collection node (Figure 2.8). The IAEA uses its own dedicated pressure sensor but has the option of using a non-invasive receiver/transmitter device installed on one of the operator's pressure gauges.

The time dependent enrichment is calculated in weight percent U-235 by relating the measured count rate in the NaI detector to the pressure and temperature dependent density. The measured count rate is based off net counts within a certain energy region of interest (ROI). The ROI can be varied between two settings about the 185.7 keV (57%) x-ray peak from U-235: one from 165 keV to 220 keV, and another from 120 keV to 220 keV. This second ROI is wider to include the 143.76 keV peak (11%) when one is attempting to maximize the number of counts measured.

The monitoring system itself is located on the high-pressure side of a unit header pipe, after the gas leaves the cascades, where there is a relatively strong gas signal. This position

upstream is also advantageous to the operators because there are fewer proprietary concerns compared to low-pressure portions of the plant [57]. The entire OLEM system is a network of collection nodes connected via a junction box for communication and backup power.

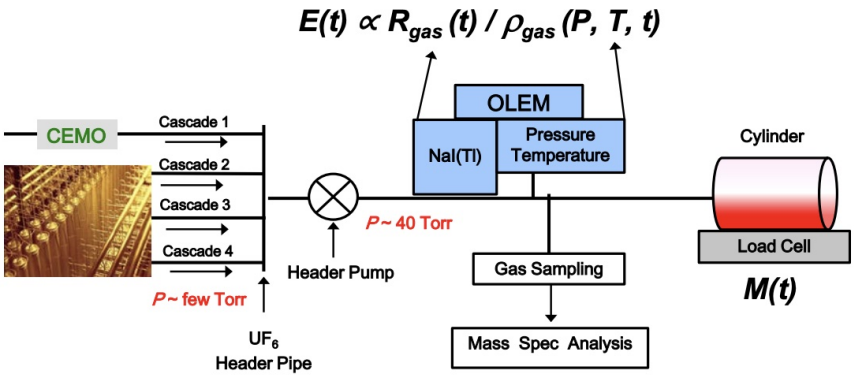

Figure 2.8: Schematic of an OLEM collection node

This work aims to use both radiation and non-radiation signals present within bulk handling facilities, to improve and develop novel near-real-time accountancy (NRTA) techniques which take advantage of existing and advanced radiation.

2.6 Structural Models and Fault Detection

The ability to detect and diagnose faults in a nuclear system is desirable not only from a safeguards standpoint but also for the operators themselves. Faults such as leaks or equipment malfunctions can result in accidents which can compromise the safety of the plant workers and the public [70]. Faults may lead to economic losses as well, stemming from the inability to recover material, the total downtime of the facility while tending to the fault, and costly retrofitting or redesigning of existing facilities to accommodate safeguards [6],[36],[19].

Fault diagnostic systems provide a valuable tool to use during the safeguards by design process to reduce the probability of adverse events from occurring. These systems employ physics-based models and measurement-based models to describe the facility's behavior. The physics-based models come from engineering designs and should describe the primary physics of interest in a prototypical system [77].

Measurement based models depend on the designer's choices, goals of the facility, and available measurement technology, and are essential in operations monitoring; without them, nothing grounds the physical models in reality. By leveraging the collective expertise of the various stakeholders in the system design process, a system of models can be created

to ultimately improve plant performance, reduce maintenance concerns, and communicate information about the facility's operation.

The aforementioned models can then be used to describe the system via a structural representation. This organizes the model's equations by the three types of parameters they contain: known variables, unknown variables, and faults. Inputs and measurements are the known variables. Unknown variables are values that change throughout operation that we do not directly control. Fault variables are used to quantify the off-normal behavior, such as nuclear material diversion or instrument malfunctions. A structured graph can be created, and then be transformed using the Dulmage-Mendelsohn (DM) decomposition [18].

The DM transformation is produced by proper and well-defined reordering of variables and equations into a sparse matrix M that appears as though it is in upper triangular form (Figure 2.9). This matrix is composed of three parts [94]:

- Structurally under-determined part M^-, where there are fewer equations than unknowns
- Structurally just-determined part M^0, where the number of equations is equal to the number of unknowns
- Structurally over-determined part M^+, where there are more equations than unknowns

The structurally overdetermined part is of particular interest from a fault diagnosis perspective because there is redundancy that can be used to potentially determine the existence or magnitude of a fault in the system. For a fault f to be considered structurally detectable in a system matrix M then the equation containing the fault e_f must exist within the overdetermined region of the model ($e_f \in M^+$). Detectability does not imply that the specific fault causing the faulted behavior is known.

It is also important to note that a structurally detectable fault is not the same as a structurally isolable fault. A fault (f_i) is structurally isolable if it is described by an equation in an overdetermined set of equations that does not include any other fault descriptions (f_j) or has a distinct signature from other fault descriptions $e_{f_i} \in (M^+ \setminus e_{f_j})$. This means that if a fault causes other faults to occur, then those faults are not isolated. However, a fault may be isolable from some faults but not others. Full isolability for a fault is only achieved if that fault can always be individually identified when it occurs [70],[77],[88]. Full fault isolability for all faults in a system is the obvious desire for facility designers ("We know something is wrong, and I know what is wrong because nothing else looks like this").

Fault isolability matrices are a convenient tool to visual analyze a model's ability to detect and isolate faults. The Fault Diagnostics Toolbox (FDT) [24], a toolbox available in MATLAB and Python, generates isolability matrices, DM decomposition matrices, residual generators, and aids in the analysis and design of fault diagnosis systems. This work utilized just a few of the FDT capabilities to perform isolability analysis on two experimental aqueous loops, constructed to emulate the movement of bulk nuclear material in a generic bulk handling facility. The objective of the experimental loops was to show experimentally

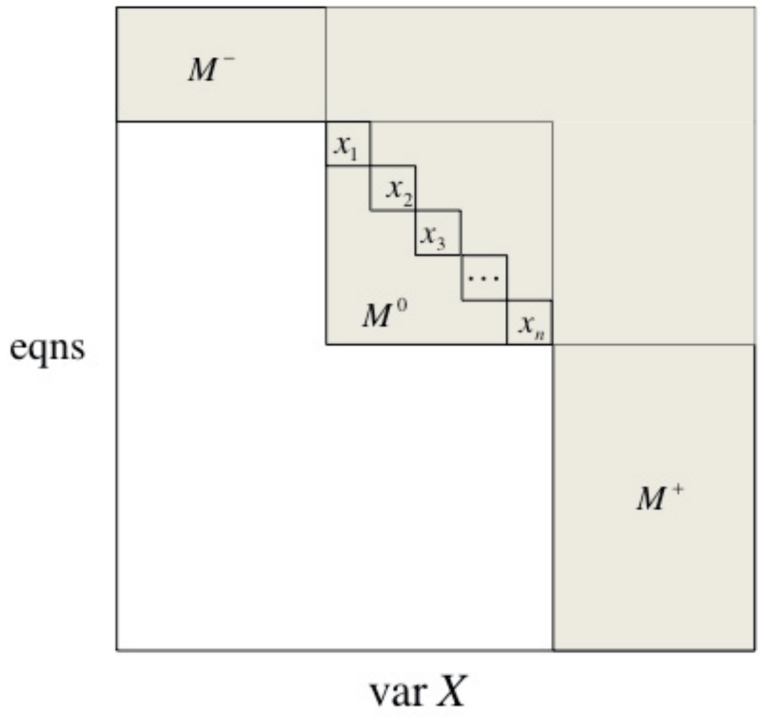

Figure 2.9: The Dulmage-Mendelsohn decomposition of a model [94]

how radiation signals and non-radiation signals can be combined to reduce measurement uncertainty and detect material holdup in bulk handling facilities by using fault detection analysis.

2.7 Simulations and Modeling

Proper system design will require predictive and confirmatory simulations of reprocessing and experimental facilities. Within aqueous reprocessing facilities, the sources are complex and extremely strong ($\sim 10^{17}$ Bq within a high activity liquid waste tank [82]), therefore robust computational methods are needed to achieve results reasonably fast. Analog Monte Carlo simulations can waste computational time by following "unimportant" particles or particles that do not interact in our detection system. To reduce computing time, advanced hybrid methods such as ADVANTG and CADIS are used. These variance reduction techniques generate coarse solutions to the adjoint flux equation and use the adjoint flux to create importance maps. Ultimately these maps can be used to weight certain regions in the model as less important than others and enable expedited MC calculations of quantities of interest with the desired statistical uncertainty and available computational resources [91].

Chapter 3

First Experimental Aqueous Reprocessing Loop

An initial and simplified closed-loop hydraulic system was constructed to leverage the existing radiation detection technology available in the Applied Nuclear Physics Program within the Department of Nuclear Engineering at UC Berkeley. The initial system aimed at modeling the movement of nuclear material between material balance areas in a commercial PUREX reprocessing plant, and simulated diversion from one or multiple areas.

3.1 Design

The simplified experimental aqueous reprocessing loop, modeled after existing reprocessing facilities such as the Rokkasho Reprocessing Plant (Japan) or Sellafield Thermal Oxide Reprocessing Plant (UK), was designed to simulate the five areas of interest in a commercial processing facility: 1) spent nuclear fuel storage, 2) dissolver tanks, 3) solid waste processing, 4) buffer tanks, and 5) the accountability tank. Because spent nuclear fuel is typically received as physical fuel assemblies after being cooled in a reactor pool, not yet chopped or dissolved, it was decided to remove that stage from the experimental loop since the focus is on the detection and quantification of aqueous solutions.

Thus, the first-generation reprocessing loop was simplified into four stages consisting of four 11.4 liter (3 gallon) PVC capacity tanks (Polyfab, Wilmington, MA, USA) to represent each stage, as well as a larger 114 liter (30-gallon) polyethylene plastic inventory tank (McMaster-Carr, Robbinsville, NJ, USA). Each of the four smaller tanks is situated progressively lower than the last to facilitate gravity-driven flow between them and for all fluid to ultimately drain to the 114 liter inventory tank. Once the radiotracer is injected into a given volume of water in the inventory tank, the radioactive mixture is circulated through a closed loop for at least 10 minutes, as shown in Figure 3.1. The mixture, discussed in more detail in the next section, is circulated through the system by an Iwaki magnet pump, Model MD-70RLZT, with a flow rate of 5.68 m^3 per hour (1500 gph) and a max head of 9.69

meters (31.8 feet). Not shown in Figure 3.1 is the unistrut structure constructed to support the weight of the tanks, radiation detectors, and lead shielding associated with each tank.

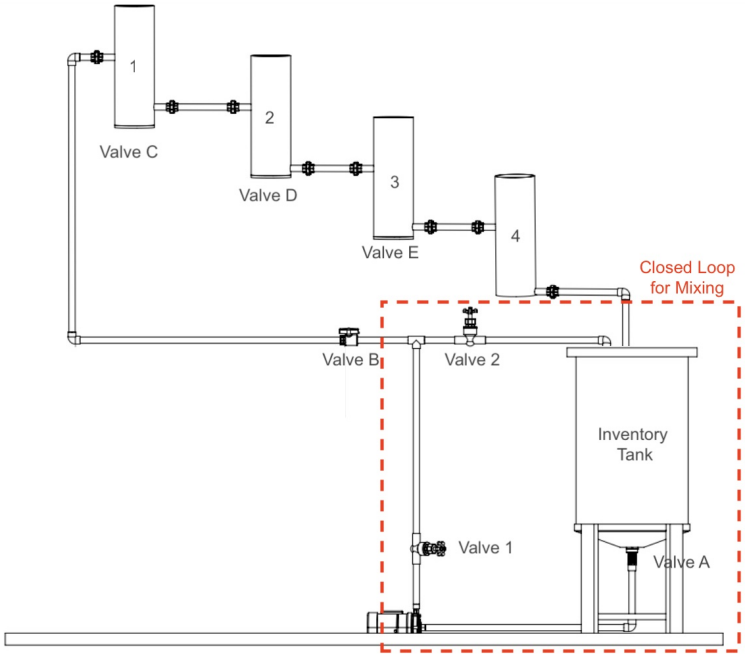

Figure 3.1: Engineering drawing of the experimental loop constructed in Solidworks 2018. Not shown is the flexible PVC tubing that is used to divert material from tanks 1, 2, and 3, which lead directly to the inventory tank

The inventory tank served multiple purposes: as a distributed background radiation source to represent the high radiation background present in bulk facilities, as a large reservoir to allow for the material to circulate continuously, as a basin to allow for the homogenous mixing of the radiotracer with the selected fluid prior to circulating it through the loop, and as a tank for all the fluid to drain into and be stored safely and in one place.

Each 11.4 liter tank is designed to hold a known amount of fluid once the pump is turned off based on the vertical positioning of the $\frac{3}{4}$-inch PVC outlet pipes that are used to connect each adjacent tank (5.7 L, 1.9 L, 3.8 L, and 0 L in tanks 1 through 4.) This was chosen to simulate a known amount of material holdup in the "facility" after processes have stopped. Material holdup and diversion may correspond to plant inefficiencies or faults such as blockages and leaks. They may also lead to unknown nuclear material streams, and it is therefore very important to understand if the plant is operating in a faulted regime [77].

3.1.1 Radiation Signals

In order to simulate both the aqueous and radioactive characteristics of dissolved spent fuel, water and a commercially available radiopharmaceutical tracer was used to form the

radioactive mixture circulated through the loop. Water was chosen as the solvent because it is readily available and does not produce mixed radioactive waste, which is more difficult and more expensive to dispose of [20]. The solute of choice was sodium pertechnetate, which contains the metastable isotope Tc-99m ($t_{1/2}$= 6.0067 hours). Tc-99m is the most commonly used radioisotope in medicine [41]. It is a pure gamma emitter with optimal photon energy (140.5 keV) – sufficient to penetrate the body, but not too large for efficient detection/protection, and has a half-life long enough to perform the investigation, with acceptable operator radiation dose. Additionally, sodium pertechnetate is relatively cheap, readily available, and completely dissolves in water making homogeneity less of a concern.

Four mechanically cooled p-type high purity germanium detectors manufactured by Ortec-Amtek (Oak Ridge, TN, USA) were selected for this experiment. These Individual Detector Modules or IDM-200 Vs was chosen for their portability (7.7 kg), sensitivity to gamma rays within the energy range of interest ($<$ 3 MeV), and energy resolution ($\leq$ 1400 eV at 122 keV and $\leq$ 2.3 keV at 1332 keV) [67]. Each detector was placed 40 cm away from the center of each tank and served as energy-sensitive gamma radiation monitors to observe any fluctuations in radioactive material present within each tank (Figure 3.2a). Figure 3.2b shows the location and orientation of the two 8" $\times$ 4" $\times$ 2" lead bricks placed in front of each of the four detectors. These lead bricks serve to reduce the amount of radiation incident on the detector face originating from the inventory tank and adjacent tanks.

The spectroscopic data collected from each IDM is processed through a multi-channel analyzer (MCA), GammaVision-32, and plots the counts detected as a function of energy during a specific acquisition time. A Gaussian model is fit to the 140.5 keV energy peak within the background subtracted spectroscopic data. The count rate within this peak ($\pm$ 1.5σ) was then summed to obtain the total count rate of Tc-99m in each tank during each operating scenario.

3.1.2 Non-Radiation Signals

Many of the non-radiation signals mentioned in the introduction, such as temperature and pressure, will not be relevant for this experimental loop since it does not contain molten salts or aqueous/organic solutions with fission products, nor does it rely on heat transfer mechanisms where these signals would be of high value to us. Thus, the primary non-radiation signals that were recorded were the tank volumes for each run, and the flow rate going into the first tank.

The tank volumes were obtained by visually inspecting each tank and estimating the volume based on the 100 mL increments on the graduated cylindrical tank. A similar method was used with the analog flow rate meter, to determine the flow rate into tank 1 in liters per minute (LPM).

The flow rate was controlled using two gate valves in the experimental loop (valve 1 and valve B) to control the flow of fluid into the first tank so that some of it recirculates back into the inventory tank to reduce the flow into the first tank. A closed loop for mixing was also implemented to ensure homogenous mixing inside the fluid. With valves 1 and 2

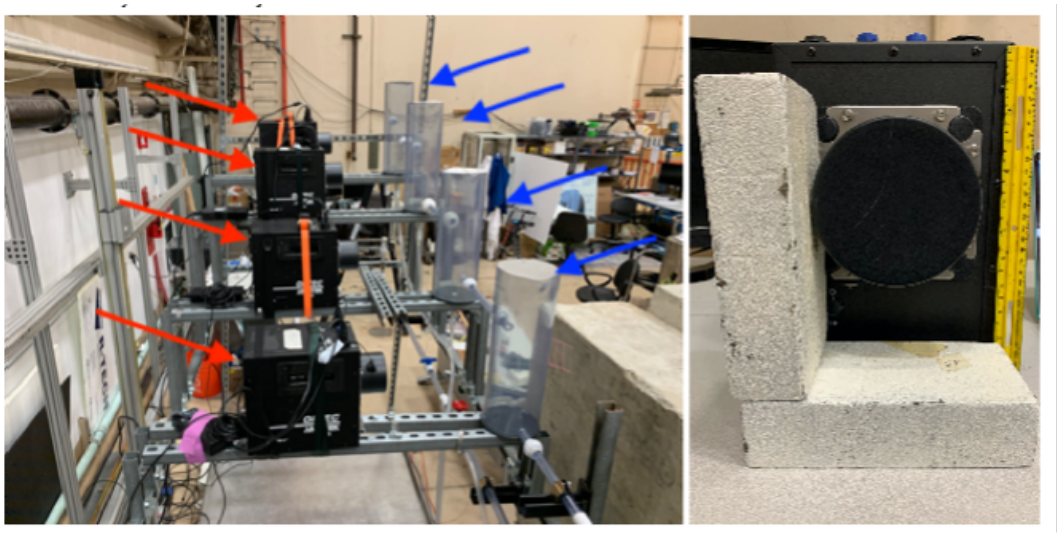

Figure 3.2: a) A side view of the experimental loop and where the corresponding mechanically cooled HPGe detectors indicated by the red arrows were placed. Each detector is suspended on the same scaffolding as the tanks themselves (indicated with the blue arrows) and are placed so that the center of the tank is 40 cm from the center of each tank. b) A front view of the 85 mm × 30 mm HPGe Detector and the two lead bricks placed to the left of the detector face and underneath to reduce the signals incident on the detectors from the inventory tank, which is located lower and to the left of the loop when facing it

partially open, valve A completely open and valve B closed, the radiotracer is injected into the inventory tank; the pump is then turned on and the tracer circulates for 10 minutes inside the closed loop for mixing indicated by the red dashed box in Figure 3.1. Once this has happened the mixture is assumed to be homogenous, and different operating scenarios were conducted. In this work, scenarios involving the loss of material are generally referred to as diversion scenarios, but may also represent leaks and faults in the system.

3.1.3 Operating Scenarios

The experimental loop was designed to operate in multiple steady state (SS) regimes, defined by two parameters: the type of diversion occurring (if at all) and the flow rate (in liters per minute) entering tank 1. Diversion from this loop is always protracted [34] and characterized by the opening of the ball valves located at the bottom of tanks 1, 2, and 3. These $\frac{1}{2}$ inch ball valves are connected to flexible tubing that leads back to the large inventory tank. When diverting, the ball valves are fully open; future experiments will explore the effect of partially opening diversion valves. Figure 3.3 illustrates the difference between SS operation (a), and SS operation while fluid is being diverted from tank 1 simultaneously (b).

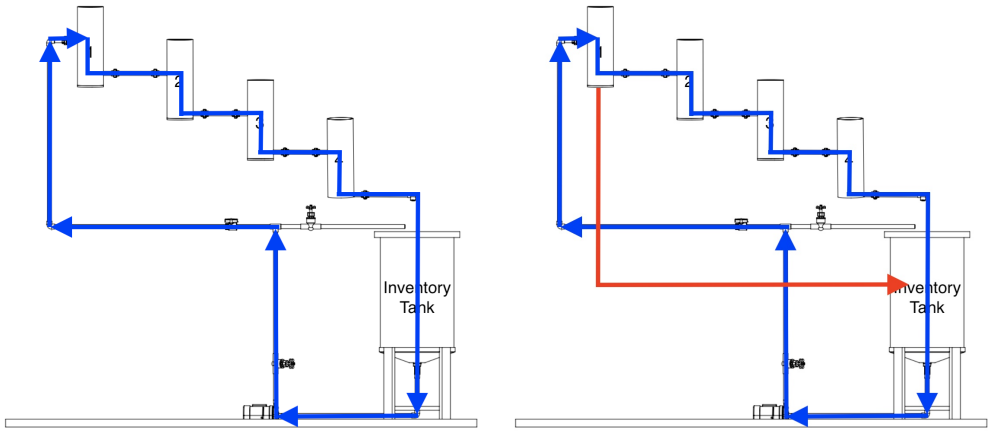

Figure 3.3: A visual representation of steady state operation of the loop shown on the left. On the right shows how various diversion scenarios occur when valves C, D, or E (Figure 3.1) are opened, and fluid is diverted straight to the inventory tank by flexible PVC pipe not shown in the image but represented by the red line

For each scenario of the following seven scenarios, four gamma spectra can be collected, one from each HPGe detector which is associated with an individual tank, each positioned 40 cm from center of the tank to the detector face. The system was configured so that during each scenario the quantities of material in each tank were constant for the duration of the measurement. This mode of operation is referred to as steady-state or SS.

Scenario 1: SS, 15.1 LPM

Scenario 2: SS, 15.1 LPM, Divert from Tank 1

Scenario 3: SS, 15.1 LPM, Divert from Tank 2

Scenario 4: SS, 15.1 LPM, Divert from Tank 3

Scenario 5: SS, 15.1 LPM, Divert from Tank 1 & 2

Scenario 6: SS, 15.1 LPM, Divert from Tank 1 & 3

Scenario 7: SS, 15.1 LPM, Divert from Tank 2 & 3

These seven scenarios were then repeated at a flow rate of 18.9 LPM, resulting in a total of 14 scenarios conducted, at 2 different flow rates, and 112 total gamma spectra collected. These spectra were then background subtracted, and time corrected back to the calibration time in order to compare quantities. Additionally, the flow rate and the heights of fluid in each 11.4-Liter tank were recorded.

3.2 Preliminary Benchmarking

In order to ensure the accuracy of the radiation transport methods employed later in this study, an MCNP model was constructed of the experimental loop and its surrounding environment. Using check sources such as a Ba-133 point source to determine each detector's efficiency, the MCNP model was coupled to the radiation detectors' response.

Figures 3.4 and 3.5 are images of the MCNP model in Vised. The rectangular boxes located near the cylindrical intermediate tanks in Figure 3.4 are the high purity germanium gamma-ray detectors used to collect spectroscopic data. For simplicity, these detectors are modeled as solid germanium with a sensitive volume of p-type high purity germanium (with dimensions: 85 mm diameter $\times$ 30 mm nominal length). A dead layer was added on the outside of the detector volume to represent the impact of the electrical contact whose thickness can be adjusted to optimize the agreement between measurements and simulations. All the mechanical and electronic components, particularly the mechanical cooler of the IDM from ORTEC was represented as a block of aluminum in the back of the detector. The large cement blocks (shown in light gray) near the large inventory tank are present in the actual experimental area, and act as radiation shield for the operators and any personnel in the surrounding area. Finally, the largest purple block is a modular room which serves as office space for employees; it was included in the model to account for dosage to individuals working in that area.

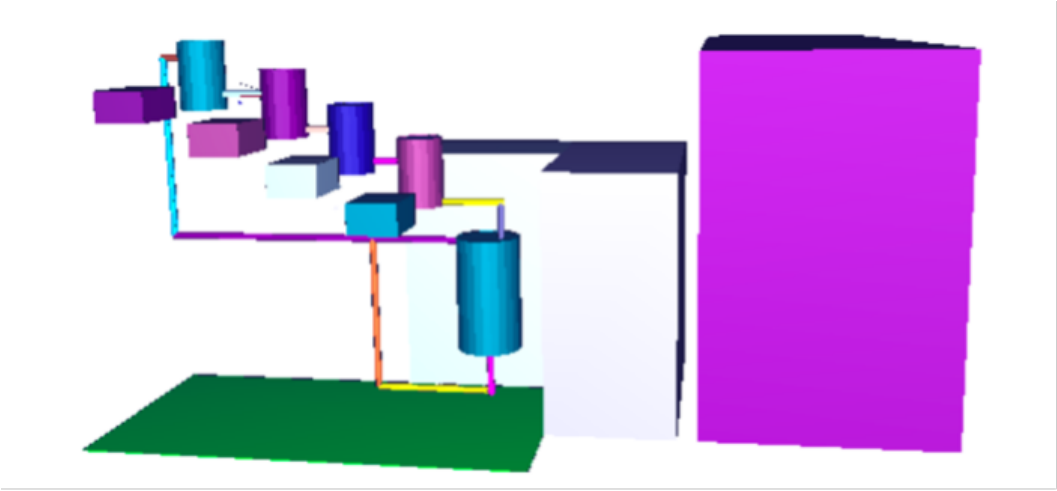

Figure 3.4: 3D Vised geometry of experimental loop and surrounding area. Tanks are represented by simple cylinders made of PVC, detectors are modeled as blocks of aluminum with a cylindrical sensitive volume (not visible from this angle) of high purity germanium in front. Also shown is the steel drip tray (dark green) machined to reduce contamination in the event of a spill, the large cement blocks (gray) used to reduce dose to personnel, and the modular room (purple) nearby

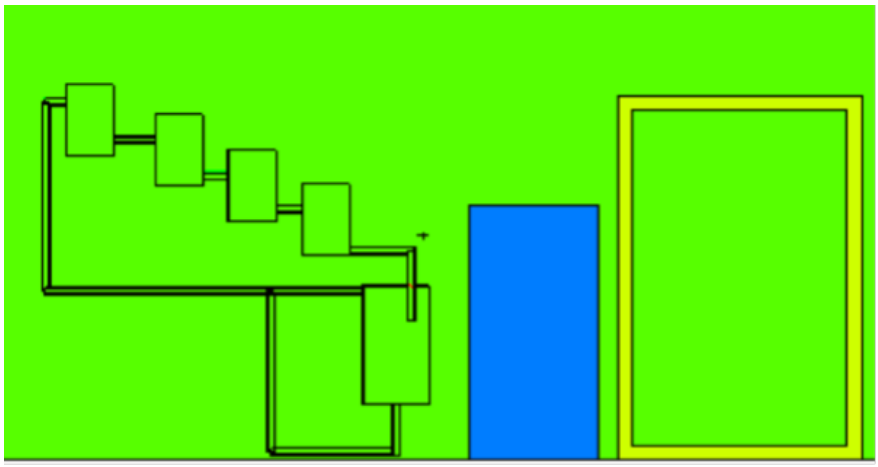

Figure 3.5: 2D Vised geometry of experimental loop and surrounding area. The four smaller tanks and larger inventory tank are visible in addition to the cement blocks (blue) and modular room (yellow) filled with air

To benchmark this model, the Ba-133 check source was placed inside of an empty tank, 12.7 cm (5 inches) above the center of an 11.4 L tank (Figure 3.6) while gamma spectra were collected using all four detectors. Then the check source was moved to an adjacent 11.4 L tank and four more gamma spectra were collected. this process was repeated for all four 11.4 L tanks, resulting in a total of 16 spectra collected.

The MCNP simulations results show good agreement with the trends expected to be observed in this experimental loop. Figures 3.7 and 3.8 demonstrate the agreement with the experimentally collected data across the entire energy range (0 to 400 keV) and specifically at the most intense full energy peak for Ba-133 (356 keV, 62%) and the highest energy of 383 keV (8.9%). Background measurements were performed separately without any radioactive sources present, and the resulting background spectra were subtracted from the spectra collected with the Ba-133 source present. All spectra were corrected for dead-time and expressed in net count rates.

As it can be seen in Figures 3.7 and 3.8 and in Tables 3.1 and 3.2, the MCNP simulations are able to reproduce experimental spectra fairly well. When the detector is closest to the source (e.g.the count rate in detector 1 when the source is in the tank 1), the MCNP simulations systematically overestimate the counts in the photopeak by about 10%. This is excluding detector 4; Detector 4 in this experiment exhibited degraded energy resolution compared to the other HPGe detectors, which is particularly visible in the fourth subplots of both Figures 3.7 and 3.8. This was determined to be due to a malfunctioning vacuum pump; subsequent experiments will use a different detector with improved resolution and performance.

Figure 3.7 and Table 3.1 illustrate that the spectral shape and counts between 0 and

400 keV are reproduced in MCNP for the detectors closest to the source very well. This agreement was achieved by adjusting the dead layer in the Ge detectors to be 1 mm which is not uncommon for such detectors. The features around 30 keV observed in the measurements are associated with x-rays emitted in the decay of Ba which were not simulated in MCNP.

The count rates in the detectors which are not the closest in the measurements — corresponding to the off-diagonal values — deviate significantly. This can be potentially attributed to uncertainties in the relative locations and materials surrounding the detectors as well as the statistical uncertainties in the background subtracted spectra. This is not of significant concern since each detector will only be used to estimate the count rate in its corresponding tank, not adjacent ones. In addition, future experiments will include more collimation making reducing the counts incident on the each detector from adjacent tanks.

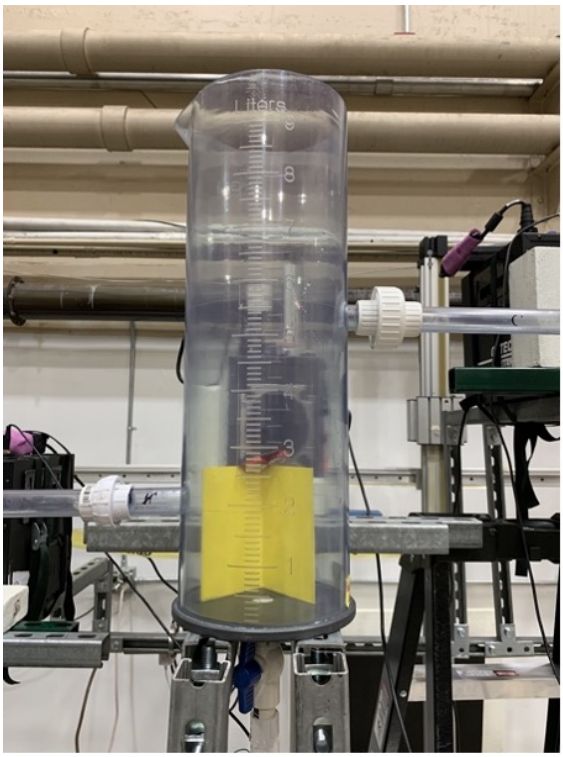

Figure 3.6: A Ba-133 point source suspended inside of an empty 11.4 L PVC tank in front of detector 2

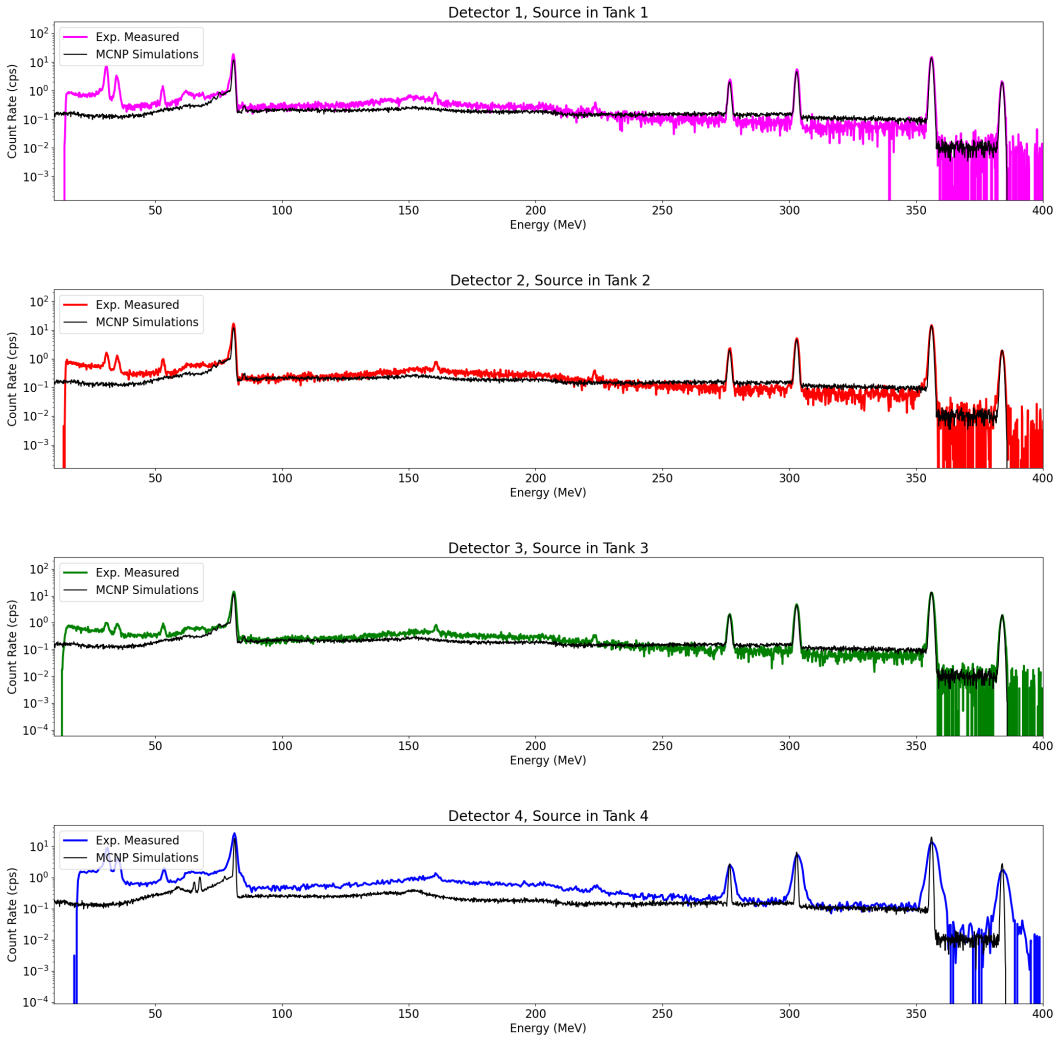

Figure 3.7: A comparison of four MCNP generated gamma spectra about the 356 keV Barium-133 gamma-line to four background-subtracted spectra collected using the experimental loop set up from 0 to 400 keV. The MCNP data is shown in the black on each of the subplots

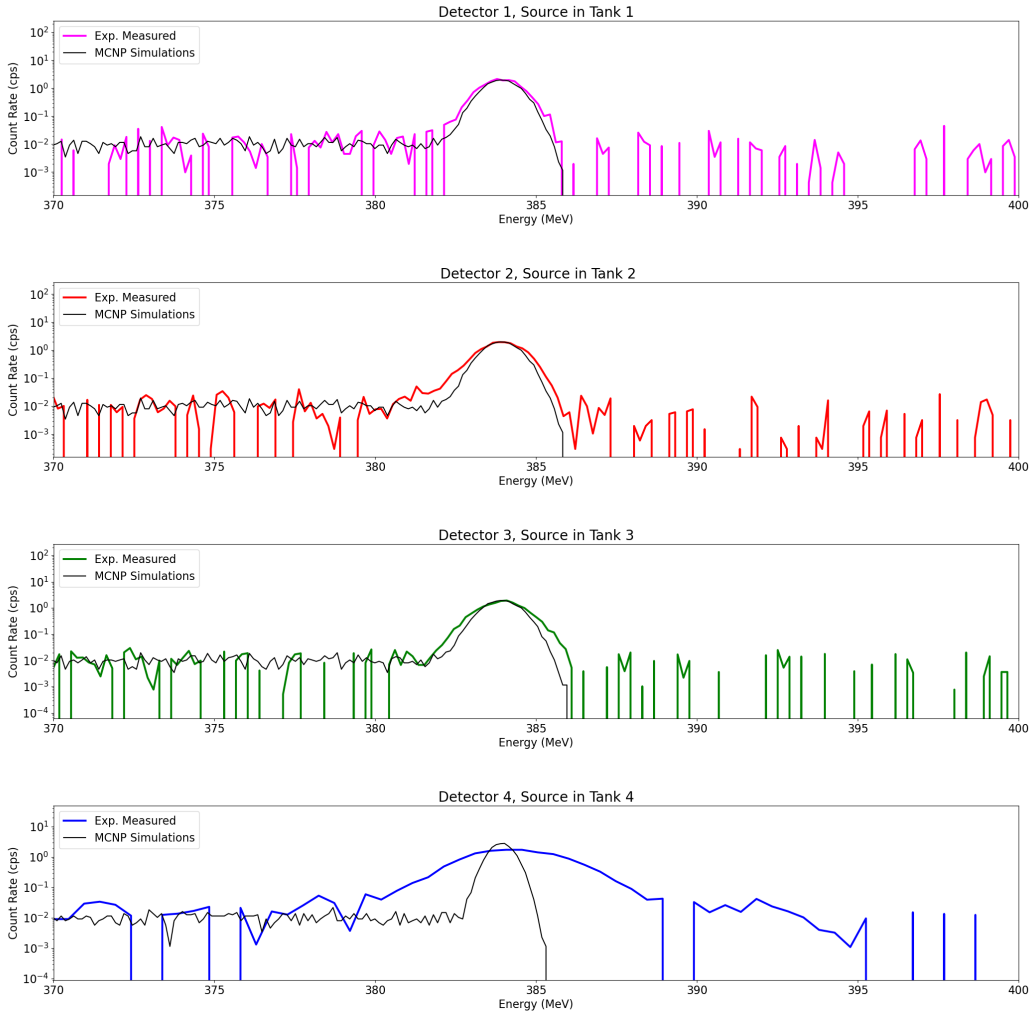

Figure 3.8: A comparison of four MCNP generated gamma spectra about the 356 keV Barium-133 gamma-line to four background-subtracted spectra collected using the experimental loop set up from 340 to 370 keV. The MCNP data is shown in the black on each of the subplots

	Detector 1	**Detector 2**	**Detector 3**	**Detector 4**
Tank 1	**1.16 ± 0.07**	0.03 ± 0.01	1.06 ± 0.13	0.09 ± 0.05
Tank 2	0.40 ± 0.07	**1.00 ± 0.07**	0.55 ± 0.05	1.25 ± 0.15
Tank 3	8.98 ± 0.89	0.47 ± 0.06	**1.00 ± 0.06**	0.05 ± 0.01
Tank 4	2.60 ± 0.70	5.50 ± 0.56	0.24 ± 0.04	**0.79 ± 0.05**

Table 3.1: A comparison of the ratios of net count rates across the entire energy spectrum (0-400 keV) observed experimentally over the net count rate determined in the MCNP simulations

	Detector 1	**Detector 2**	**Detector 3**	**Detector 4**
Tank 1	**0.89 ± 0.08**	0.0003 ± 0.001	1.06 ± 0.18	0.04 ± 0.05
Tank 2	0.35 ± 0.08	**0.86 ± 0.08**	0.53 ± 0.07	1.52 ± 0.22
Tank 3	25.13 ± 3.33	0.41 ± 0.07	**0.88 ± 0.08**	0.01 ± 0.01
Tank 4	84.52 ± 29.6	14.54 ± 1.94	0.21 ± 0.05	**0.70 ± 0.06**

Table 3.2: A comparison of the ratio of count rates inside the Ba-133 full energy peak (356 keV ± 2σ) observed experimentally over those seen in the MCNP simulations

3.3 Results

To investigate the sensitivity and specificity in the detection and quantification of holdup and diversion in a bulk handling facility, a closed-loop hydraulic system (Figure 3.1) was constructed using PVC and unistrut. Water and the commercially available radioisotope Tc-99m were used simulate bulk nuclear material which moves from one process area to the next within a generic PUREX reprocessing facility, represented by four smaller cylindrical tanks and one large inventory tank. This experiment serves to guide the development of sufficient detection limits and quantification capabilities for the ultimate goal of safeguarding bulk handling facilities.

Cardinal Health delivered a 3 cc (15 mCi) syringe of sodium pertechnetate, calibrated for 12:00 pm on the day of the experiment. Due to the short half-life of Tc-99m (6.0067 hours), within an hour of the syringe being received, it was removed from the lead-lined shipping container and completely emptied into the inventory tank and permitted to mix within the closed mixing loop for ten minutes.

3.3.1 Measured Volume and Count Rate

As the volume of fluid inside each tank increases, so should the number of counts detected in each tank. Figure 3.9 plots the total count rate within the 140.5 keV full energy peak registered for each detector as a function of the volume measured in tanks 1, 2, and 3. The expected positive correlation between those two values is observed. Had the detectors been sufficiently collimated so that only the corresponding tank is in the detector field of view, one would expect that the lines for all three detectors should overlap. Meaning, that for a specified volume in the same sized tanks with properly calibrated detectors, one should observe the same count rate. This was not observed due to minimal collimation being used. More care should be taken for future experiments to ensure better and more efficient use of the available collimation to preserve the structural integrity of the loop while reducing the cross talk between radiation detectors.

During the experiment the level of fluid in tank 4 was observed to vary greatly in somewhat of an oscillatory manner, resulting in large uncertainties associated with the estimated volume in that tank for each steady state measurement scenario. This behavior was determined to be a result of the turbulent flow of fluid out that tank, which allowed air bubbles into the pipe that drained fluid from tank 4 into the inventory tank. This outlet pipe had been designed to be below the fluid surface to prevent splashing and radioactive contamination of the experimental lab space. However due to the accumulation of air bubbles in the pipe itself, the volume in tank 4 needed to fill to a certain amount to overcome the pressure from the accumulated air bubbles in order to force fluid from tank 4 into the inventory tank.

This resulted in a periodic increase in volume in tank 4 followed by a rapid decrease in volume due to the rapid draining of fluid into the inventory tank. This preliminary loop experiment only measured steady state volumes in tanks, and because this oscillatory behavior could not be captured in the time-independent measurements collected, the data collected

from detector 4, positioned directly in front of tank 4, is omitted from the subsequent discussion.

Comparisons can be made between the measured volume in tanks 1-3 and the calculated volume in that tank using the linear regression model fitted to the data in Figure 3.9. When computing the calculated volume, care must be taken to ensure uncertainties are propagated not only from the count rate value itself, but also the uncertainties in the model. The results are shown in Figure 3.10a.

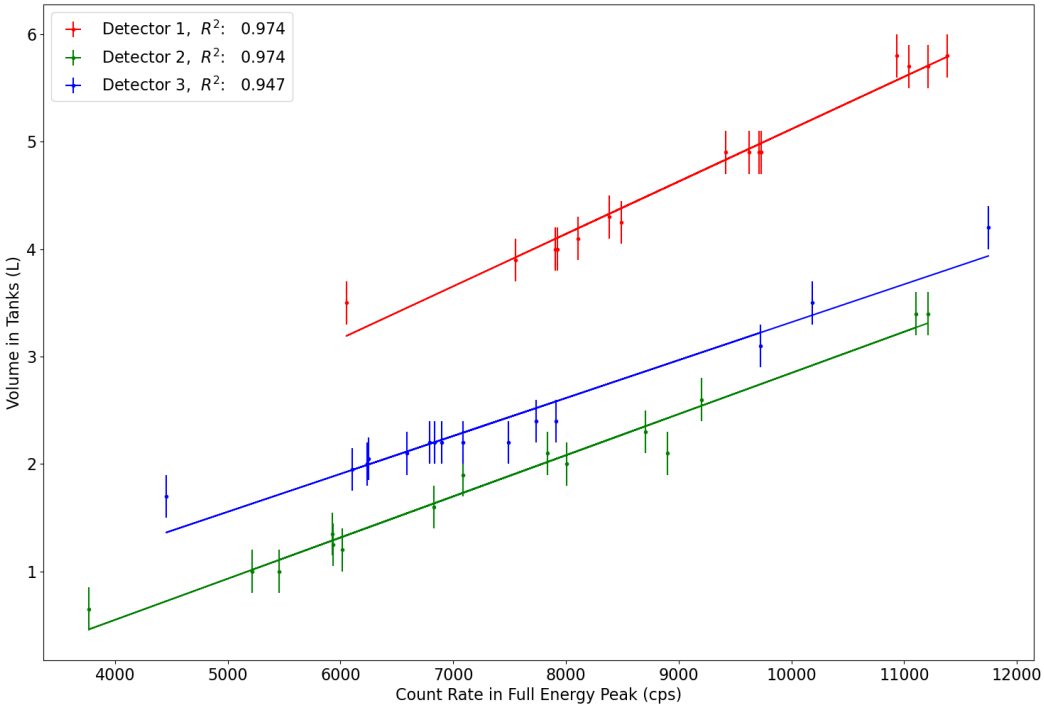

Figure 3.9: The net count rates in the 140.5 keV peak observed detectors 1, 2, and 3 which were placed in front of tanks 1, 2, and 3 respectively is plotted against the volume measured in each tank in each of the operating scenarios

If the calculated volume value for each tank/scenario was equal to the measured value, then the points would line on the diagonal. Figure 3.10b takes another approach to comparing these values by plotting the residual (observed - expected)/(expected) as a percent for each data point. The mean residual value was 0.2% with a standard deviation of 6.3%. This shows decent agreement, however with improved collimation/detector geometry and more precise measurements of volume better agreement could be obtained from future experiments.

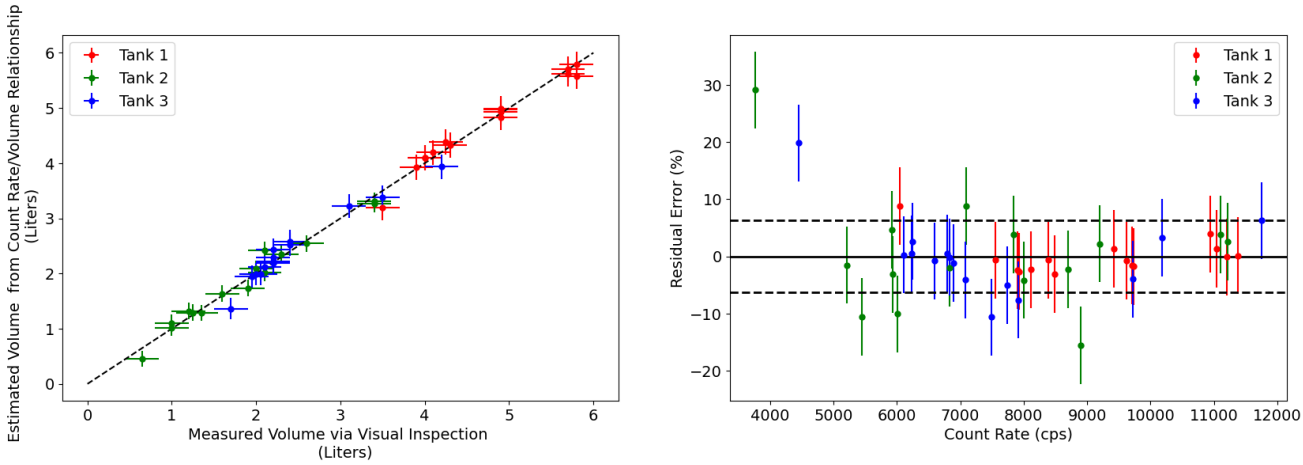

Figure 3.10: a) Using the linear regression model which relates count rate in the 140.5 keV peak at each detector to volume of material in each tank, the explicitly measured volume is plotted against the estimated volume based upon each regression model for each tank. b) The detected count rate is plotted as a function of the residual error (%). The residual error of the calculated volume of the tank (which is a function of count rate) compared to the measured value of the tank. The horizontal solid and dashed lines represent the mean and standard deviations respectively of the residual distribution: 0.02% ± 6.3%

3.3.2 Diversion Scenarios

The volume of radioactive fluid in each tank for each of the seven scenarios, at the two different flow rates, was plotted on top of one another (Figure 3.11). The uncertainties in these values were estimated to be ± 100 mL based on the tank increments. The shapes of the trend lines are similar when comparing each tank value to its flow rate complement, however it is clear that changing the flow rate does alter the volume observed in each tanks as well as the shape of the volume vs scenario curve.

Figure 3.12 overlays the volume data in each tank from both flow rates (15.1 LPM and 18.9 LPM) on the same plot. The observed count rate or the calculated volume from that count rate could have also been plotted but would show similar results since they only differ by a constant. Figure 3.13 presents the volume at a given flow rate for each diversion scenario relative to the volume observed at the same flow rate during steady state operation without any diversion occuring. For example, the volume registered in tank 1 at 15.1 LPM when material is being diverted from tank 1 is divided by the volume obtained in tank 1 at 15.1 LPM when no material is being diverted from any tank, and is indicated by the red circular marker. While a red triangular marker represents the same ratio but at a higher flow rate of 18.9 LPM. The dashed dotted line at unity represents when the volume at a certain flow rate during a diversion scenario is equal to the volume at the same flow rate without diversion (SS, no diversion).

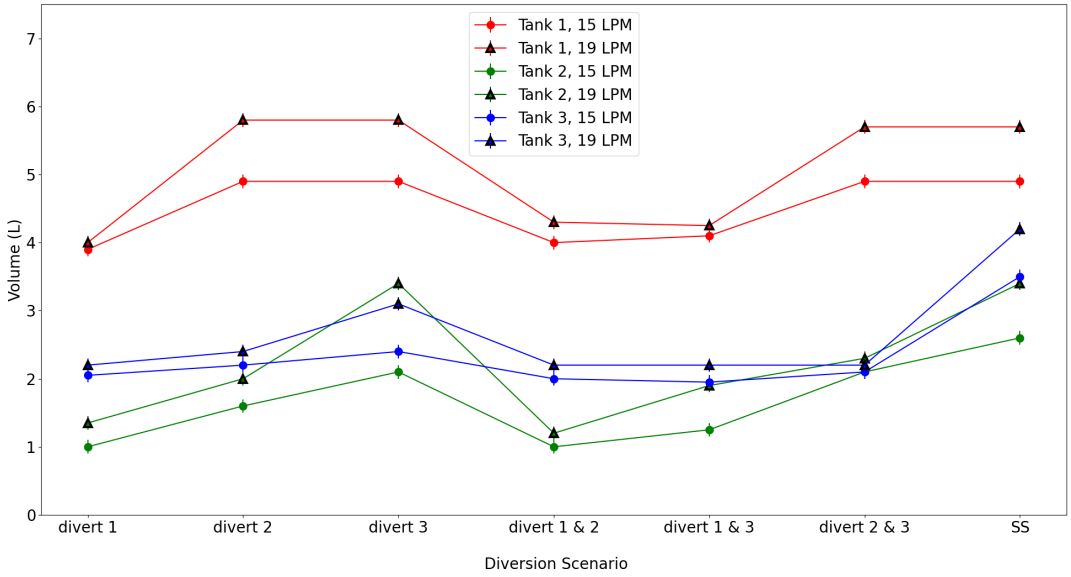

Figure 3.11: The volume in each tank is plotted as function of the scenario. The circle markers represent volumes at a flow rate of 15.1 liters per minute. The triangular markers represent the volumes measured during the same seven scenarios but at a flow rate of 18.9 liters per minute

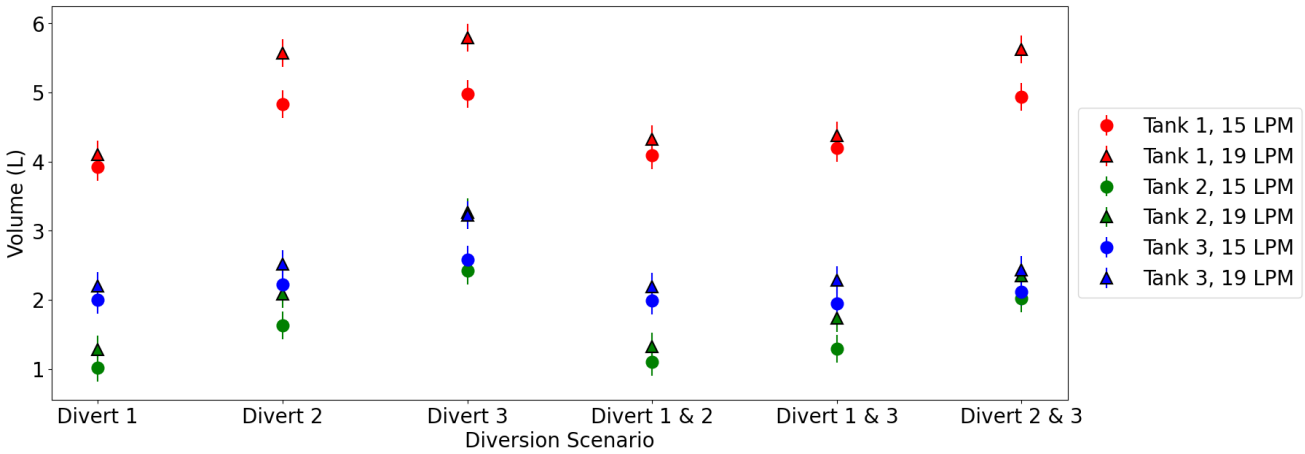

Figure 3.12: The measured volume in each tank is plotted for each of the six diversion scenarios at two flow rates: 15.1 LPM (circular markers) and 18.9 LPM (triangular marker)

For tank 1 (shown in red), when material is diverted from tank 2, tank 3, or both tanks 2 and 3 (divert 2, divert 3, divert 2 & 3) the volume ratio appears to stay relatively close to unity (Figure 3.13). Similarly, when material is diverted from tank 3 (divert 3), the volume in tank 2 (shown in green), remains near its steady state value, but this relationship

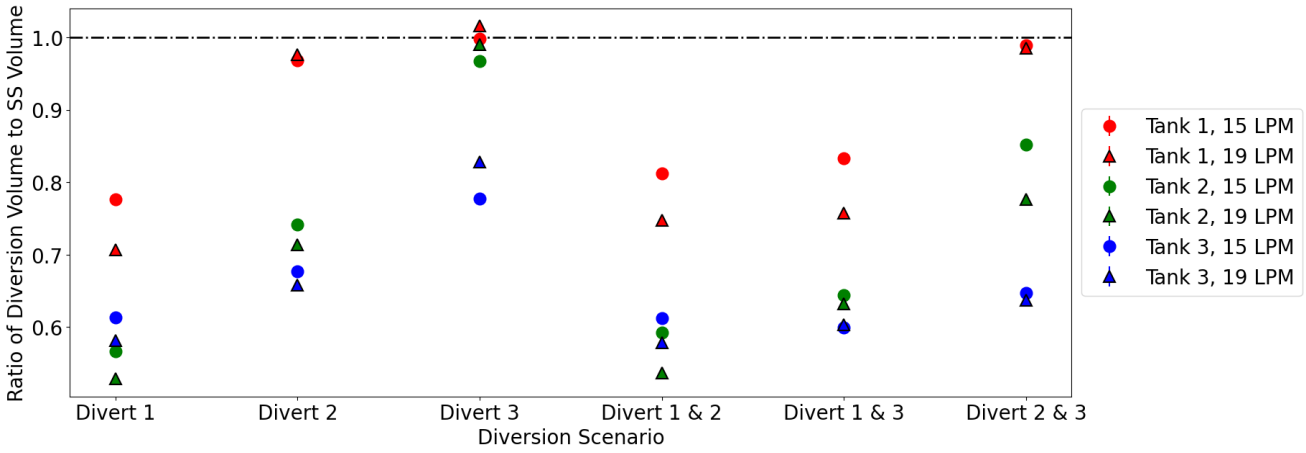

Figure 3.13: The ratio of the measured volume in each tank at a certain diversion scenario over the measured volume during steady state operation at the same flow rate is plotted for each of the six diversion scenarios at two flow rates: 15.1 LPM (circular markers) and 18.9 LPM (triangular marker)

does not hold for diversion from tanks 1 & 3, or 2 & 3. It appears that when diversion happens downstream from a tank, but not including the tank itself then its volume (and its corresponding measured count rate) will stay near the steady state value. This confirms our intuition that the count rate for a tank would not be affected by downstream diversion. Further research is needed into the fluid dynamics of this system to understand the remaining tank behavior. If downstream effects propagate, then that might explain why all values for tank 3 remain distant from their steady state without diversion complements.

This data provides useful information related to the relationships between volume and count rate measurements when the source is distributed. When using the count rates registered in the high purity germanium detector to calculate the volume inside a tank, 95% of the time those measurements fell within ± 13% of the actual measured volume value. Future experiments should explore this relationship further and utilize more precise instrumentation for measuring the non-radiation signals so that more certainty can be gained from those values. In fact, with the additional instrumentation planned to be installed within the next generation loop (e.g. more measurement points for flow rate and more precise fluid level sensors) these values can then be used to draw more precise conclusions on detection limits of diversion.

3.3.3 Fault Detection

In this experiment we measured nine signals directly: the height of all four tanks, the count rate in the 140.5 keV Tc-99m peak in each of the four detectors, and the flow rate into tank 1 (q_1). Faults were defined as malfunctions in instrumentation or as discrepancies in

quantities that are supposed to be preserved such as the total volume in the system. The 13 faults variables which were included in the structural model were faults of the flow rate going into tanks 1-4 (fQ_i), faults in the count rate recorded in each tank (fCR_i), faults in the volume measured in each tank (fV_i), and a fault in the estimated total volume in the system (fV_{tot}).

The resulting structural representation of this loop is illustrated in Figure 3.14. This was generated using the Fault Diagnostics Toolbox and is a graphical representation of the all known equations used to model the loop. The full numbered list of equations can be found in Appendix A. Equation numbers are listed in descending order along the y-axis. The three types of values listed along the x-axis are variables, faults, and measured signals. A dot is placed in a specific position if the variable in x appears in that equation y. Variables are shown in blue and include for example the volume in each tank (V_i). Differentiated or integrated variables are denoted by a blue "D" or blue "I". Fault variables are shown in red, and measured signals are marked in black.

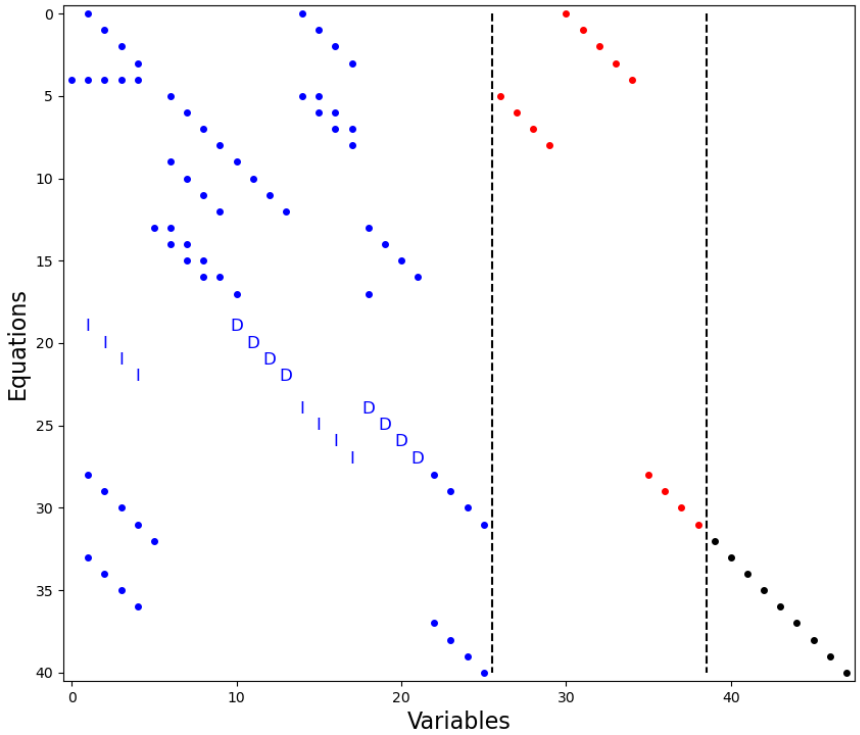

Figure 3.14: Structural model of the first generation loop

The structural model can then be manipulated in such a way to produce the Dulmage-Mendelsohn Decomposition matrix. In this specific example the equations create both a just-determined (no. of equations = no. of variables) and over-determined (no. of equations > no. of variables) system. These correspond to the two sub matrices which are separated

by blue boxes along the diagonal of the matrix shown in Figure 3.15. The matrix in the lower right hand corner is the over-determined portion, which can be further organized into equivalence classes. These can be thought of as sets of equations for which every constituent equation is necessary to make a set of equations that is over determined. Equivalence classes of equations are indicated by the gray squares in the plot. Faults may be overdetermined using just one equation, and therefore the equivalence class consists of just one equation and appears as a red dashed line through that specific equation. Red dotted lines indicate which equation a given fault will affect.

In order for a fault to be isolable there must only be one fault in each equivalence class. If multiple faults cross through the same gray square, it means these faults are not distinguishable from each other. Ideally faults should be completely isolable because there would be a unique response in the case of each fault. For example, our response to a fault in the height of a fluid might differ from a response to a fault in a flow rate meter. If a fault doesn't appear in an portion of the over-determined part of the matrix, including the just-determined region, it is deemed not detectable.

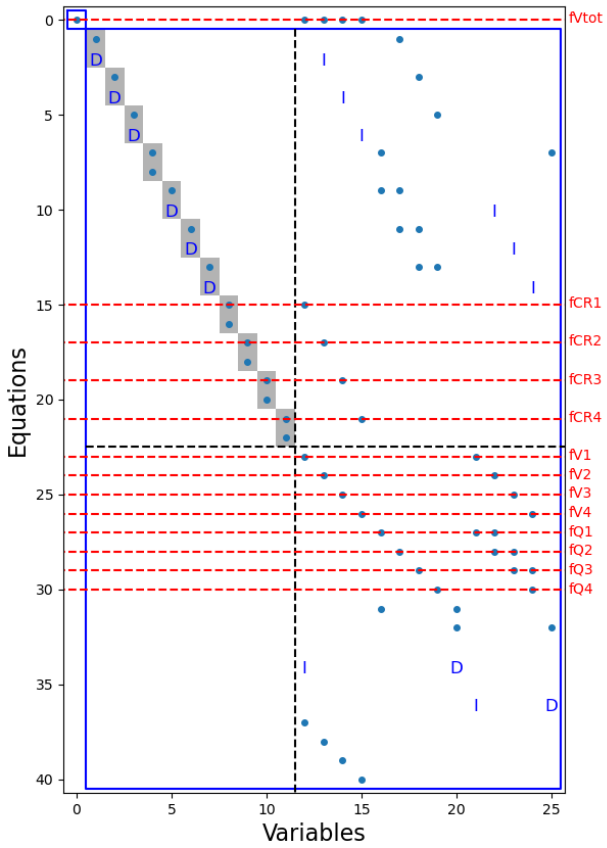

Figure 3.15: The Dulmage-Mendelsohn decomposition for the first generation loop

To further understand this concept, we look to Figure 3.16 which illustrates the degree of isolability of this loop. The x axis and y axis represent different faults occurring. Here, a blue dot in position (i, j) indicates, that fault i will occur if fault j is present. Based off the isolability matrix, if a fault occurs in the total volume of the system, no other faults should appear. But if any other fault occurs in the system then those faults cannot be distinguished from a fault in the total volume. This is how undetectable faults appear in an isolability matrix, with that undetectable fault being able to occur and for it to not be able to be isolated from any other fault.

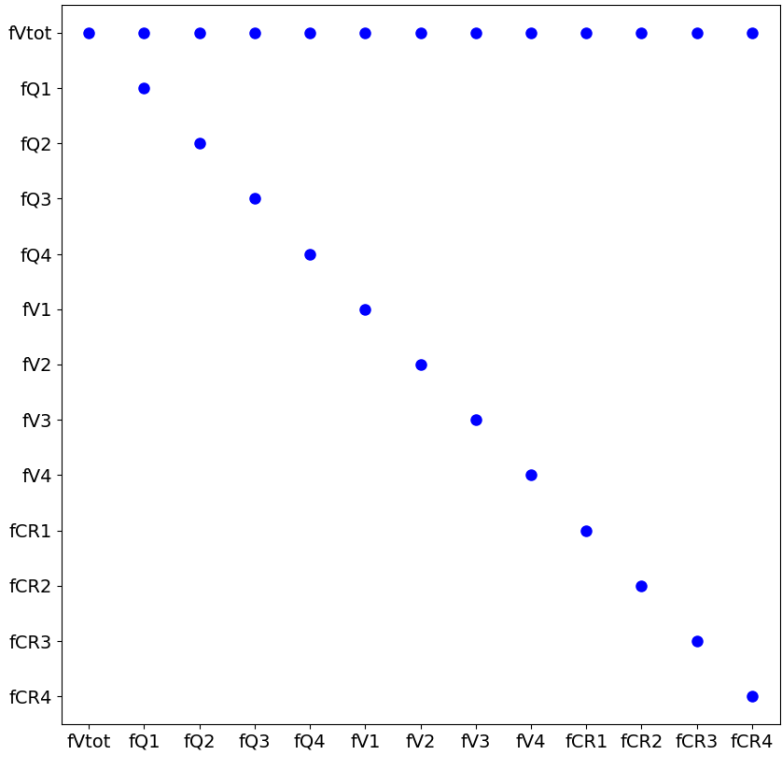

Figure 3.16: The corresponding isolability matrix for the first generation loop

This lack of detectability of a fault in the total volume makes sense given the construction of this specific system. No sensors are present to measure the volume in the inventory tank so there is never a way to explicitly verify the total amount of fluid in the system. For this loop iteration the loop designers were not concerned with total volume being removed from the system, especially since that would potentially result in radioactive contamination of the lab space. Even though any other fault is not able to be distinguished from a fault in the total volume in this system, by design if one fault does occur the operators in this case can be confident that that fault is not due to a loss of fluid volume.

The power of DM decomposition and isolability matrices is that the isolability of faults can be considered in the design process as opposed to post-construction of an experiment. If this loop were to be improved upon the additional measurement signals required can be explored prior to testing. In this case simply adding a device which measures the volume in the inventory tank would improve isolability and make all of the system's faults completely isolable. This is shown in Figures 3.17 and 3.18. The same 13 faults exist however an additional measurement signal (and corresponding equation) is added to the structural model. This results in full isolability. Now there is no longer a just-determined part of the system, and a new equivalence class is formed involving fV_{tot} making it both detectable and isolable. The isolability matrix confirms complete isolability of all faults. Now every defined fault that could appear in this system will always be identified as itself and only itself.

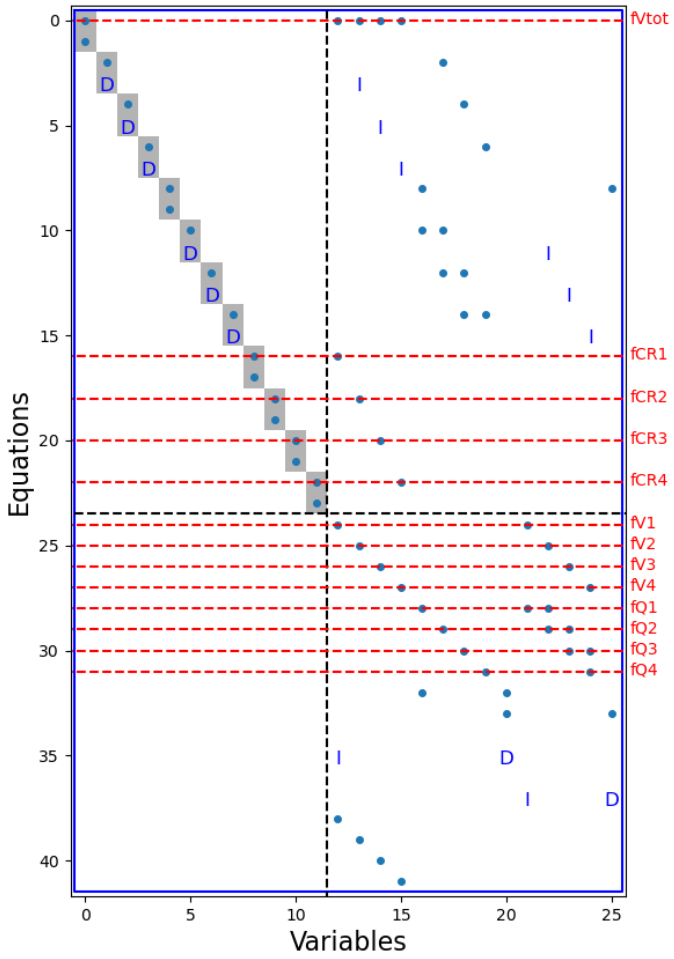

Figure 3.17: The revised DM decomposition matrix for the first generation loop, with the addition of a sensor to measure the volume in the inventory tank

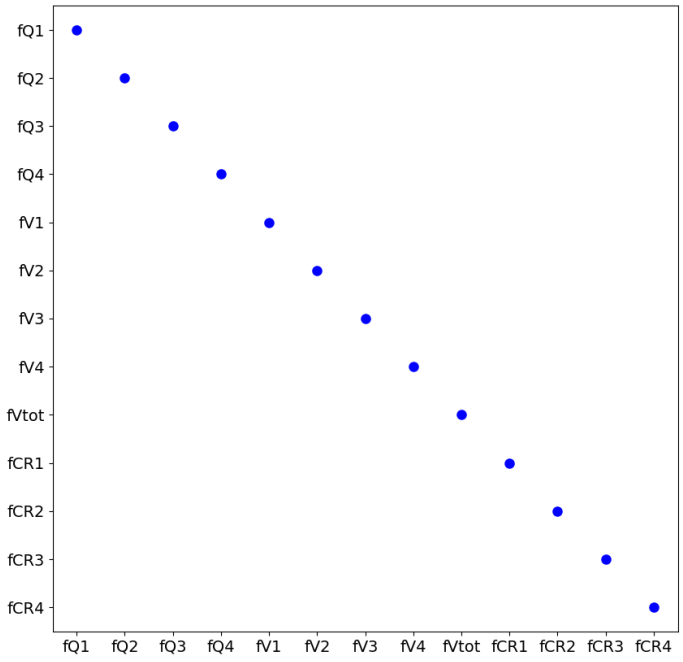

Figure 3.18: The revised isolability matrix for the first generation loop, with the addition of a sensor to measure the volume in the inventory tank

3.4 Conclusion

A simplified experimental aqueous reprocessing loop was constructed to investigate the ability of existing technology to detect and quantify diversion in a PUREX plant using both radiation and non-radiation signals. Using radiolabeled sodium pertechnetate (Tc-99m) dissolved in water, we were able to show preliminary results indicating the expected relationship: the larger the volume in an area, the higher the count rate observed within that area of interest. This loop proved to be a sufficient proof of concept for the ability to couple radiation transport simulations with experiments and of the strength of fault diagnostics, especially during the design process.

Future experiments conducted on this loop would benefit from more accurate and precise instrumentation. The flow rate meter and level height measurements proved to be the largest source of error. More precise level indicators and flow rate meters implemented at more locations in the loop will greatly reduce the uncertainties in measurements and allow for more precise estimation of faults. Additional signals may also be detected and measured

such as weight, pressure, temperature, etc.

Although the large activities present permitted the measurement time to be minimal (approximately 3 minutes), further work should be done to investigate diversion, both abrupt and protracted, and its relationship to acquisition/detection time. Additional shielding and collimation would also be useful for subsequent measurements. Currently, the detectors are seeing more of the "facility" than necessary and reducing their field of view and the background radiation incident on the detector should make the relationship between volume and count rate more certain and allow for higher precision estimates.

The design and construction of a second closed loop hydraulic system for simulating aqueous reprocessing facilities and other bulk handling facilities will be discussed in the next chapter. This system had fewer tanks, to better isolate and control the material inventory. Instead of focusing further on more accurately modeling a specific facility, since the facility designs can vary greatly, this loop will focus on further investigating the limits of measurement uncertainty and the fault detection models with greater accuracy. Additional sensors (flow rate meters and ultrasonic height level meters) with more precision will be implemented, as well as multiple radiotracers will be used simultaneously to simulate an even more complex radiation environment.

Chapter 4

The Next Generation Loop

The Next Generation Loop (NGL) is a second generation closed-loop hydraulic system. The NGL simulates the movement of nuclear material in a generic aqueous reprocessing facility using water and commercially available radiotracers. The NGL can operate in a variety of configurations and boasts control of individual process streams while employing both radiation and non-radiation sensors to observe and detect off-normal behavior.

4.1 Design

The current iteration of the aqueous reprocessing loop contains two 18.9 liter (5-gallon) PVC tanks and retains the 114 liter (30-gallon) PVC inventory tank and the Iwaki magnetic pump from its predecessor (Figure 4.1). This design was selected to allow for more control of process flows between tanks via strategically placed gate valves, and to enable a greater variety of operating configurations to be tested. The inventory tank still serves the same purpose: as a distributed background radiation source to represent the high radiation background present in bulk facilities; as a large reservoir to allow for the material to circulate continuously; as a basin to allow for the homogenous mixing of the radiotracer with the selected fluid prior to circulating it through the loop; and as a tank for all the fluid to drain into and be safely stored in one place once operation is complete.

The radiation signals present in a reprocessing plant are not only very intense but extremely complex [8]. To mimic the presence of multiple radioisotopes in a mixture, Tc-99m ($t_{1/2}$= 6.0067 hours) and F-18 ($t_{1/2}$=109.77 minutes) were selected to create the radioactive mixture present in the loop. Radiolabeled technetium pertechnetate and fluorodeoxyglucose both readily dissolve in water and are two of the most common and affordable radioisotopes on the market today [41]. Both have reasonably short half-lives for observation in a laboratory setting, and gamma ray energies sufficient but not too large for efficient detection/protection. Water was chosen as the solvent because it too is readily available and does not produce mixed radioactive waste, which is difficult and expensive to dispose of [20].

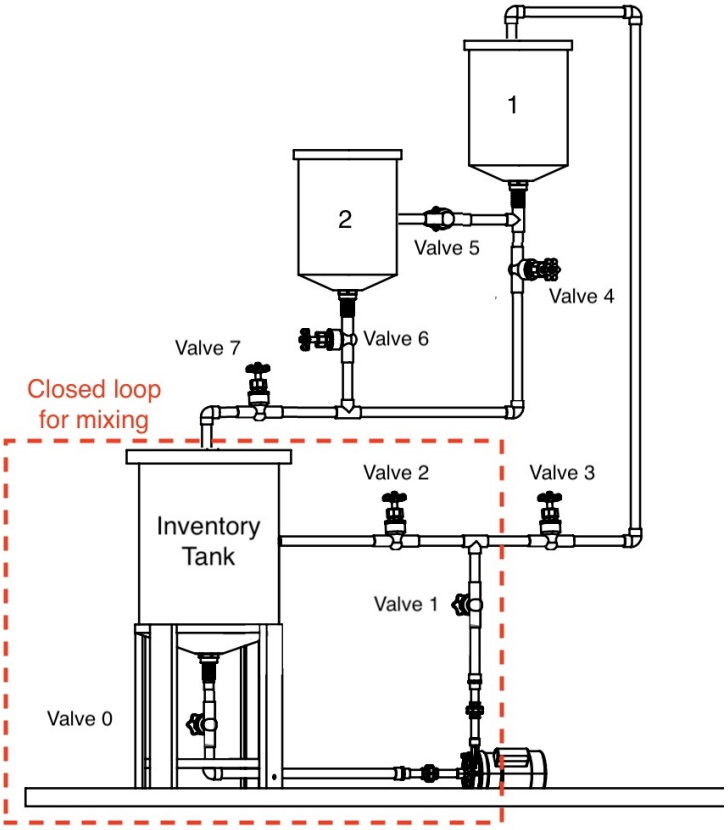

Figure 4.1: An engineering drawing of the NGL constructed in Solidworks 2018. The loop consists of two 18.9 liter (5-gallon) tanks and one large 114 liter (30-gallon) inventory tank. They are connected to one another using $\frac{3}{4}$ inch PVC piping with $\frac{3}{4}$ inch PVC gradual on/off gate valves to attenuate the flow between tanks. The closed loop for mixing the radiotracers in with the water is shown by the red dashed line

4.1.1 Measurement Signals Available

The Next Generation Loop employs sensors which collect gamma radiation data and instrument based non-radiation data such as volume, weight, and flow rate at various locations in the system. Three mechanically cooled p-type high purity germanium detectors called Individual Detector Modules (IDM-200 Vs) [16] are positioned 20 cm above each of the three tanks in the NGL. IDMs were chosen for their large crystal volume (85 mm $\times$ 30 mm), great energy resolution within the energy range of interest ($\leq$ 1400 eV at 122 keV and $\leq$ 2.3 keV at 1332 keV), and their non-reliance on liquid nitrogen for cooling. Each of these detectors were shielded by four hevimet (8" $\times$ 4" $\times$ 1") or lead blocks (8" $\times$ 4" $\times$ 2") to reduce the amount of radiation incident on the detector face originating from adjacent tanks (Figure 4.2).

Figure 4.2: An angled view of the 85 mm × 30 mm HPGe detector (crystal volume not visible) shielded by four white painted lead bricks (8" × 4" × 2") sitting atop of a half inch thick square of plywood. The detector sits 20 cm above the 114 L inventory tank. 2-inch-wide black Velcro straps ensure stability of the bricks while an orange ratchet strap secures the detector to the unistrut structure

The volume in each tank was determined using three Madison U3M-148 ultrasonic level sensors (Madison Company, Branford, CT) which were secured to the lid of each tank. The total mass of fluid in the inventory tank was also measured using an Arlyn Platform Scale with a 227 kg × 0.45 kg (500 lb × 0.1 lb) capacity (Arlyn Scales, East Rockaway, NY). Both the ultrasonic level sensors and the scale produced analog current output signals (4 to 20 mA). Finally, the flow rate going into the highest tank and into the inventory tank were measured using two Omega turbine flow meters (Omega Engineering, Norwalk, CT) with a high frequency pulse output (K-factor = 20 pulses/liter = 75.7 pulses/gallon) and detectable flow rate range 0.76 to 76 LPM (0.22 to 20 gallons per minute). All six of these non-radiation process sensors' data were collected and stored using a Labjack T4 (Labjack Corporation, Lakewood, CO) data acquisition system every 5 ms.

4.1.2 Operating Scenarios

The Next Generation Loop was designed to run in multiple configurations to simulate different operating regimes in a bulk handling facility. Each scenario can be characterized by the number of tanks involved, which valves were open/closed, and whether the pump was

on (forced circulation) or off (gravity flow) (Table 4.1). What is considered off-normal behavior can vary from scenario to scenario. This behavior may include material hold up and diversion, which can correspond to plant inefficiencies, faults such as blockages or leaks, or unknown/unauthorized nuclear material streams. For example, in the two tanks plus holdup scenario, tank 1 and the inventory tank represent the "normal" movement of material from one material balance area to another. Tank 2 is used as a repository for protracted diversion [7] from the two-tank system.

Scenario	**Valves Open**
Closed loop for mixing	0, 1, 2
Two Tank Gravity Flow [Two tanks, no pump]	4, 7
Three Tank Gravity Flow [Three tanks, no pump]	5, 6, 7
Three tanks Gravity Flow, all open	4, 5, 6, 7
Two tanks, forced circulation	0, 1, 3, 4, 7
Three tanks, forced circulation	0, 1, 3, 5, 6, 7
Three tanks, forced circulation, all open	0, 1, 3, 4, 5, 6, 7
Two Tanks, plus diversion (accumulated in tank 2)	0, 1, 4, 5, 7

Table 4.1: Operating scenarios of the Next Generation Loop

4.1.3 Fault Detection

Before the structural representation of this system is generated, its known, unknown, and fault variables should be determined. Variables that were considered known were the measured quantities from the nine sensors installed in the system. Note that the inventory tank may sometimes be referred to as tank 0 for conciseness.

Known (measured) variables:

V_i = volume of fluid in tank i measured by an ultrasonic level sensor (i=0,1,2)

$A_{i,Tc-99m}$ = total count rate in 140.5 keV peak from Tc-99m decaying in tank i (i=0,1,2)

$A_{i,F-18}$ = total count rate in 511 keV peak of F-18 decaying in tank i (i=0,1,2)

m_0 = mass measured in inventory tank by the weigh scale

q_1 = the flow rate (in LPM) of fluid entering tank 1 (after valve 3)

q_5 = the flow rate (in LPM) of fluid leaving tanks 1 and 2 and entering the inventory tank (after valve 7) (before valve 7)

Unknown variables are values that change throughout operation that we do not directly control. For brevity not all unknown variables are listed. The full system of equations

used to generate the structural model and corresponding isolability matrices are included in Appendix B.

dh_i = change height of fluid in tank i; this is used to show how the changing height in a tank relates to net flow rate in that tank

q_2 = the flow rate (in LPM) of fluid entering tank 2 (after valve 5)

q_3 = the flow rate (in LPM) of fluid leaving tank 1 and entering the inventory tank (after valve 4)

q_4 = the flow rate (in LPM) of fluid leaving tank 2 and entering the inventory tank (after valve 6)

q_6 = the flow rate (in LPM) of fluid re-entering the inventory tank (after valve 2)

Lastly, the 17 possible faults were selected to be malfunctions in instrumentation (i.e., the level sensor recording an incorrect height), or in discrepancies in quantities that are supposed to be preserved. For example:

fV_i = fault affecting the volume of fluid in each tank (i=0,1,2)

fQ_j = fault affecting the flow rate of fluid into/out of each tank (j=1,2,3,4,5,6)

fM_0 = fault affecting the mass of fluid measured in the inventory tank

f_{Vtot} = fault in the total amount of fluid in the system, which should be conserved

$fA_{Tc,i}$ = fault in the measured count rate within the 140.5 keV Tc-99m peak for each tank (i=0,1,2)

$fA_{F,i}$ = fault in the measured count rate within the 511 keV annihilation peak from F-18 for each tank (i=0,1,2)

4.2 Results

The Next Generation Loop (NGL) is an experimental aqueous loop with optional forced circulation composed of three PVC tanks connected by PVC piping with a unistrut supporting frame. The NGL serves to simulate the movement of nuclear material from one material balance area to the next within a generic aqueous reprocessing facility (Figure 4.3). Water and commercially available radiotracers were used to mimic the aqueous material and its radioactive properties. These experiments intend to improve the understanding of radiation and non-radiation signals within a bulk handling facility and leverage novel fault detection methods to improve upon existing safeguards techniques within these facilities.

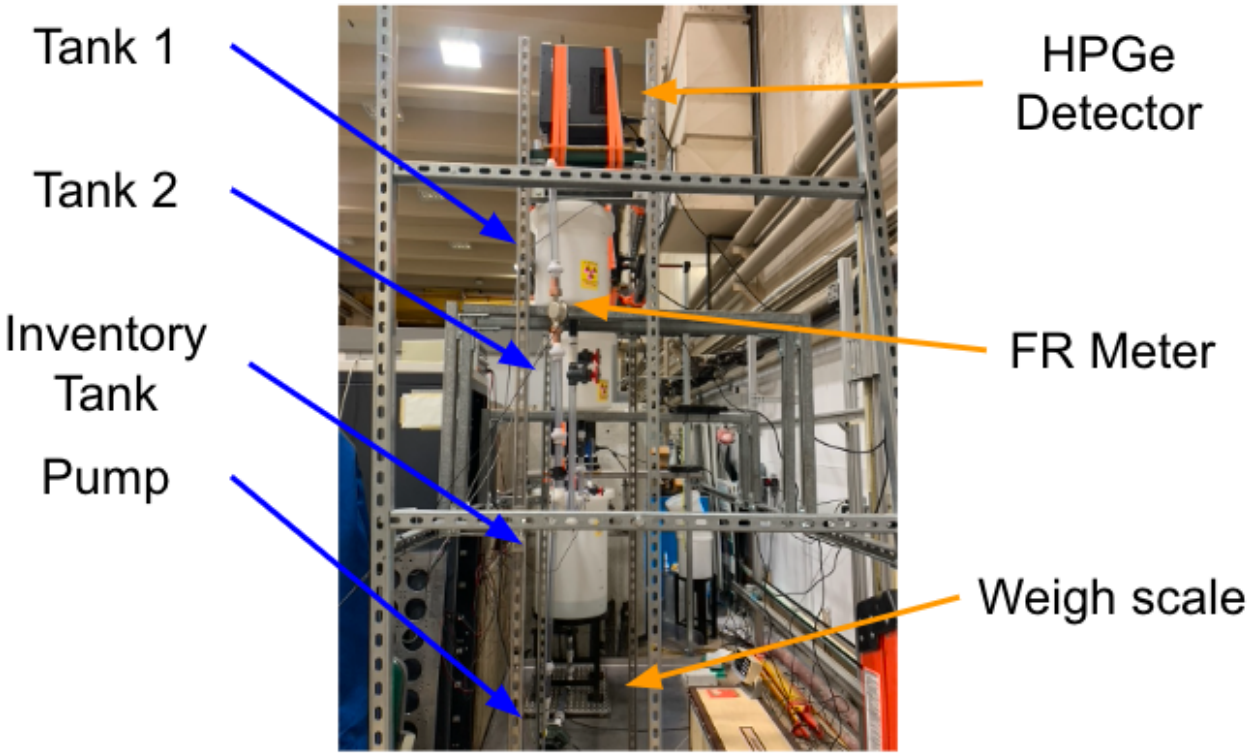

Figure 4.3: A side view of the Next Generation Loop. The loop components are indicated by the blue arrows on the left of the image. The measurement devices installed in the loop are indicated by the orange arrows on the right side of the image. There are a total of 3 tanks, 3 HPGe detectors, 3 ultrasonic level sensors, 2 flow rate meters, and 1 weigh scale

Cardinal Health delivered two syringes: one containing 3 cc of sodium pertechnetate with 5 mCi of activity, and the other containing 3 cc of fluorodeoxyglucose also with 5 mCi of activity. Upon receipt, both syringes were removed from the lead-lined shipping container and completely emptied into the inventory tank. The pump was turned on and the material was circulated within the closed mixing loop for ten minutes to enable sufficient mixing of the tracers with approximately 60 kg of water. Figure 4.4 shows that the mechanically cooled HPGe detectors possess sufficient resolution to resolve both the 140.5 keV gamma ray produced during Tc 99m decay, and the 511 keV annihilation photon from the β^+ decay of F-18.

4.2.1 Fault Detection and Isolability

The structural model for the Next Generation Loop is shown in Figure 4.5. This was generated using the Fault Diagnostics Toolbox and is a graphical representation of the equations

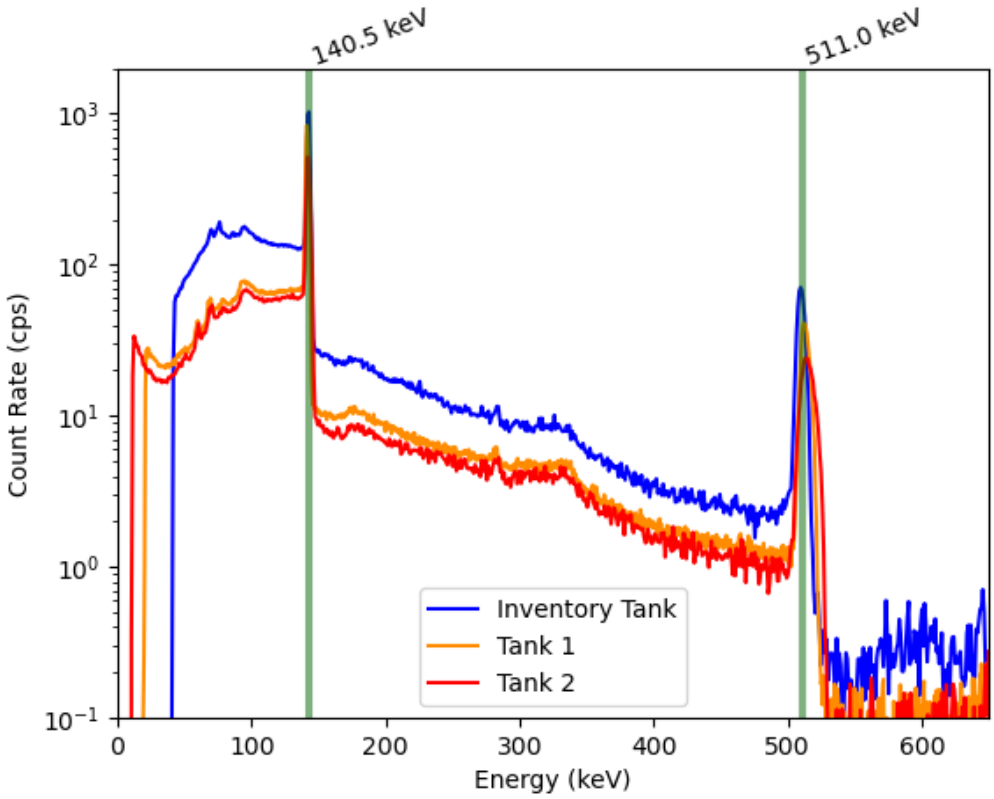

Figure 4.4: A sample gamma ray spectra observed above each of the three tanks in the NGL

used to model the NGL (see Appendix B). Equation numbers are listed in descending order along the y-axis. The three types of values listed along the x-axis are variables, faults, and measured signals. A dot is placed in a specific position if the value in x appears in that equation y. Variables are shown in blue and include for example the volume in each tank (V_i). Differentiated or integrated variables are denoted by a blue "D" or blue "I". Fault variables are shown in red, and measured signals are marked in black.

Taking the structural model one step further, the Dulmage-Mendelsohn decomposition can be performed, resulting in the plot shown in Figure 4.6. Here equations that together create an over-determined system (no. of equations > no. of variables) are reorganized into equivalence classes. These can be thought of as sets of equations for which every constituent equation is necessary to make a set of equations that is over determined. Equivalence classes of equations are indicated by the gray squares in the plot. Red dotted lines indicate which equation a given fault will affect. In order for a fault to be isolable there must only be one fault in each equivalence class. If multiple faults cross through the same gray square, it means these faults are not distinguishable from each other. Ideally faults should be isolable because there would be a unique response in the case of each fault. For example, our response

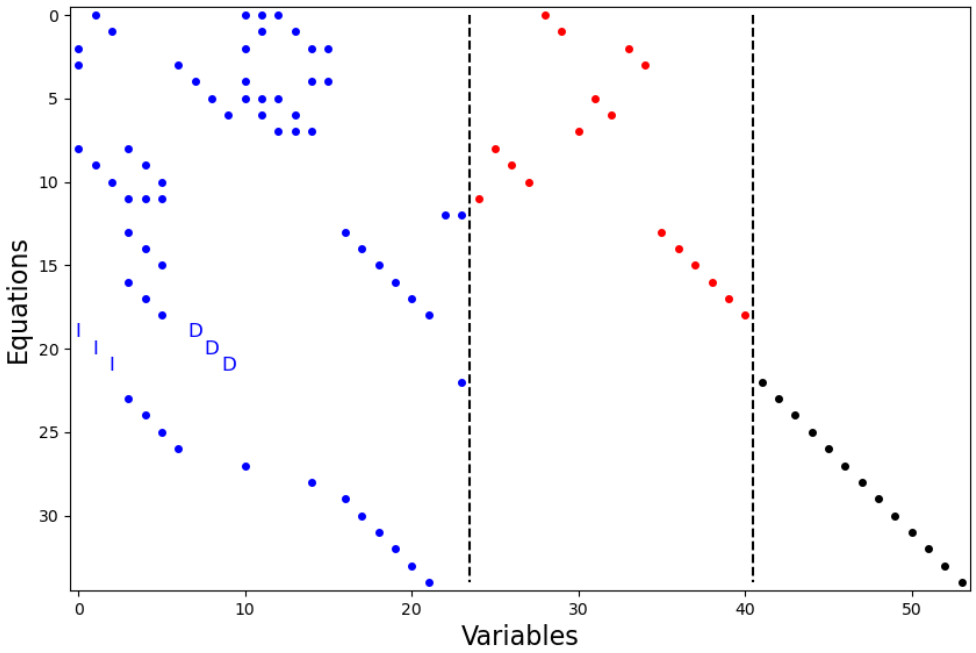

Figure 4.5: The structural representation of the NGL using the Fault Diagnostics Toolbox. Blue markers are variables (Blue D's denotes differential relations, blue I's denotes integral relations). Red markers are fault variables, and black markers are measured signals

to a fault in the level sensor might differ from a response to a fault in a flow rate meter.

The isolability matrix for the NGL system (Figure 4.7) reveals that all faults are detectable and completely isolable from one another. Each fault is listed along the x and y-axis of the matrix. If the fault on the y-axis occurs, the model allows it to be identified as any of the corresponding fault(s) on the x-axis for which it has a blue dot filled in. In the case of the NGL, if a fault is observed, the only fault that it could possibly correspond to in this system is that individual fault, making each fault both detectable and isolable from the others.

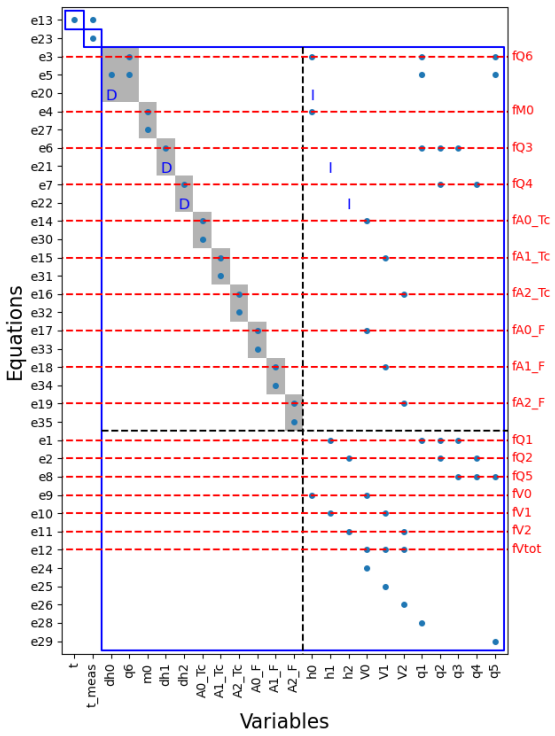

Figure 4.6: Dulmage-Mendelsohn decomposition of the Next Generation Loop

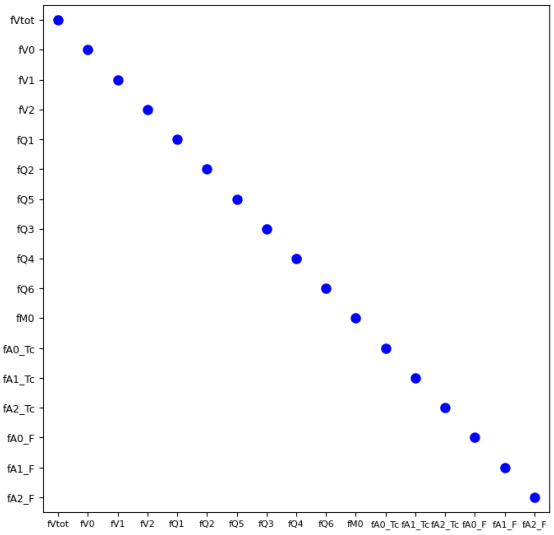

Figure 4.7: Isolability matrix of the Next Generation Loop

4.2.2 NGL Operating Scenario Examples

Before moving on to operating the NGL in its diversion configuration, some simple examples are included to highlight what different operating scenarios look like using the installed instrumentation.

In the static case, where the circulation pump is turned off and there is no material moving between process tanks, the expectation is to observe constant signals with uncertainty values within those quoted in Tables 2.7 and 2.8. Figure 4.8 illustrates this scenario, when approximately all the fluid is contained within the inventory tank. The left subplot displays the volume of fluid in liters contained within each tank as measured by the three ultrasonic level sensors. Depending on the magnitude of the signal, the standard deviation from random measurement errors ranged from 0.39% to 12% of the mean volume.

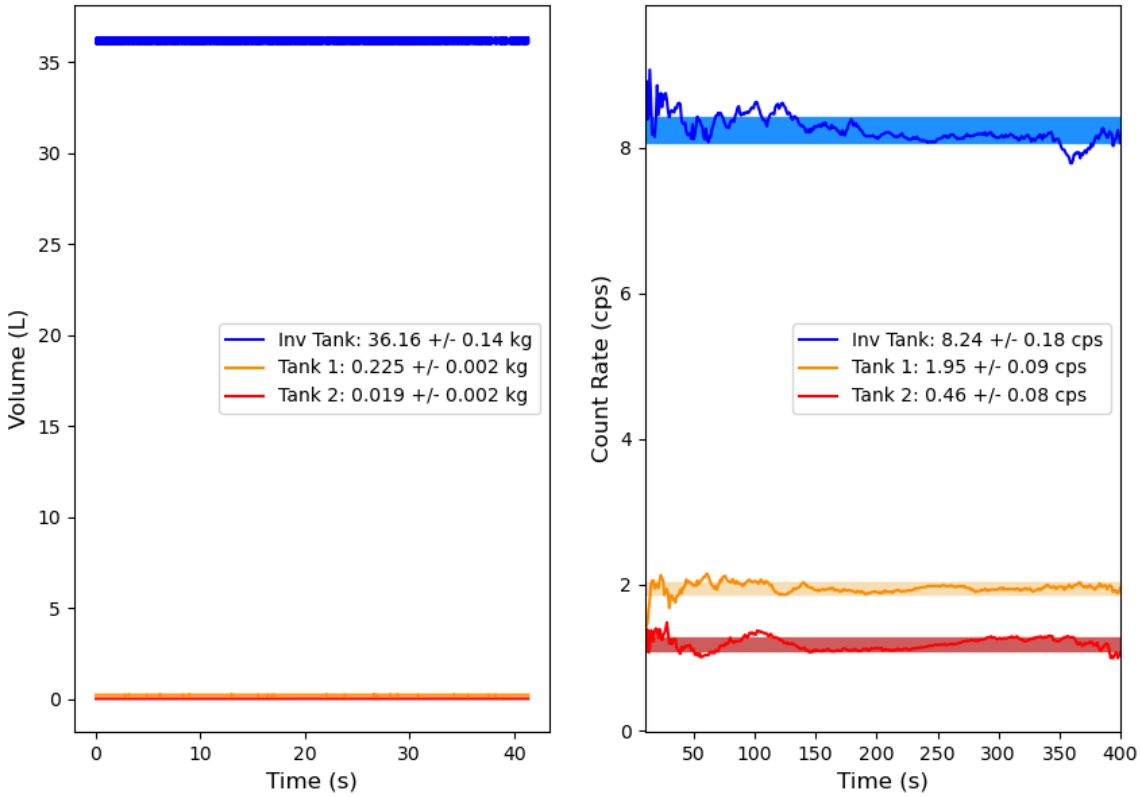

Figure 4.8: Left) The volume data measured by the ultrasonic level sensors in all three tanks when approximately all fluid is contained within the inventory tank. Right) The count rate data within the Tc-99m full energy peak measured when approximately all fluid is contained within the inventory tank.

Although the upper range of these uncertainties does exceed the international target value

for volume measurements in process tanks (1%), it is important to remember that quoting the uncertainty as a percent doesn't always provide the full picture of what is occurring. In the case of the ultrasonic level sensors, the random uncertainties in measurements is due to the static noise present when the output voltage is measured, leading to perturbations from the mean measured voltage. This noise remains around the same amplitude however that amplitude becomes less and less relevant as the voltage increases, resulting in a smaller percent uncertainty.

A similar relationship is observed in the right subplot of Figure 4.8, where the standard deviation of the background subtracted count rate measured within the 140.5 keV Tc-99m peak ranged from 2.2% to 7.4%, which agrees with NDA ITV values. The shaded areas represent $\pm$ 1σ about the mean background subtracted count rate observed in each tank. Including this example is important because it shows how different radiation signals and non-radiation signals vary when quantities in the loop are being help constant.

Going one step further, the following example operating scenario involves the movement of a finite volume of material from the inventory tank into tank 1, and then draining that volume back into the inventory tank. A color-coded schematic of this scenario is shown in Figure 4.9.

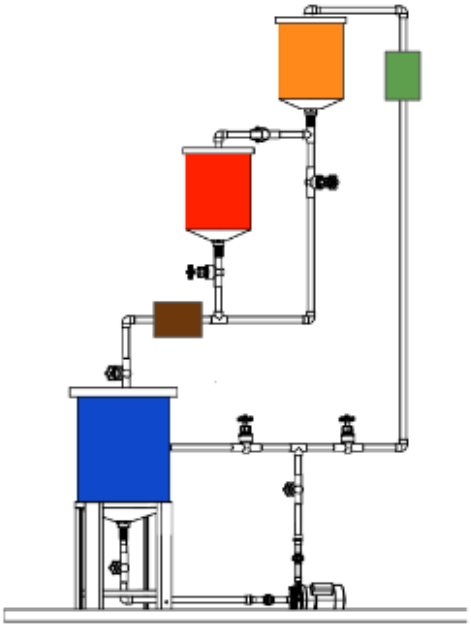

Figure 4.9: Schematic of the filling and draining of tank 1 in the NGL

The three ultrasonic level sensors and two flow rate meter readings are shown as a function of time in Figure 4.10. For conciseness, no weigh cell data or radiation data is including in

this plot although it was recorded during this trial. Fluid from the larger inventory tank (shown in blue) is pumped up to the higher of the two 11.4 L tanks. Valve 5, which connected tank 1 to tank 2, is closed for this entirety of this example. Valve 4, which situated below tank 1, is open allowing for fluid to begin draining almost immediately once it enters tank 1.

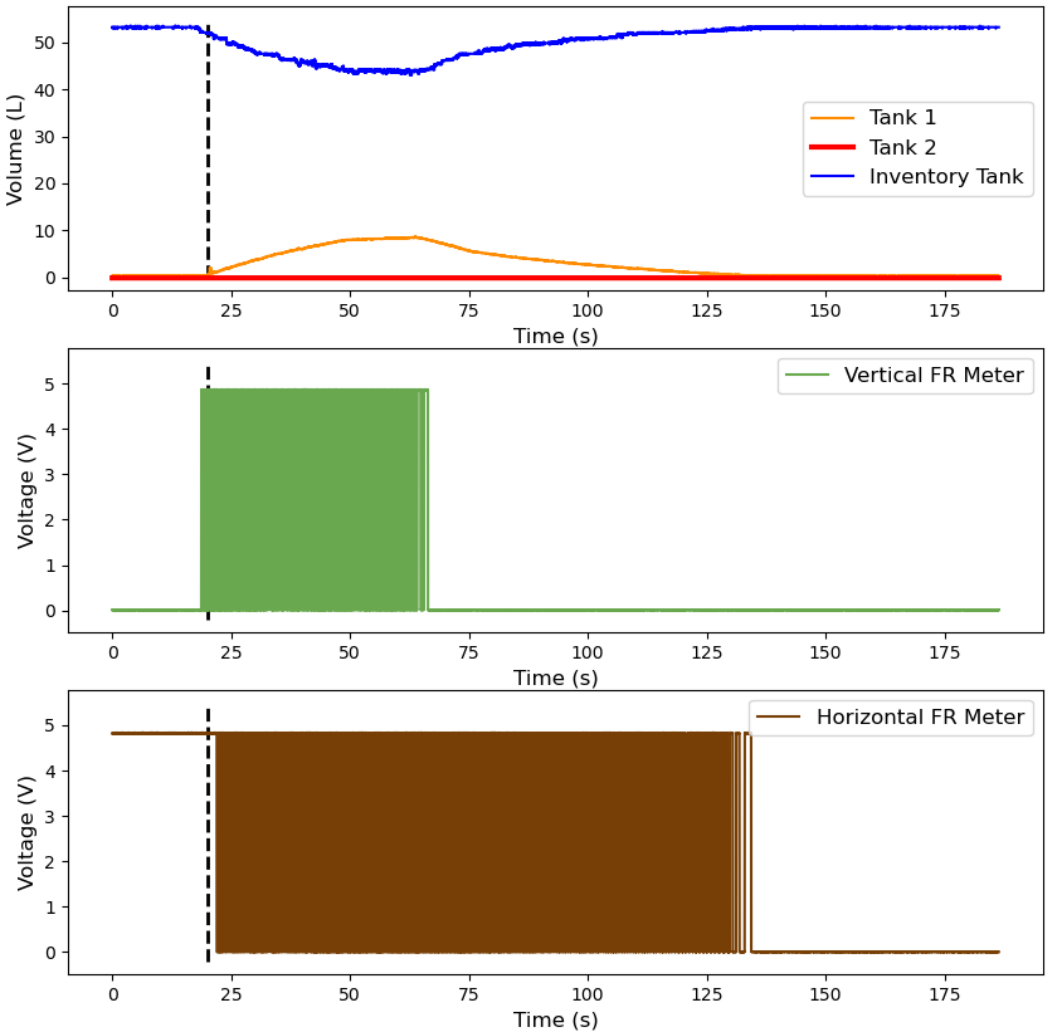

Figure 4.10: Filling and draining of tank 1 in the NGL

The dashed black line indicates approximately when material begins to accumulate in tank 1. Notice how that time occurs after the volume in the inventory tank starts decreasing as it is forcibly pumped upwards, and after the vertical flow meter begins to register fluid flowing through it. This behavior reflects the continuity of fluid flow in the loop: that the

only way for fluid to enter tank 1 is for that fluid to first be pumped from the inventory tank through the vertical flow rate meter. A few seconds later the fluid has had time to reach the horizontal flow meter shown in brown, as it recirculates back to the inventory tank.

Both turbine flow meters send a square voltage pulse to the data acquisition system for every 0.05 liters that passes through them. After about 70 seconds from the start of this run, the hydraulic pump is turned off and no more fluid is pumped into tank 1. Shortly after the vertical flow meter stops registering fluid flow and the measured volume in tank 1 begins to decrease while the volume in the inventory increases until all fluid has drained back into the inventory tank.

In an extreme case of the previous scenario, the ultrasonic level sensor temporarily faults mid measurement. This behavior is well documented by the sensor manufacturer and is the result of when the fluid in a tank rises too high towards the top of the container into the sensor's 10.2 cm (4 inch) dead zone. A discontinuity appears in the output signal of the faulted tank 1 sensor, and the pre-existing linearity between fluid level height and voltage amplitude disappears.

Figure 4.11 illustrates this behavior. This plot's y-axis is now in units of mass to account for the fact that the weigh cell signal does not directly indicate the volume in the inventory tank, but rather the combined mass of the tank and its structural surroundings. Other tanks' contents have been approximated to mass as well since the density of water was assumed to not change from the addition of just a few milliliters or radioactive material.

By designing the NGL system to have a high degree of redundancy, there were multiple ways to detect the fault in ultrasonic sensor's behavior. A straight forward way of estimating this fault is by taking advantage of the known volume initially input into the system which should be known by the operator. Using the ultrasonic level sensors in all three tanks, the volume missing from the system (with some room for a finite amount being held up in the pipes) can be calculated from the difference of the total volume and the volume in all three tanks.

Similarly, instead of using the ultrasonic level sensor in the inventory tank, one can use the weigh cell to calculate the volume of fluid in the inventory tank and combine that with the remaining ultrasonic sensor data. These two methods are denoted by fV_{tot} (US Sensor) and fV_{tot} (Weigh Cell) respectively in Figure 4.12. The third method used in that figure involves calculating the cumulative fluid volume that flowed through the vertical flow rate meter and subtract that from the cumulative volume that flowed out the horizontal sensor back into the inventory tank, fV_{tot} (FR Meters).

The faulty sensor temporarily produces a negative fault signal indicating that approximately 4 L of material had abruptly gone missing. Then after 40 seconds, the missing volume returns to zero. The fault signal produced from the flow rate meter calculation shows a second deviation from the other two fault signals immediately after the negative jump to 4 L. This was attributed to the linearly interpolated manner that cumulative volume was calculated. The flow rate meters only pulse every 50 mL while the rate at which fluid was flowing out of tank 1 was shown to increase at a faster rate when observed by the ultrasonic level sensors.

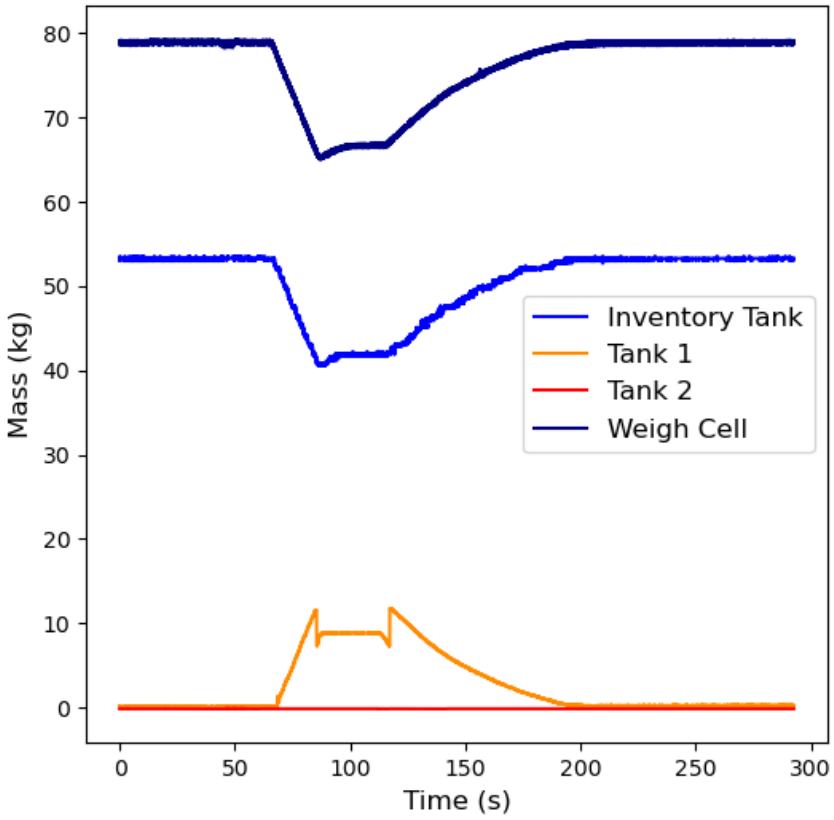

Figure 4.11: Tank 1 is filled and then drained back into the inventory tank. The contents of the tank reached above the recommended 10 L maximum into the sensor's dead zone and a temporary fault was observed

This highlights the trade-offs with using different instruments to measure different signals. In this case the faulted volume signal eventually returned to zero, as if nothing had ever been missing in the first place. The multiple fault signals were able to confirm this eventual return to zero and one could conclude that this was a temporary instrument malfunction. Had material actually been removed from the system, the fault signal would remain non-zero to indicate material went missing and stayed missing throughout the measurement period.

This example serves to remind stakeholders that even with advanced fault detection techniques, sound knowledge and understanding of the system is required by operators to be able to operate machinery within their operating limits and adequately diagnose faults especially in more advanced facilities.

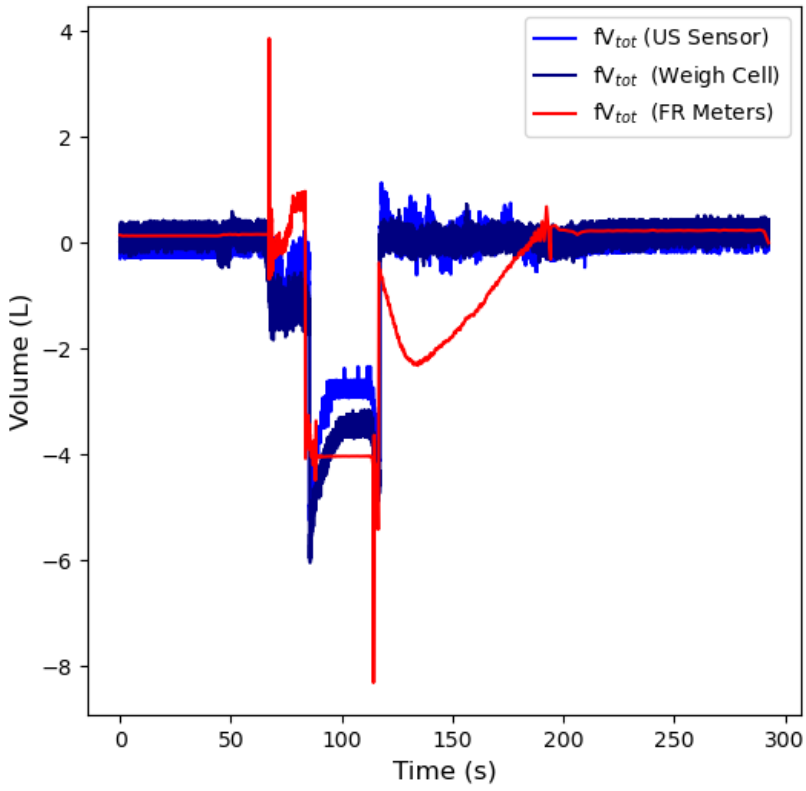

Figure 4.12: Using three different methods, three different fault signals were generated to indicate the defective behavior of the ultrasonic level sensor in tank 1

4.2.3 Diversion Scenario

One of the benefits of the NGL system over its predecessor is the ability to make repeatable diversion experiments with added instrumentation installed to better quantify the amount of diverted material. While operating in the diversion configuration, material was diverted from a two-tank system (higher tank/tank 1 and inventory tank/tank 2) to a tertiary tank (Figure 4.13).

The two-tank system employed forced circulation via the hydraulic pump, and after a certain point in time, valve 5 was opened, initiating diversion from the two tank system. The diverted material accumulated in the diversion tank, which appears as a "black box" to the system and in the schematic of the diversion scenario in Figure 4.13. This is because the diversion tank is viewed as "unknown" to the two-tank system, and thus the accumulation of material in it results in a net loss of material in the two-tank system. So as valve 5 is opened, the amount of material in both the inventory tank (blue) and the entire system (green) decreased.

According to the isolability matrix, this diversion will be detected and isolated. The

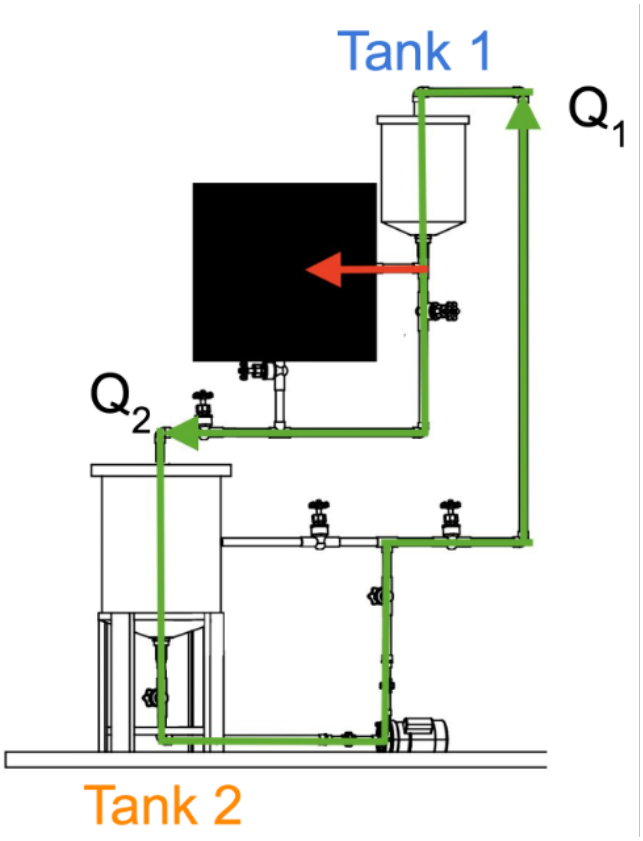

Figure 4.13: A schematic of the two-tank diversion system. Diversion is indicated by the red arrow leaving the system going into a third tank which is not known to the system and is thus represented by a black box

fault is expected to occur in the measured flow rate of material re-entering the inventory tank (Q_2). Therefore, the faulted signal fQ_2 will be equal to the water flowing into tank 1 (Q_1) plus the adding flow rate provided by the accumulated material in tank one, subtracted by the amount of material leaving tank 1 (Q_2). If there was no diversion then the fault would be zero.

$$fQ_2 = Q_1 + A_{spout,1}\sqrt{2gh_1} - Q_2 \tag{4.1}$$

By having a level sensor on the diversion tank itself, the amount diverted can be compared to the fault signals generated in this scenario, acting as a ground truth. Figure 4.14 shows this graphically: the material accumulating in the diversion tank, compared to the calculated accumulated material from the faulted flow rate, and the missing total volume in this system. Note that fQ_2 estimate is slightly lower than the other two signals. This is due to the finite amount of hold up present in the horizontal piping connecting tank 2 and the diversion tank, as well as holdup in the diversion tank itself from its sloped bottom and the small amount

of piping between the bottom of the diversion tank and the gate valve that closes that tank off from the rest of the system. The simplified fluid dynamics equation which described the fault (fQ_2) might be too idealized and therefore not accurately describe the behavior actually occurring. This all appears to result in an underestimate of the volume diverted.

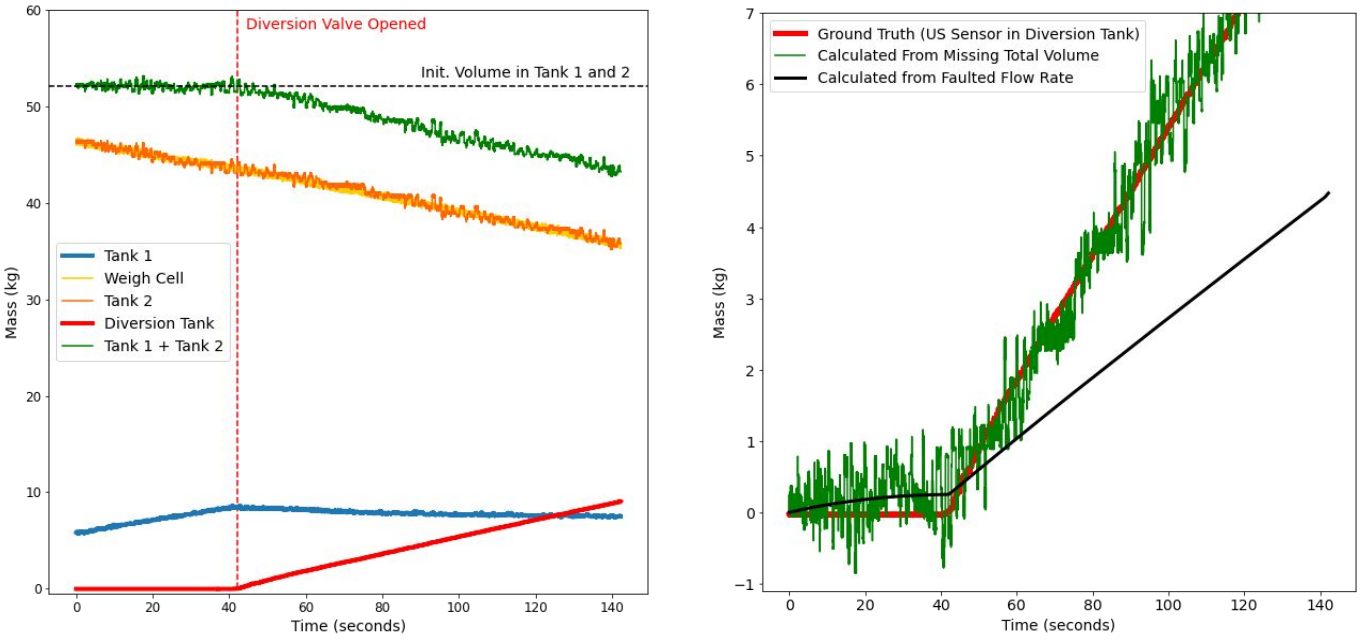

Figure 4.14: Left) The measured mass of fluid inside of a two-tank system, where the large inventory tank is tank 1 and a smaller 11.4 L tank is tank 2. At approximately 79 seconds the gate valve connected tank 1 to a separate diversion tank was opened. Right) An estimation of the diverted as is shown based on the three ways it was calculated: from the difference of the known total volume and what is measured in tanks 1 and 2, the estimated mass from the difference in flow rates denoted by fQ_2, and the actual measured mass inside the diversion tank

Fault detection is useful because faults can be calculated a variety was ways and this will improve the operator's confidence in the existence of a fault. Figure 4.14 uses a method to calculate the flow rate fault using volume in tank 1 based upon the level sensor's estimation of volume. But one can also estimate volume based on the observed count rates in the different full energy peaks present. Figure 4.15 shows the degree of agreement between the measured volume using the level sensors in each tank compared to the estimated volume using the 140.5 keV Tc-99m peak and the 511 keV F-18 peak.

Tank 1 shows decent agreement however tank 2 and even the diversion tank shows large discrepancies in the estimation of the volume in each tank. This results in large uncertainties when comparing the missing volume to estimates of it based on this method. Figure

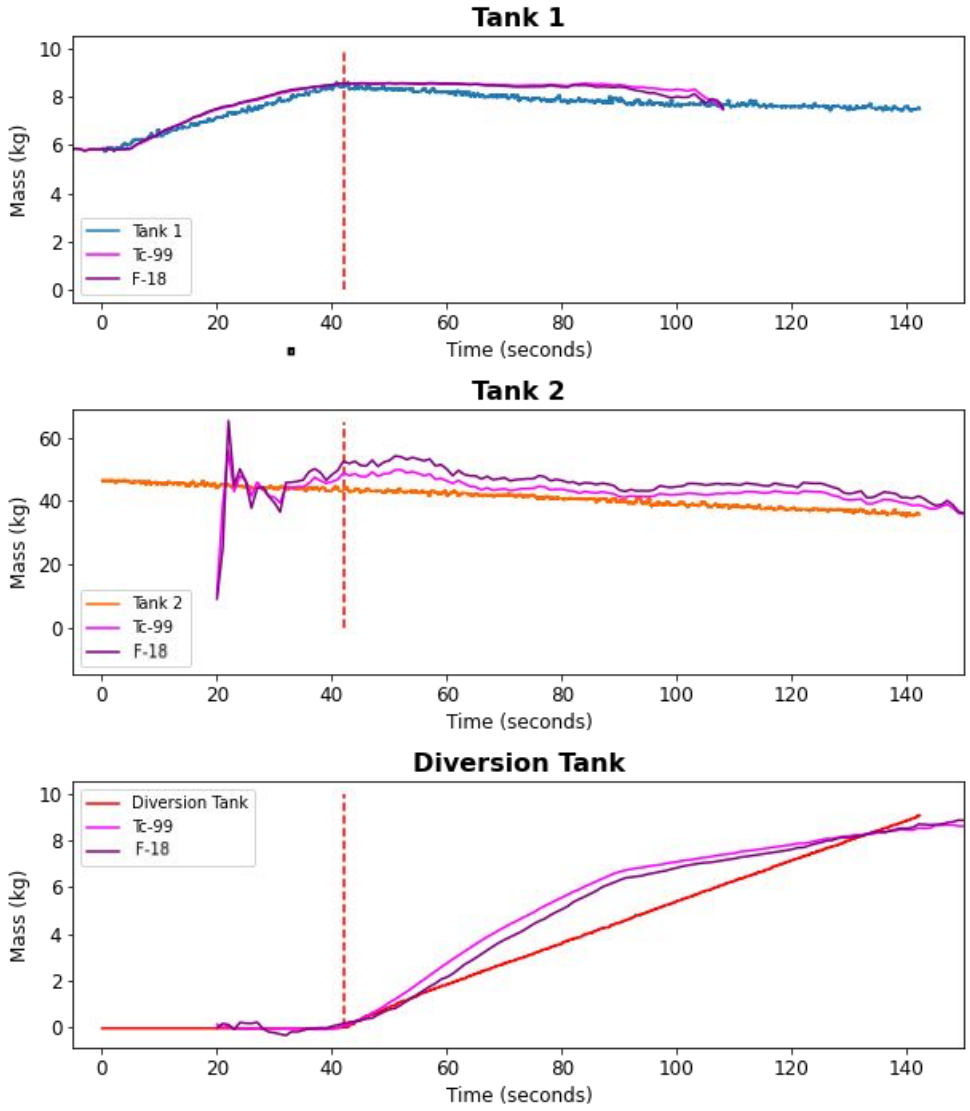

Figure 4.15: The volume in each tank as measured by the ultrasonic level sensor compared to the volume estimates using the Tc-99m and F-18 gamma ray emission peaks to relate measured count rate to volume.

4.16 shows how beginning when the diversion valve was opened, the estimated mass in the diversion tank does trend upward but is extremely noisy. Even using the estimation of volume of the diversion tank's radiation detector shows deviations up to 50% but the positive correlation between volume and count rate is still observed.

With improved shielding between each successive tank, the measurement variations should be reduced. More shielding was present in the NGL than its predecessor however the wide field of view still resulted in some cross talk between tanks. Additionally, the height of the

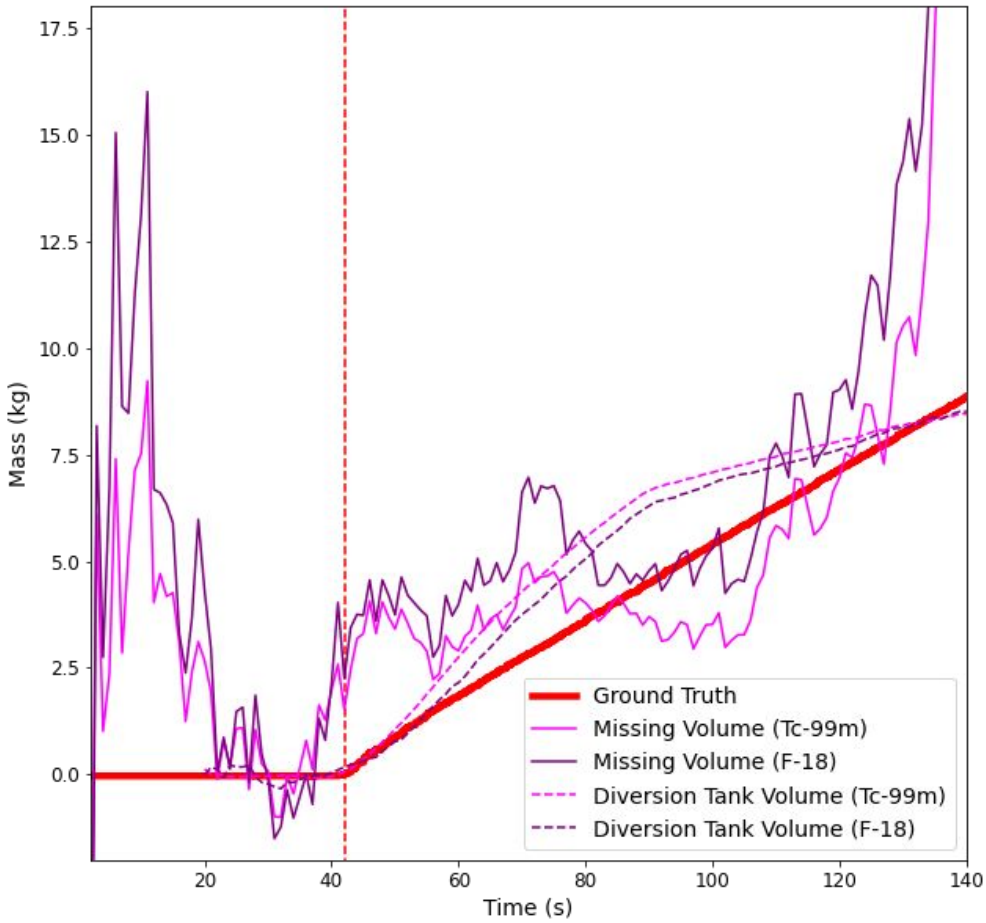

Figure 4.16: The volume in each tank as measured by the ultrasonic level sensor compared to the volume estimates using the Tc-99m and F-18 gamma ray emission peaks to relate measured count rate to volume.

inlet pipe opening of each tank was positioned at the top of each tank, closer to the detector face than the fluid which accumulated at the bottom, potentially altering the measured count rate during forced circulation.

Lastly, the perturbation at the beginning of tank 2's experimental data is worth discussing briefly. Since the estimate of diverted material can be based on missing volume from the entire system (∼60 kg), and 75% of the total volume was in contained within tank 2, these fluctuations in measured count rate had a larger effect on the missing volume estimate. More care should be taken to begin collecting the list mode data earlier before each operating scenario is began to prevent this disturbance from affecting future diversion estimates.

4.3 Conclusion

Fault detection and the Fault Diagnostics Toolbox are valuable tools to meet the growing need of improved material accountancy. By iterating on designs and implementing fault diagnostics into the design process, new technology can be rapidly prototyped while keeping the safeguarding of material in mind throughout the design process. It is worth noting that more complex residual generators can be employed for fault diagnostic work but that these generators may be computationally expensive, potentially making them less likely for plant operators to use. Employing machine learning algorithms may also be beneficial but suffer from the same disadvantages of being computationally expensive the more complex they become. Care must be taken when selecting residual generators to optimize for computational complexity and the ability to cover the entire systems' faults. If all of the systems' faults are not covered, new first principle relationships, alternative formulations, or additional instruments may be added.

Small scale experiments like the Next Generation Loop are important towards the creation of novel safeguards technology to answer these calls. This work demonstrated the feasibility of new fault detection approaches which combined radiological and non-radiological signatures to detect faults in the operation of a simple aqueous loop. This work focused on gamma-ray detection, but the methodology can easily be extended to include neutron radiation signals as well.

Upgrades to the Next Generation Loop will include finer collimation for the detectors to suppress the count rate when higher activity materials are present. Additional collimated detectors should be employed for pipe interrogation, while pressure transducers can be added for improved holdup quantification or leak detection in piping. Advances in radiation transport methods can help benchmark these experiments and ultimately apply these models to even more complex facilities in the future.

Chapter 5

Modeling and Simulation

In order to develop novel safeguards approaches for reprocessing plants, the source term in these facilities must be well understood. With that, measurement instrumentation can be chosen to optimize detection capabilities and performance. Sandia National Laboratories developed the Separations and Safeguards Performance Model (SSPM) as a tool to accomplish this [11]. SSPM is a MATLAB/Simulink toolbox used to track nuclear material and bulk materials through various unit operations in a generic 200 tHM/year PUREX reprocessing plant. SSPM provides great detail on modeling flow rates, inventories, separations, and timing sequences across the following 11 locations within the plant:

- Shredder/Voloxidizer
- Input Accountability Tank
- Electrolytic Reduction
- Uranium Electrorefiner
- Metal Processing
- U Product Processing
- U/TRU Product Processing
- U/TRU Drawdown
- Salt Purification
- Oxidant Production
- Fission Product Waste

The graphical user interface to SSPM is shown in Figure 5.1. Elements and isotopes are tracked in real time to simulate actual plant conditions from a startup state with a 24-hour dissolution cycle. The toolbox allows for the burnup, initial enrichment, and cooling time of the incoming spent fuel assembly to be varied as well. SSPM can also simulate diversion, both direct loss and substitution loss, however these capabilities were not studied at this time.

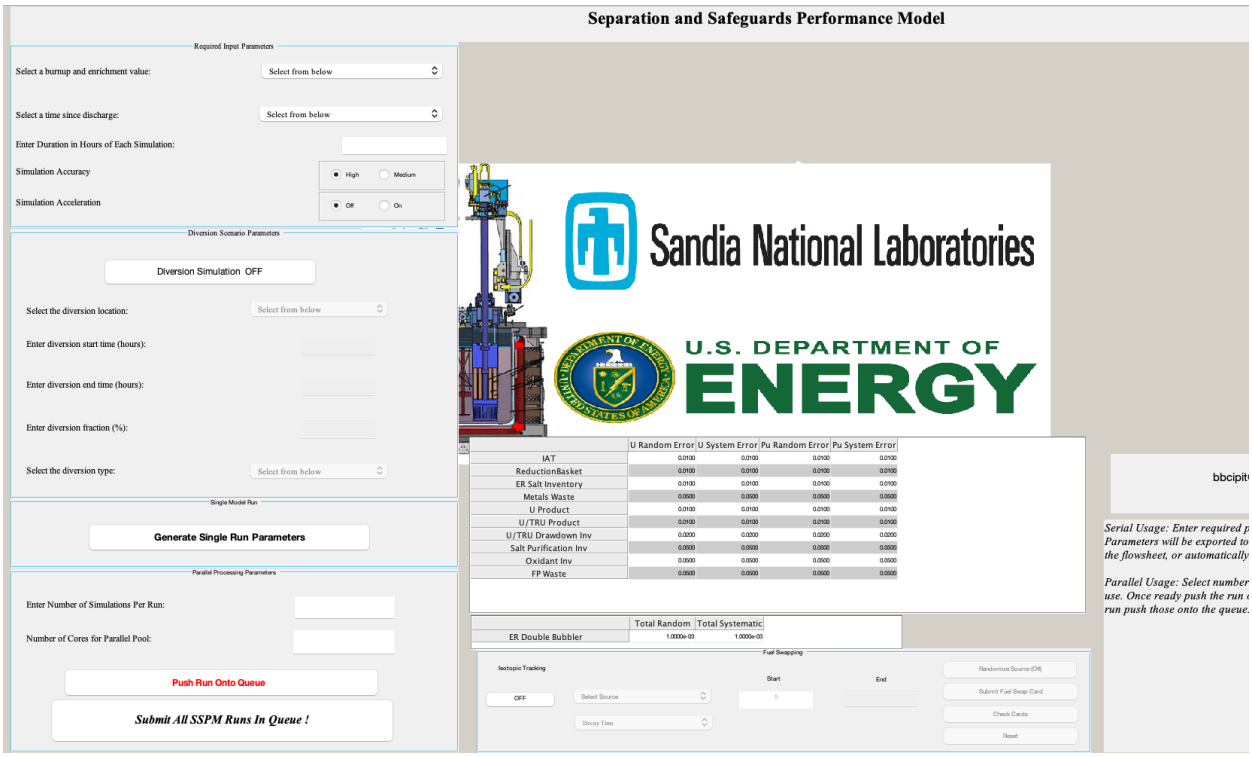

Figure 5.1: The SSPM Graphical User Interface (GUI)

5.1 Gamma Spectroscopy in Aqueous Reprocessing

The objective of nuclear safeguards is to ensure that nuclear materials are not diverted from the peaceful utilization of nuclear technology. A growing area of interest is near-real-time accountancy (NRTA), which involves using in-process inventory estimation through direct methods (i.e. volume, flow, or concentration measurements) and indirect methods such as historical data like burnup and cooling time [75]. The combination of these two methods allows for improved timeliness of detection of material loss to supplement existing material balance methodologies. Instruments such as the solution measurement and monitoring system (SMMS) [39] exist to accurately monitor solution process tanks in reprocessing facilities for disturbances in plutonium-bearing materials. SMMS accomplishes this based on observed volume, density and temperature data. This work hopes to provide the basis for similar technologies that utilizes gamma spectroscopy measurements in addition to the non-radiation signals being collected.

For the purposes of this study energy range and energy resolution were prioritized over other properties such as cost, maintenance, cooling requirements, etc. A high purity germanium (HPGe) detector was selected as the primary detection system for the following

simulations. Its excellent resolution combined with appropriate shielding and collimation should result in a detailed spectra of the radioisotopes present in the field of interest. Such fine energy resolution (0.2% at 662 keV) should be sufficient to observe Cs-134, Cs-137, and Eu-154, three important isotopes for fuel burnup determination [1].

5.1.1 Methodology

SSPM offers time-dependent isotope specific material inventories at specific locations within a generic 200 tHM/year PUREX reprocessing facility. Using this data and the Monte Carlo N-Particle Transport Code (MCNP) [92], an input accountability tank (IAT) was modeled with the following fuel burnups and initial enrichments after cooling for one year:

33 GWd, 2.6 %, 3.3%, 4.0%
45 GWd, 3.3%, 4.0%, 4.7%
60 GWd, 4.03%, 4.73%, 5.43%

The IAT is the front end of the reprocessing process and is considered the first and most important point where an accurate assessment of the amount of plutonium produced in reactors can be made. Verifying the presence of these materials is crucial not only from a safeguards perspective but also for the verification of process losses. Normally this is done through isotope dilution spectrometry, however the isotope correlation technique, which uses correlations between Pu to U and various other heavy element or fission product isotope ratios, has shown promise as well [58],[71]. One known correlation is that the activity ratio of Cs-134 to Cs-137 is proportional to the burnup of LWR fuel [1].

Under the assumption that input accountability tanks are similar in design to waste collection tanks in existing nuclear facilities, the dimensions and fill proportions of the IAT were based on the High Activity Waste tank at the Tokai Reprocessing Plant in Japan [82]. The IAT is has a diameter of 1.726 m, height of 1.222 m, and the stainless-steel wall is 2.2 cm thick. The tank is enclosed in a concrete hot cell 4 m $\times$ 4 m $\times$ 6 m with 1.22 m (4 ft) thick walls as illustrated in Figure 5.2.

Cylindrical hole collimation through the 1.22 m of concrete with diameters of 1.0 cm, 3.2 mm, and 1.6 mm, were selected to observe how the count rate at the detector face changes as a function of collimator diameter. This detector configuration is similar to the experimental setup at the Molten Salt Reactor Experiment (MSRE), designed to study the fission products at various locations throughout the MSRE facility [29]. After concrete blocks were removed to access a given hot cell in the MSRE, gamma spectrometry measurements were taken from approximately 4.6 m (15 ft) above through narrow apertures in a biological shield. The aperture diameter was either 3.175 mm ($\frac{1}{8}$ inch) or 1.59 mm ($\frac{1}{16}$ inch).

Due to advances in semiconductor technology and fabrication, this study employs a state-of-the-art, mechanically cooled high purity germanium (HPGe) detector, 85 mm in diameter and 30 mm long, instead of the 36.7 mm by 28.5 mm lithium-drifted germanium detector used at the MSRE. Various types of shielding were employed at the MSRE but were not in

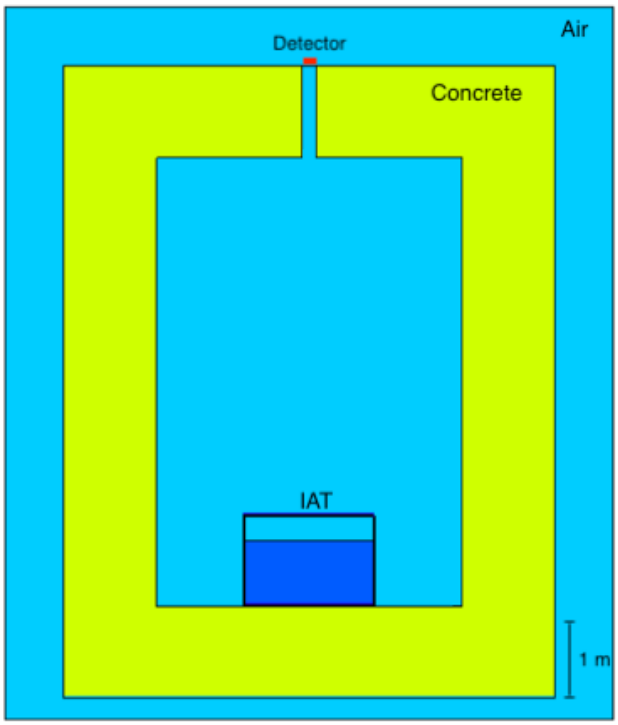

Figure 5.2: A MCNP model of an input accountability tank of a 200 tHM/year PUREX plant. The tank is made of 2.2 cm thick stainless steel and has dimensions of 1.726 m (diameter) and 1.222 m (height). It is surrounded by 1.22 m (4 feet) of concrete and shown with a 10 cm wide collimated hole directly above the tank. The tank is shown filled to 75% of its capacity

this study because of the attenuation provided by the 4 feet of concrete in this experiment, which was not available in the MSRE study, was sufficient.

Over 200 isotopes across 99 elements were tracked inside the Input Accountability Tank using SSPM. The following data is representative of when the amount in the IAT is at its maximum, or halfway through a 24-hour dissolution cycle, indicated by the red dashed lines in Figure 5.3. In addition to uranium and zirconium which dominate the dissolved spent fuel by mass, other prominent elements such as cesium and strontium are shown to be present in large quantities. The proportions from Figure 2.2 are reflected in this elemental data, namely that approximately 1% of the fuel is composed of plutonium, and there is 2-3 times more plutonium present than cesium and strontium.

This elemental data is further divided into isotopes by SSPM. Due to the complexity of this source term, an Automated Variance Reduction Parameter Generator, or ADVANTG [62] was employed to reduce the computational time required to obtain precise tally estimates in MCNP to generate quality gamma spectra.

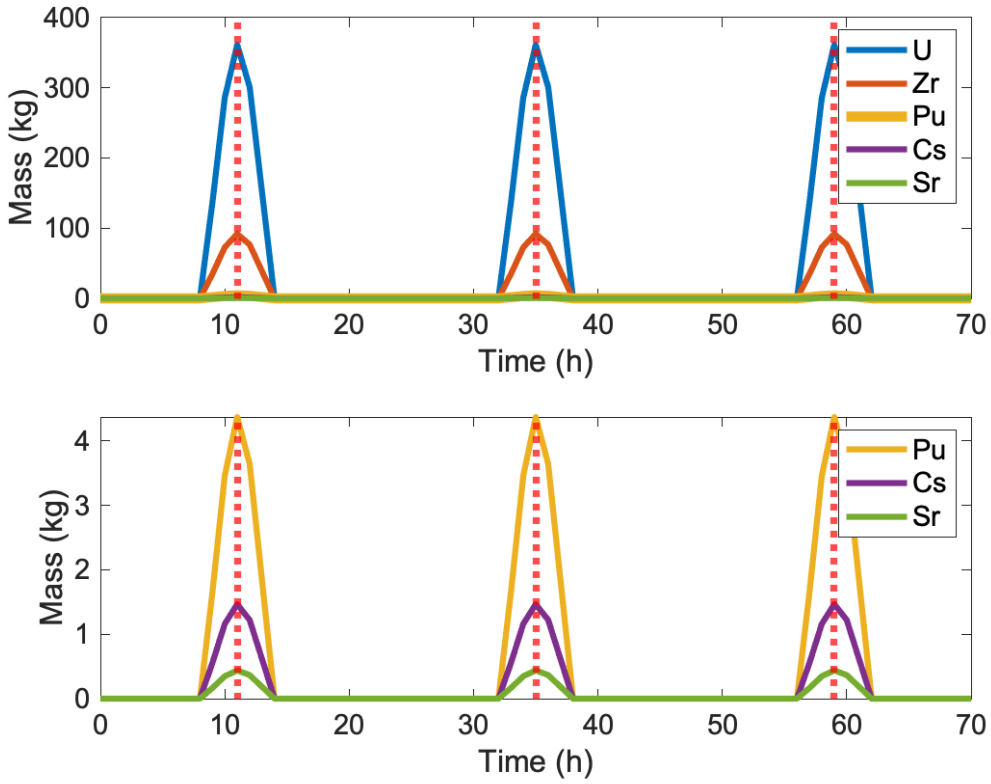

Figure 5.3: The elemental composition of spent fuel (45 GWd, 4% initial enrichment, 1 year cooling time) is shown a function of time. The red dashed lines indicate that maximum amount of material present in the input accountability, which occurs every 24 hours

5.2 Results

Material accountancy within PUREX facilities relies heavily on destructive sampling and off-site analysis. New technology is needed to provide real time process monitoring and that technology needs to be benchmarked with accurate and precise data. SSPM generates isotopic inventory data at various locations within a facility to assist in the testing of new measurement instrumentation and analysis of diversion scenarios.

This work focuses on the material present within the front end of the spent fuel reprocessing cycle: the input accountability tank (IAT). The following results use the inventory data when the material inside the IAT is at a maximum or halfway through its 24-hour dissolution cycle.

Within the hot cell itself, count rates were estimated to be on the order of 10^{11} counts per second. This would require a detector to have ∼picosecond timing to resolve the energies

of individual gamma rays. Most HPGes have time resolutions between 2-12 nanoseconds [51],[13], however recent advancements in high resolution gamma spectroscopy at high count rates has produced detectors that can operate at a rate as high as 1 Mcps and still maintain sufficient energy resolution (e.g. $\leq 0.3\%$) [12].

With this upper limit on count rate in mind, a cylindrical hole was inserted in the concrete ceiling directly above the center of the input accountability tank. This served to reduce the intensity of radiation incident on the detector, thereby lowering the count rate and deadtime. Figure 5.4 plots the spectra produced when the radiation detector is placed directly above the IAT with three different cylindrical collimator diameter holes (1 cm, 0.32 cm, and 0.16 cm). The intensity of these count rates ($\sim 10^5$ cps) are much lower than within the cell and are within the range of operation of the latest generation of HPGe detectors.

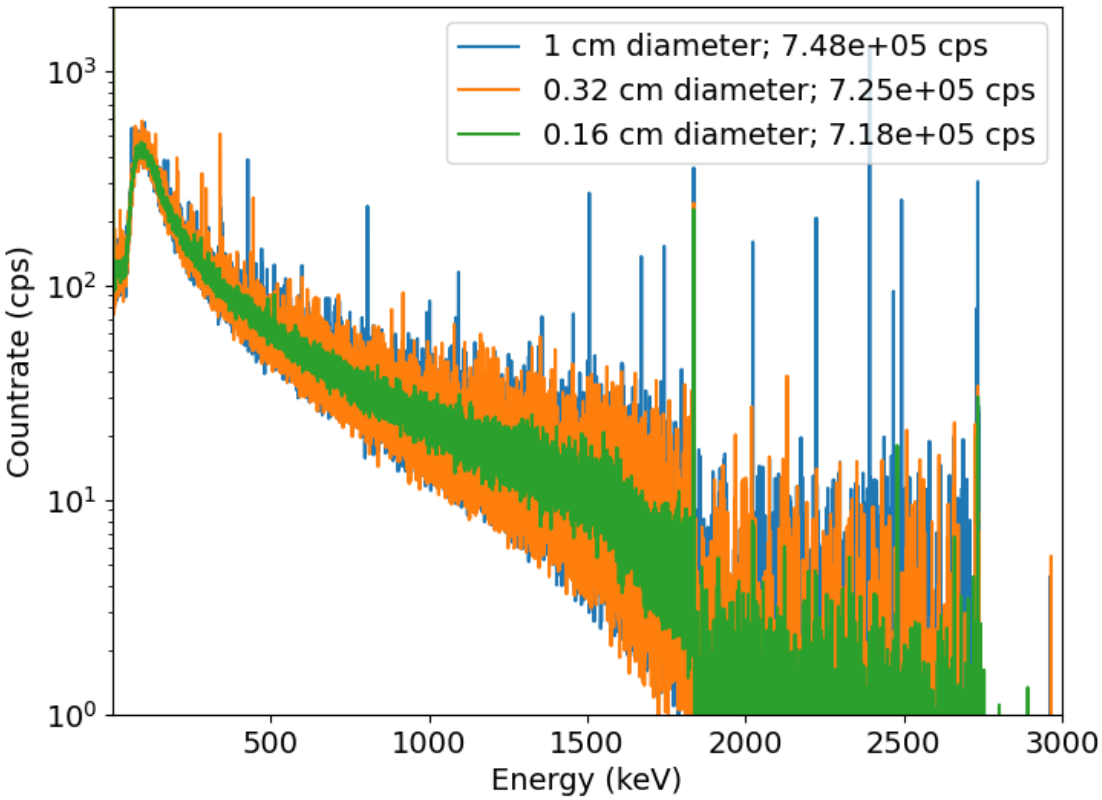

Figure 5.4: Gamma spectra collected from an HPGe detector without additional surrounding it. The detector was looking down through varying diameter holes in 1.2 meters of concrete directly above the center of the IAT. The fuel used had a burnup of 45 GWd, initial enrichment of 4.0% and had cooled for 1 year

Taking a closer look at the 1 cm diameter collimated hole setup, a multitude of gamma

peaks are readily resolvable from the data. Figure 5.5 replots the spectra this time overlaid with all discernible peaks with signal- to-noise ratios (SNRs) above 5. This cutoff was chosen arbitrarily, and many more peaks can be measured with an even lower cutoff of 2, however, to get sufficient statistics an SNR equal to 5 will be used for the time being.

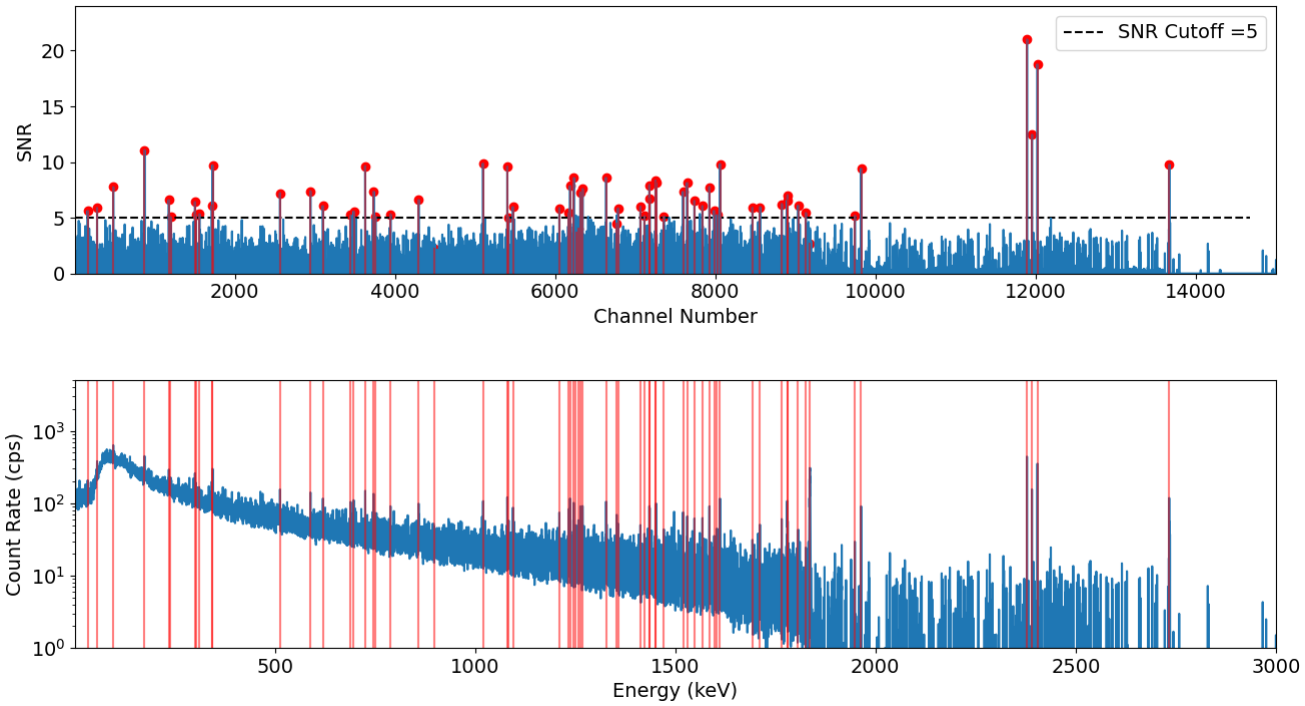

Figure 5.5: Top) The signal to noise ratio (SNR) of a gamma spectrum collected directly above the center of the IAT through a 1 cm diameter hole in the concrete hot cell. The cutoff value of what peaks were tabulated was an SNR equal to 5. Bottom) the corresponding gamma spectrum for the spent fuel with a burnup of 45 GWd, initial enrichment of 4.0% and had cooled for 1 year

Numerous peaks were observed in the nine different burnup and enrichment scenarios using 1 cm of collimation above the input accountability tank using spent fuel that had been cooled for one year. Although this cooling time is much shorrter than what spent fuel entering reprocessing plants typically undergo ($\geq$ 3 years), this data can still provide insight into the readily identifiable isotopes in this set and their relationship to the source term.

Table 5.1 lists the most prominent and relevant isotopes detected with signal to noise ratios above 2 and multiple known gamma peaks present that were unique and distinguishable from any other known isotope gamma emission lines within 1 keV. Because of this somewhat wide energy window for identification, it is unsurprising that most of the distinguishable isotopes are above 800 keV, away from lower energy x-ray emission lines which overlap

tremendously. Y-88 and Bi-214 were the only isotopes that with clearly resolvable peaks that appear in all nine scenarios. The complete list of scenarios, isotopes, and the identified gamma rays is included in Appendix C.

33 GWd 2.6% IE	**33 GWd 3.3% IE**	**33 GWd 4.0% IE**	**45 GWd 3.3%IE**	**45 GWd 4.0% IE**	**45 GWd 4.7% IE**	**60 GWd 4.03% IE**	**60 GWd 4.73% IE**	**60 GWd 5.43% IE**
Y-88	Y-88	Y-88	Y-88	Y-88	Y-88	Y-88	Y-88	Y-88
Bi-214	Bi-214	Bi-214	Bi-214	Bi-214	Bi-214	Bi-214	Bi-214	Bi-214
	La-140	La-140					La-140	La-140
				Ag-110		Ag-110		Ag-110
			Np-240		Np-240			Np-240
			Tl-208			Tl-208		Tl-208
			Rh-106			Rh-106	Rh-106	
		Pb-211	Pb-211					
			Ac-228				Ac-228	
				Pa-234		Pa-234		
					Pu-239			
					Eu-154			

Table 5.1: Isotopes Expected to be Observed in All Scenarios

Table 5.2 shows the half-lives, average emission rates, and average activity of the isotopes identified in the nine scenarios based on the source terms provided by SSPM. Each isotope included in the table is discussed in more detail below:

Y-88: The presence and prominence of the twin Y-88 peaks aligns with the large activity (10^{12} Bq) present in each spent fuel batch. This large activity is attributed to the presence of yttrium and other rare earth elements like lanthanum that are often added as stabilizers to uranium fuel in order to raise the melting point and improve mechanical properties [26]. Its half-life is reasonably long enough for it be observed after a year of cooling, however other isotopes should be identified for use at larger cooler times. These longer cooling times are more relevant to spent fuel that undergoes reprocessing.

Bi-214: With a 19.9 minute half-life and a small emission rate it is somewhat surprising that Bi-214 appears in all nine simulated scenarios. Bi-214 is a gamma-emitting daughter in the U-238 decay chain; while it should not provide any information about cooling time, burnup, initial enrichment, or power history, it has the possibility of indicating the time since the uranium was chemically processed [93].

La-140: This isotope has appreciable thermal fission yields and fast fission yields in U-233, U-235, Pu-239, and Pu-241; it also has a non-zero fast fission yield in Th-232

and U-238 [52], [53]. It is commonly used in combination with Ba-140 for investigating irradiated nuclear fuel, and as a fission rate monitor [66].

Ag-110: Control rods in nuclear reactors are made in part of natural silver (52% Ag-107, 48% Ag-109) because of the two main isotopes' high neutron absorption cross section. The (n,γ) reaction on these silver atoms creates shorter lived isotopes such as Ag-110 and Ag-110m which can contribute to the contamination of auxiliary systems within a nuclear facility [14],[72].

Np-240: This isotope an extremely short lived daughter product in the decay chain of Pu-244, the longest lived known plutonium isotope. The ratio of Pu-244 to Pu-239 is one of many isotopic fingerprints used to assess the origin of radioactive contamination [2]. However, because of Np-240's short half life it is not of interest from a material recovery perspective nor for material accountancy purposes.

Tl-208: Like Bi-214, Tl-208 is a gamma-emitting daughter product of the U-238, and in Th-232 decay series. These two isotopes are often used in uranium exploration, via airborne or car-borne radiometry to survey large areas rapidly [25]. Tl-208 is also present in the U-232 decay chain. U-232 is present in virtually all weapons grade HEU, and is often used along with Tl-208 as effective tracers for HEU [65].

Rh-106: Rh-106 has appreciable thermal fission yields and fast fission yields in U-233, U-235, Pu-239, and Pu-241; it also has a non-zero fast fission yield in Th-232 and U-238 [52], [53]. For this reason, spent fuel is typical cooled for three or more years to reduce the presence of Rh-106/Ru-106 contamination by allowing these relatively short-lived isotopes to decay substantially [63].

Pb-211: This isotope is a short-lived daughter product within the U-235 and Pu-239 decay chains. Pb-211's short radioactive half life and extremely low total activity within spent fuel disqualifies it for future spent fuel characterization methods.

Ac-228: No actinium was present in the source term inputted into the MCNP model. However, Ac-228 is apart of the Th-232 decay chain, and Th-232 is the daughter product of the alpha decay of U-235. Ultimately, Ac-228's short half life and extremely low total activity within the spent fuel make it an improbable candidate for future spent fuel characterization methods as well.

Pa-234: The grand daughter of U-238's radioactive decay, Pa-234 short half life precludes it from use in spent fuel reprocessing accountancy methods.

Pu-239: This fissile plutonium isotope is used to produce nuclear weapons and has been proven to be a viable nuclear fuel material in thermal reactors. Being able to detect decay radiation from this Pu-239 is extremely important from a material accountancy and nuclear safeguards perspective. In this study, only the 1057.3 keV gamma ray (4.5 E-08 %) was identified in just one scenario.

Eu-154: Similar to Rh-106, Eu-154 has non-zero thermal and fast fission yields in U-233, U-235, Pu-239, and Pu-241; it also has a non-zero fast fission yield in Th-232 and U-238 [52], [53]. Eu-154 was expected to appear in all spent fuel scenarios given its known relationship to initial enrichment, however this was not the case.

Isotope	Half-life	Emission Rate (1/g/s)	Activity (Bq)
Y-88	106.6 d	8.10 E+10	5.58 E+12
Bi-214	19.9 m	7.85 E-11	2.29 E-20
La-140	1.68 d	1.94 E+2	5.53 E-07
Ag-110	249.7 d	9.93 E+1	2.24 E-07
Np-240	61.9 m	1.31 E-06	2.67 E-07
Tl-208	3.05 m	5.78 E+4	2.67 E-07
Rh-106	131 m	5.44 E+09	2.07 E+05
Pb-211	36.1 m	1.74 E-01	1.92 E-13
Ac-228	6.15 h	3.25 E-17	5.75 E-27
Pa-234	6.70 h	7.25 E+02	6.61 E-08
Pu-239	24110 y	3.64 E+05	8.42 E+08
Eu-154	8.60 y	4.61 E+08	7.11 E+08

Table 5.2: Average Emission Rates and Average Total Activity for Detected Isotopes. Uncertainties are set within SSPM and depend on the spectra collection time. They can be assumed to be +/- 5%

None of the Cs-134 or Cs-137 emission lines were observed during these preliminary simulations despite their thermal and fast fission yields in U-233, U-235, Pu-239, and Pu-241, and fast fission yields in Th-232 and U-238. Cs-134 ($t_{1/2}$=2.06 years) was expected to be easily resolvable with such a short cooling cooling time used in all scenarios, but that was not the case. In other bulk handling facilities like molten salt reactors, online gamma ray measurements could benefit from the characterization and quantification of this isotope because of its known relationship with burnup and cooling time of spent fuel. Other isotopes of interest include U-235, U-238, and Am-241 were not seen despite their high emission rates and total activity within the IAT (Table 5.3). Even with though they possess much longer half-lives, the sheer magnitude of material present and the large disintegration rate of U-235 and U-238 should have resulted in some decay radiation being detected.

Using what information was available, the two Y-88 peaks (1835.7 keV (99.2%) and 2734.0 keV (0.71%)) that were present and prominent during all nine scenarios were used to establish a relationship between count rate and mass. By summing the count rates within 3σ of the peaks and tabulating the mass of Y-88 from the SSPM source term Figure 5.6 was generated. The nine scenarios are grouped by the fuel burnup. As the fuel burnup increases so does the mass of Y-88 within the fuel, and a weak positive correlation is present between

Isotope	Halflife	Emission Rate (1/g/s)	Activity (Bq)
Cs-134	2.07 y	7.02 E+09	5.31 E+11
Cs-137	30.08 y	1.33 E+08	8.98 E+10
U-235	7.04 E+08 y	8.29 E+02	2.93 E+06
U-238	4.47 E+09 y	1.06 E+03	3.76 E+08
Am-241	432 y	1.22 E+09	6.64 E+08

Table 5.3: Important isotopes for MC&A and safeguards. Uncertainties are set within SSPM and depend on the spectra collection time. They can be assumed to be +/- 5%

mass of fuel and count rate observed in the peaks. There are times when the count rate also increases with initial enrichment within each scenario however it is not consistent across all nine.

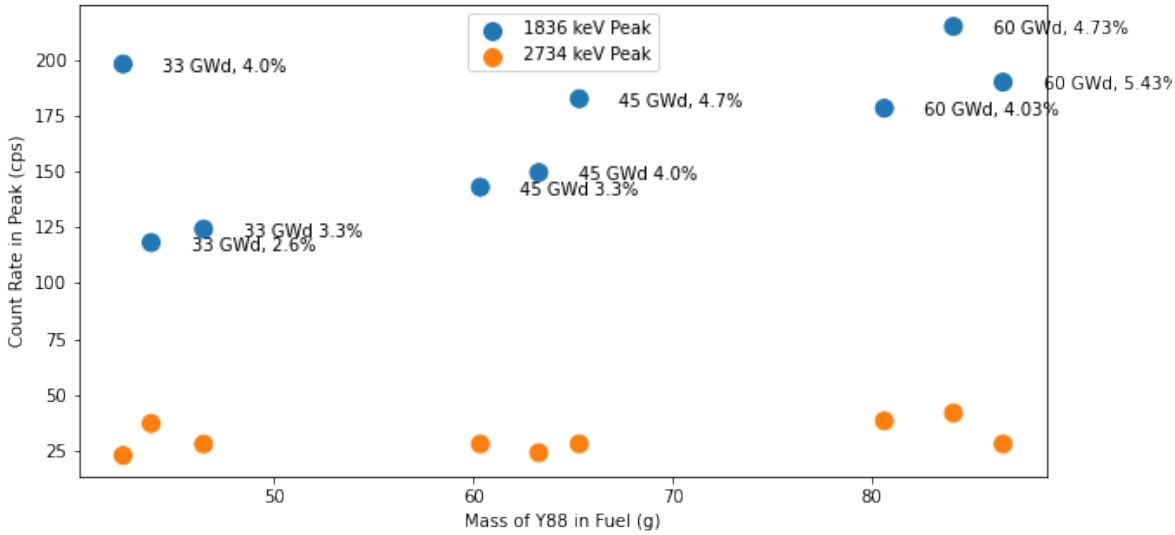

Figure 5.6: The sum of the count rate within two prominent Y-88 gamma peaks (1836 keV and 2734 keV) plotted as a function of mass with each spent fuel assembly for nine different scenarios burnup and initial enrichment combinations

5.3 Conclusion

Verifying the amount of special nuclear material within any nuclear facility is crucial to ensure the peaceful use of nuclear technology. With emerging high count rate high resolution gamma spectroscopy instruments [12] and narrow enough collimation through the thick concrete walls of a typical hot cell, various fission product decay radiation can be resolved. It is worth noting that this is an idealized scenario; this iteration of the MCNP model did not include the various types of instrumentation that are installed on top, around, or even inside the IAT (e.g. sampling probes, bayonet tubes for heating/cooling, etc.). This instrumentation would undoubtedly alter the intensity of gamma radiation detected at the HPGe detector face. Having a hole in the concrete shielding of a hot cell, even a few millimeters in diameter could be a potential radiological hazard for personnel working in the surrounding area. At the Tokai Reprocessing Plant for example, curved inspection pipes exist to sample the radiation environment inside the cell and conduct various experiments[82]. Future models should employ non-linear geometries of inspection pipes similar to these.

This research was made possible by tools like ADVANTG which greatly reduced the computation time needed to perform simulations of such large and complex sources. This study only focused on a relatively short lived but very prominent isotope: Y-88. Other isotopes such as Cs-134, Cs-137, and Eu-154 should be investigated further because of their known correlation to spent fuel characteristics. Cs-134 in particular was expected to be observed in all nine scenarios especially given the fuel's short cooling time however none of its decay radiation was resolved.

Additional shielding and attenuation were not applied because the count rate at reasonably obtainable hole diameters was low enough to resolve numerous emission lines. Future studies should also factor in the presence of neutrons for detection and identification and simulate the spent fuel at longer cooling times and different time points within a 24-hour dissolution cycle.

The nuclear facility landscape is continuing to change as countries begin to pivot towards Generation IV reactors and beyond to meet their energy needs. The characterization of high radiation fields present in aqueous reprocessing facilities serves as a valid benchmark for novel safeguards technology to be deployed in bulk handling facilities.

Even if countries choose not to reprocess, these new advanced reactor facilities will contain complex radiation sources that need to be better understood and properly safeguarded. Tools like SSPM and ADVANTG may help reduce the computational burden and expedite the study of more advanced nuclear reactor types including but not limited to molten salt reactors.

Chapter 6

Conclusion and Future Work

The modeling and simulation capabilities developed in this study allowed for a better understanding of the advanced recycle facilities and how advanced radiation detection and imaging, combined with advances in radiation transport methods, and fault detection capabilities can be leveraged to improve material accountancy.

Two experimental aqueous reprocessing loops were constructed to simulate the movement of radioactive material from one area to another within a bulk handling facility and served as a test bed for fault detection methodologies involving both radiation and non-radiation-based measurement signals. Future work will improve upon the Next Generation Loop by adding more detection systems (e.g., pressure transducers and pipe interrogators) and use neutron detection to improve accountancy measures. Furthermore, the existing fault detection methods used will be refined to connect fault monitoring to control optimization and feedback. Filtering techniques will be employed to further investigate alarm/detection threshold definitions.

Preliminary simulations using advanced hybrid methods showed promise in the ability to resolve many gamma rays with some collimation at appropriate count rates based on newly available source terms for high throughput PUREX plants. This data will be put to further use to study how the measured signals change as material inventory and fuel characteristics such as cooling time, burnup and enrichment are varied. More robust quantification methods will be developed to better identify important isotopes and their relationship to material inventory.

Lastly, this work serves as a basis for the safeguards by design process within bulk handling facilities including advanced reactor facilities such as molten salt reactors. These facilities vary widely in design and function but by leveraging the collective expertise of the various stakeholders in the system design process, we can employ system to ultimately improve plant performance, reduce maintenance concerns, and communicate information about the facility's operation to better safeguard nuclear material.

Bibliography

[1] C Alejano, D Boulanger, M Brady-Raap, R Brennetot, V Chrapciak, et al. "Spent nuclear fuel assay data for isotopic validation". In: *Nuclear Energy Agency OECD, NEA/NSC/WPNCS/DOC* (2011).

[2] JA Corcho Alvarado, S Röllin, H Sahli, and P McGinnity. "Isotopic signatures of plutonium and uranium at Bikar atoll, northern Marshall Islands". In: *Journal of Environmental Radioactivity* 242 (2022), p. 106795.

[3] Antech. *Active-passive well coincidence counter data sheet, N2442*. 2017.

[4] Antech. *High-level neutron coincidence counter data sheet N2018*. 2018.

[5] S Balsley. "Destructive nuclear material analysis for safeguards: importance and future trends". In: *IAEA symposium on international safeguards, Vienna. IAEA-CN-184/278*. 2010.

[6] C Bassett. "High cost of nuclear power plants. [Retroactive safety standards account for over half of cost]". In: *Public Util. Fortn.* 101-9.7100178 (Apr. 1978).

[7] O Beneš and P Souček. "Chapter 6: Molten salt reactor fuels". In: *Advances in Nuclear Fuel Chemistry*. Ed. by Markus H.A. Piro. Woodhead Publishing Series in Energy. Woodhead Publishing, 2020, pp. 249–271. ISBN: 978-0-08-102571-0.

[8] J Bruno and RC Ewing. "Spent nuclear fuel". In: *Elements* 2.6 (2006), pp. 343–349.

[9] M Bunn, JP Holdren, S Fetter, and B Van Der Zwaan. "The economics of reprocessing versus direct disposal of spent nuclear fuel". In: *Nuclear Technology* 150.3 (2005), pp. 209–230.

[10] T Burr, MS Hamada, and J Howell. "Modelling and simulation for nuclear material accounting and process monitoring in nuclear safeguards". In: *International Journal of Research and Reviews in Applied Science* 8.3 (2011), pp. 270–282.

[11] BB Cipiti and N Shoman. "Bulk handling facility modeling and simulation for safeguards analysis". In: *Science and Technology of Nuclear Installations* (2018).

[12] RJ Cooper, M Amman, and K Vetter. "High resolution gamma-ray spectroscopy at high count rates with a prototype high purity germanium detector". In: *Nuclear Instruments and Methods in Physics Research Section A: Accelerators, Spectrometers, Detectors and Associated Equipment* 886 (2018), pp. 1–6.

[13] FCL Crespi, V Vandone, S Brambilla, F Camera, B Million, S Riboldi, and O Wieland. "HPGe detectors timing using pulse shape analysis techniques". In: *Nuclear Instruments and Methods in Physics Research Section A: Accelerators, Spectrometers, Detectors and Associated Equipment* 620.2-3 (2010), pp. 299–304.

[14] F Dacquait, M Bultot, G Pipet, J Francescatto, F Broutin, M Benfarah, and P Mondit. "^{110m}Ag behaviour in PWRs: Lessons learnt from the EMECC campaigns". In: *NPC 2016 (Nuclear Plant Chemistry)-International Conference on Water Chemistry of Nuclear Reactor Systems*. The Nuclear Institute. 2016.

[15] M DeWitt. *Review of S-1030 scrubber event Columbia Fuel Fabrication Facility*. Oct. 2016.

[16] MP Dion, LG Worrall, S Croft, and LM Scott. *Molten salt reactor signatures and modeling study*. Tech. rep. ORNL, Nov. 2021. DOI: 10.2172/1761616.

[17] J Doyle. *Nuclear safeguards, security and nonproliferation: achieving security with technology and policy*. Elsevier, 2011, pp. 175–176.

[18] AL Dulmage and NS Mendelsohn. "Coverings of bipartite graphs". In: *Canadian Journal of Mathematics* 10 (1958), pp. 517–534.

[19] MH Ehinger and SJ Johnson. *Lessons learned in international safeguards-Implementation of safeguards at the Rokkasho reprocessing plant*. Tech. rep. ORNL/TM-2010/23. Oak Ridge National Lab. (ORNL), Oak Ridge, TN (United States), 2010.

[20] Office of Environment Health and Safety (EH&S) at UC Berkeley. *Safety information fact sheet: Hazardous waste management*. June 2014.

[21] EB Firmage. "The treaty on the non-proliferation of nuclear weapons". In: *American Journal of International Law* 63.4 (1969), pp. 711–746.

[22] V Fortakov. *Nuclear verification: what it is, how it works, the assurances it can provide*. Tech. rep. 1998.

[23] The Generation IV International Forum. *Molten salt reactor (MSR)*. 2018.

[24] E Frisk, M Krysander, and D Jung. "A toolbox for analysis and design of model based diagnosis systems for large scale models". In: *IFAC-PapersOnLine* 50.1 (2017), pp. 3287–3293.

[25] C Ganguly. *Human resource development for uranium production cycle*. June 2014.

[26] J Guon, LF Grantham, and ER Specht. *Yttrium and rare earth stabilized fast reactor metal fuel*. US Patent 5,112,534. May 1992.

[27] Health and Safety Executive (HSE). *Report of the investigation into the leak of dissolver product liquor at the Thermal Oxide Reprocessing Plant (THORP), Sellafield, notified to HSE on 20 April 2005*. Feb. 2007.

[28] K Hogue. "Introduction to safeguards by design". In: (Oct. 2018).

[29] A Houtzeel and FF Dyer. *Study of fission products in the molten-salt reactor experiment by gamma spectrometry*. Tech. rep. Oak Ridge National Lab., Tenn., 1972.

[30] IAEA. *2015 Review conference of the parties to the treaty on the Non-Proliferation of Nuclear Weapons (NPT)*. 2015.

[31] IAEA. "Developing the first ever facility for the safe disposal of spent fuel". In: *IAEA Bulletin* (July 2019).

[32] IAEA. *Facility design and plant operation features that facilitate the implementation of IAEA safeguards*. Vol. IAEA-STR-360. IAEA, 2009.

[33] IAEA. *Hydrogen production using nuclear energy*. Nuclear Energy Series NP-T-4.2. 2013. ISBN: 978-92-0-135110-4.

[34] IAEA. *IAEA safeguards glossary. - 2001 edition*. OSTI ID: 20267262. 2002.

[35] IAEA. *International safeguards in nuclear facility design and construction*. Vol. No. NP-T-2.8. IAEA, 2013.

[36] IAEA. *International safeguards in the design of reprocessing plants*. Nuclear Energy Series NF-T-3.2. Vienna: International Atomic Energy Agency, 2019. ISBN: 978-92-0-104519-5.

[37] IAEA. *Molten salt reactors*. 2016.

[38] IAEA. *Physical protection of nuclear material and nuclear facilities (Implementation of INFCIRC/225/Revision 5)*. 2018.

[39] IAEA. *Safeguards techniques and equipment. – 2011 edition*. 2011.

[40] IAEA. *Safeguards–an introduction*. Tech. rep. IAEA/SG/INF/3, Vienna, Austria, 1981.

[41] IAEA. *Seven things to know about radioisotopes*. 2014.

[42] IAEA. *Status and trends in pyroprocessing of spent nuclear fuels*. 2021.

[43] IAEA. "Status and trends in spent fuel reprocessing". In: *IAEA-TECDOC-1467* (2005).

[44] Institut de Radioprotection et de Sûreté Nucléaire. *Incident in the THORP reprocessing plant at Sellafield*. May 2005.

[45] ER Irish and W Ho Reas. *The purex process: a solvent extraction reprocessing method for irradiated uranium*. Hanford Atomic Products Operation, 1957.

[46] Japan Atomic Energy Agency. *Reprocessing Technology Development*. 2004.

[47] SJ Johnson. *The safeguards improvement plan for the Tokai Reprocessing Plant*. Tech. rep. IAEA-SM-351/143. IAEA Department of Safeguards, 1997.

[48] SJ Johnson, R Abedin-Zadeh, C Pearsall, K Hiruta, C Creusot, M Ehinger, E Kuhn, et al. "Development of the safeguards approach for the Rokkasho Reprocessing Plant". In: *IAEA SM* 367.IAEA-SM-367/8/01 (2001), p. 01.

[49] SJ Johnson and M Ehinger. *Designing and operating for safeguards: Lessons learned from the Rokkasho Reprocessing Plant (RRP)*. Tech. rep. PNNL-19626. Pacific Northwest National Lab.(PNNL), Richland, WA (United States), 2010.

[50] J Kendrick, C Poresky, C Alivisatos, G Batie, V Goss, L Shi, P Peterson, R Slaybaugh, and K Vetter. *Non-radiation Safeguard signals and detection for special nuclear material holdup and diversion detection*. Internal report prepared in fullment of DOE NEUP Project No. 17-12824. May 2019.

[51] GF Knoll. *Radiation detection and measurement*. John Wiley & Sons, 2010.

[52] A Koning, R Forrest, M Kellett, R Mills, H Henriksson, et al. *The jeff-3.1 nuclear data library-jeff report 21*. Tech. rep. Organisation for Economic Co-operation and Development, 2006.

[53] A Koning, R Forrest, M Kellett, R Mills, H Henriksson, and Y Rugama. *Joint Evaluated Fission and Fusion File, Incident-neutron data*. Oct. 2006.

[54] M Kotzalas. *Report on lessons learned from uranium accumulation in scrubber and ventilation systems at Westinghouse Columbia Fuel Fabrication Facility*. Tech. rep. U.S. Nuclear Regulatory Commission, Oct. 2016.

[55] JJ Laidler, JE Battles, WE Miller, JP Ackerman, and EL Carls. "Development of pyroprocessing technology". In: *Progress in Nuclear Energy* 31.1 (1997). The Technology of the Integral Fast Reactor and its Associated Fuel Cycle, pp. 131–140. ISSN: 0149-1970.

[56] Nuclear Waste Partnership LLC. "WIPP history/timeline". In: (Apr. 2021).

[57] H March-Leuba, J Garner, J Younkin, and DW Simmons. *On line enrichment monitor (OLEM) UF6 tests for 1.5" sch40 SS pipe revision*. Tech. rep. Oak Ridge National Lab.(ORNL), Oak Ridge, TN (United States), 2016.

[58] CK Mathews, HC Jain, VD Kavimandan, and SK Aggarwal. "Tracer techniques for the input accountability of plutonium in reprocessing plants: MAGTRAP and LEAD-TRAP". In: *Nuclear Technology* 42.3 (1979), pp. 297–303.

[59] J McFarlane, PA Taylor, DE Holcomb, and W Poore III. *Review of hazards associated with molten salt reactor fuel processing operations*. Tech. rep. Oak Ridge National Lab.(ORNL), Oak Ridge, TN (United States), 2019.

[60] HO Menlove. *Description and operation manual for the active well coincidence counter*. Tech. rep. Los Alamos Scientific Lab., 1979.

[61] JC Miles, JE Glancey, and SE Donelson. *Use of process monitoring data for the enhancement of nuclear material control and accounting*. Vol. 1013. The Division, 1979.

[62] SW Mosher, SR Johnson, AM Bevill, AM Ibrahim, CR Daily, TM Evans, JC Wagner, et al. *ADVANTG: An automated variance reduction parameter generator, rev. 1*. Tech. rep. ORNL, Aug. 2015. DOI: 10.2172/1210162.

[63] KL Nash and GL Lumetta. *Advanced separation techniques for nuclear fuel reprocessing and radioactive waste treatment*. Elsevier, 2011.

[64] Office of Nuclear Energy. *TRISO particles: The most robust nuclear fuel on Earth*. July 2019.

[65] RB Oberer, LG Chiang, MJ Norris, CA Gunn, and BC Adaline. *The use of TI-208 gamma rays for safeguards, nondestructive-assay (NDA) measurements*. Tech. rep. Oak Ridge Y-12 Plant (Y-12), Oak Ridge, TN (United States), 2009.

[66] JB Olomo and TD MacMahon. "Gamma-ray emission probabilities in the decay of 140Ba and 140La". In: *Journal of Physics E: Scientific Instruments* 17.2 (1984), p. 124.

[67] ORTEC Advanced Measurement Technology. *IDM-200-V: Interchangeable HPGe detector module (IDM) brochure*. 2019.

[68] H Ottmar and H Eberle. "The hybrid K-edge/K-XRF densitometer: principles - design - performance". In: Citeseer, 1991.

[69] D Parvin. "Validation and performance test of the plutonium inventory measurement system (PIMS) at the Rokkasho Reprocessing Plant (RRP)". In: *British Nuclear Group, Project Services Limited* (2007).

[70] G Pérez-Zuñiga, J Sotomayor-Moriano, R Rivas-Perez, and V Sanchez-Zurita. "Distributed fault detection and isolation approach for oil pipelines". In: *Applied Sciences* 11.24 (2021), p. 11993.

[71] PJ Persiani, RG Bucher, RB Pond, and RJ Cornella. *Fuel reprocessing data validation using the isotope correlation technique*. Tech. rep. Argonne National Lab., 1990.

[72] DA Petti. "Silver-indium-cadmium control rod behavior in severe reactor accidents". In: *Nuclear technology* 84.2 (1989), pp. 128–151.

[73] JR Phillips, TR Bement, K Kaieda, and EG Medina. *Nondestructive verification of relative burnup values and cooling times of irradiated MTR fuel elements*. Tech. rep. Los Alamos Scientific Lab., 1979.

[74] TH Pigford. *Actinide burning and waste disposal*. Tech. rep. International Atomic Energy Agency, 1990.

[75] KKS Pillay. *Fundamentals of materials accounting for nuclear safeguards*. Tech. rep. LA-11569-M. Los Alamos National Laboratory, Apr. 1989. DOI: 10.2172/6347788.

[76] R Plenteda, A Alessandrello, W Deringer, M Frankl, M Lang, LM Cronholm, D Breban, C Creusot, and K Baird. *Hardware and software upgrade for the solution measurement and monitor system at Rokkasho Reprocessing Plant*. Tech. rep. 2015.

[77] C Poresky. "Model network methodology for experimental development of industrial monitoring systems". PhD thesis. University of California, Berkeley, 2019, pp. 18–39.

[78] D Reilly, N Ensslin, H Smith Jr, and S Kreiner. *Passive nondestructive assay of nuclear materials*. Tech. rep. Nuclear Regulatory Commission, Washington, DC (United States), 1991.

[79] RC Robertson. "MSRE design and operations report part I: Description of reactor design (ORNL-TM-728)". In: (1965).

[80] C Rofer. "Why did the US abandon a lead in reactor design?" In: *Physics Today* (2015). DOI: 10.1063/PT.5.2029.

[81] S Rouquette-Sanchez, J Finne, and G Picard. "Assessment of pyrochemical methods for the molten salt reactor fuel clean-Up". In: *ECS Proceedings Volumes* 2004.1 (2004), p. 738.

[82] M Sekine, H Tomikawa, T Matsuki, K Tsutagi, N Nishida, T Kitao, et al. *Final report on feasibility study of Pu monitoring and solution measurement of high active liquid waste containing fission product at reprocessing facility*. Tech. rep. Japan Atomic Energy Agency, 2020.

[83] Y Shatilla. "7 - Nuclear desalination". In: *Nuclear Reactor Technology Development and Utilization*. Ed. by Salah Ud-Din Khan and Alexander Nakhabov. Woodhead Publishing Series in Energy. Woodhead Publishing, 2020, pp. 247–270. ISBN: 978-0-12-818483-7.

[84] LE Smith and AR Lebrun. "Design, modeling and viability analysis of an online uranium Enrichment Monitor". In: *2011 IEEE Nuclear Science Symposium Conference Record*. 2011, pp. 1030–1037.

[85] European Nuclear Society. *PUREX process*. 2019.

[86] Mirion Technologies. *Waste Crate Assay System (WCAS)*. 2002.

[87] Office of Technology Assessment. *Nuclear Safeguards and the International Atomic Energy Agency*. 1995. ISBN: 9781422348802.

[88] MES Trothe, HR Shakerand M Jradi, and K Arendt. "Fault isolability analysis and optimal sensor placement for fault diagnosis in smart buildings". In: *Energies* 12.9 (2019), p. 1601.

[89] U.S. Government Accountability Office. *Nuclear fuel cycle options: DOE needs to enhance planning for technology assessment and collaboration with industry and other countries*. Washington, DC, USA, Oct. 2011, p. 8.

[90] JD Vienna. "Nuclear waste vitrification in the United States: recent developments and future options". In: *International Journal of Applied Glass Science* 1.3 (2010), pp. 309–321.

[91] JC Wagner, DE Peplow, SW Mosherand TM Evans, et al. "Review of hybrid (deterministic/Monte Carlo) radiation transport methods, codes, and applications at Oak Ridge National Laboratory". In: *Progress in nuclear science and technology* 2 (2011), pp. 808–814.

[92] CJ Werner, JS Bull, CJ Solomon, FB Brown, GW McKinney, ME Rising, DA Dixon, RL Martz, et al. *MCNP version 6.2 release notes*. Tech. rep. Los Alamos National Lab.(LANL), Los Alamos, NM (United States).

[93] J White, WS Charlton, A Solodov, and SJ Tobin. "Applications of x-ray fluorescence and fission product correlations for nuclear forensics". In: *Proceedings of the 51st Annual Meeting for the Institute of Nuclear Materials Management, Baltimore, Maryland*. 2010, pp. 11–15.

[94] J Zhang and G Rizzoni. "Functional safety of electrified vehicles through model-based fault diagnosis". In: *IFAC-PapersOnLine* 48.15 (2015), pp. 454–461.

[95] K Zhao et al. *International target values 2010 for measurement uncertainties in safeguarding nuclear materials*. Tech. rep. International Atomic Energy Agency (IAEA), 2010.

Appendix A

First Generation Loop Equation Set

1. $V_1 = A_1 h_1 + \mathbf{fV1}$
2. $V_2 = A_2 h_2 + \mathbf{fV2}$
3. $V_3 = A_3 h_3 + \mathbf{fV3}$
4. $V_4 = A_4 h_4 + \mathbf{fV4}$
5. $V_{tot} = V_0 + V_1 + V_2 + V_3 + V_4 + \mathbf{fVtot}$
6. $q_1 = \frac{\rho g(h_1 - h_2)}{R_1} + \mathbf{fQ1}$
7. $q_2 = \frac{\rho g(h_2 - h_3)}{R_1} + \mathbf{fQ2}$
8. $q_3 = \frac{\rho g(h_3 - h_4)}{R_1} + \mathbf{fQ3}$
9. $q_4 = \frac{\rho g(h_4)}{R_1} + \mathbf{fQ4}$
10. $q_1 = \frac{dV_1}{dt}$
11. $q_2 = \frac{dV_2}{dt}$
12. $q_3 = \frac{dV_3}{dt}$
13. $q_4 = \frac{dV_4}{dt}$
14. $\dot{h_1} = \frac{q_0 - q_1}{A_1}$
15. $\dot{h_2} = \frac{q_1 - q_2}{A_1}$
16. $\dot{h_3} = \frac{q_2 - q_3}{A_1}$
17. $\dot{h_4} = \frac{q_3 - q_4}{A_1}$
18. $\frac{dh_1}{dt} = \dot{h_1}$
19. $\frac{dh_2}{dt} = \dot{h_2}$
20. $\frac{dh_3}{dt} = \dot{h_3}$
21. $\frac{dh_4}{dt} = \dot{h_4}$
22. $\frac{dV_1}{dt} = \dot{V_1}$
23. $\frac{dV_2}{dt} = \dot{V_2}$
24. $\frac{dV_3}{dt} = \dot{V_3}$
25. $\frac{dV_4}{dt} = \dot{V_4}$
26. $V_1 = C_1 * CR_1 + \mathbf{fCR1}$
27. $V_2 = C_2 * CR_2 + \mathbf{fCR2}$
28. $V_3 = C_3 * CR_3 + \mathbf{fCR3}$
29. $V_4 = C_4 * CR_4 + \mathbf{fCR4}$
30. $y_1 = q_0$
31. $y_2 = V_1$
32. $y_3 = V_2$
33. $y_4 = V_3$
34. $y_5 = V_4$

35. $y_6 = CR_1$
36. $y_7 = CR_2$
37. $y_8 = CR_3$
38. $y_9 = CR_4$

Appendix B

Next Generation Loop Equation Set

1. $q_1 = q_2 + q_3 - A_{spout,1}\sqrt{2gh_1} + \mathbf{fQ1}$
2. $q_2 = q_4 - A_{spout,2}\sqrt{2gh_2} - \mathbf{fQ2}$
3. $q_5 = q_1 - q_6 - A_{spout,0}\sqrt{2gh_0} + \mathbf{fQ6}$
4. $m_0 = \pi\rho_{fluid}R_{tank0}^2 h_0 + \boldsymbol{fM_0}$
5. $dh_0 = \frac{q_5+q_6-q_1}{A_{tank0}}$
6. $dh_1 = \frac{q_1-q_2-q_3-\boldsymbol{fQ3}}{A_{tank1}}$
7. $dh_0 = \frac{q_2-q_4-\boldsymbol{fQ4}}{A_{tank2}}$
8. $q_5 + \boldsymbol{fQ5} = q_3 + q_4$
9. $V_0 = \pi R_{tank0}^2 h_0 + \boldsymbol{fV_0}$
10. $V_1 = \pi R_{tank1}^2 h_1 + \boldsymbol{fV_1}$
11. $V_2 = \pi R_{tank2}^2 h_2 + \boldsymbol{fV_2}$
12. $V_{total} = V_0 + V_1 + V_2 + \boldsymbol{fV_{tot}}$
13. $t = t_{meas} - t_{cal}$
14. $V_0 = c_{0,Tc} * (A_{Tc,0} + \boldsymbol{fA_{Tc,0}}) + b_{0,Tc}$
15. $V_1 = c_{1,Tc} * (A_{Tc,1} + \boldsymbol{fA_{Tc,1}}) + b_{1,Tc}$
16. $V_2 = c_{2,Tc} * (A_{Tc,2} + \boldsymbol{fA_{Tc,2}}) + b_{2,Tc}$
17. $V_0 = c_{0,F} * (A_{F,0} + \boldsymbol{fA_{F,0}}) + b_{0,F}$
18. $V_1 = c_{1,F} * (A_{F,1} + \boldsymbol{fA_{F,1}}) + b_{1,F}$
19. $V_2 = c_{2,F} * (A_{F,2} + \boldsymbol{fA_{F,2}}) + b_{2,F}$
20. $\frac{dh_0}{dt} = \dot{h_0}$
21. $\frac{dh_1}{dt} = \dot{h_1}$
22. $\frac{dh_2}{dt} = \dot{h_2}$
23. $y_t = t_{meas}$
24. $y_1 = V_0$
25. $y_2 = V_1$
26. $y_3 = V_2$
27. $y_4 = m_0$
28. $y_5 = q_1$
29. $y_6 = q_5$
30. $y_7 = A_{0,Tc-99m}$
31. $y_8 = A_{1,Tc-99m}$
32. $y_9 = A_{2,Tc-99m}$
33. $y_{10} = A_{0,F-18}$
34. $y_{11} = A_{1,F-18}$
35. $y_{12} = A_{2,F-18}$

Appendix C

Table of Isotopes and Identified Gamma Rays in 9 IAT Scenarios

Spent Fuel Scenario	Detected Gamma Energy (keV)	Identified Gamma Energy (keV)	Identified Isotope
33 GWd 2.6% IE	1751.4	1751.6	Bi-214
	1836.1	1836.1	Y-88
	2733.0	2734.0	Y-88
33 GWd 3.3% IE	1543.2	1543.3	Bi-214
	1561.0	1561.0	Pr-144
	1835.7	1836.1	Y-88
	2482.5	2482.8	Bi-214
	2521.5	2521.4	La-140
	2734.2	2734.0	Y-88
33 GWd 4.0% IE	1196.3	1196.3	Pb-211
	1599.6	1599.6	Bi-214
	1835.3	1836.1	Y-88
	1924.6	1924.6	La-140
	2026.0	2026.7	Eu-156
	2735.0	2734.0	Y-88
45 GWd 3.3% IE	1095.7	1095.7	Ac-228
	1196.1	1196.3	Pb-211
	1222.3	1223.0	Np-240
	1248.1	1247.1	Ac-228
	1380.9	1381.1	Tl-208
	1583.0	1583.2	Bi-214
	1725.2	1724.6	Rh-106
	1835.5	1836.1	Y-88
	2733.2	2734.0	Y-88

Spent Fuel Scenario	**Detected Gamma Energy (keV)**	**Identified Gamma Energy (keV)**	**Identified Isotope**
45 GWd 4.0% IE	1360.9	1360.2	Rh-106
	1421.1	1420.3	Ag-110
	1435.7	1436.6	Sb-124
	1477.7	1476.9	Sb-126
	1602.2	1601.8	Pa-234
	1835.7	1836.1	Y-88
	2252.4	2251.6	Bi-214
	2733.2	2734.0	Y-88
45 GWd 4.7% IE	1056.5	1057.3	Pu-239
	1104.7	1104.6	Bi-214
	1122.7	1122.0	Rh-106
	1487.9	1488.2	Np-240
	1673.2	1673.9	Eu-154
	1835.7	1836.1	Y-88
	2734.4	2734.0	Y-88
60 GWd 4.03% IE	1363.5	1363.8	Eu-152
	1498.5	1498.8	Rh-106
	1553.6	1553.8	Pa-234
	1697.8	1698.8	Ag-110
	1743.4	1744.0	Tl-208
	1835.9	1836.1	Y-88
	2287.4	2287.7	Bi-214
	2733.8	2734.0	Y-88
60 GWd 4.73% IE	1149.5	1150.2	Rh-106
	1226.3	1226.7	Bi-214
	1405.3	1405.2	La-140
	1836.1	1836.1	Y-88
	2733.8	2734.0	Y-88
60 GWd 5.43% IE	885.1	884.7	Ag-110
	1323.9	1323.6	Rh-102
	1333.3	1332.5	Co-60
	1440.9	1441.1	Ag-108
	1577.8	1577.2	Rh-106
	1600.4	1599.6	Bi-214
	1743.6	1744.0	Tl-208
	1836.1	1836.1	Y-88
	2075.6	2074.8	Np-240
	2733.4	2734.0	Y-88